Phosphate recovery

From Nanoparticles to Membrane Technology

Paltrinieri, Laura

DOI
10.4233/uuid:8ae79702-2689-4235-89a7-202afdf5e358

Publication date
2019

Document Version
Final published version

Citation (APA)
Paltrinieri, L. (2019). *Phosphate recovery: From Nanoparticles to Membrane Technology*. [Dissertation (TU Delft), Delft University of Technology]. https://doi.org/10.4233/uuid:8ae79702-2689-4235-89a7-202afdf5e358

PHOSPHATE RECOVERY

From Nanoparticles to Membrane Technology

Laura PALTRINIERI

PHOSPHATE RECOVERY

From Nanoparticles to Membrane Technology

Dissertation

For the purpose of obtaining the degree of doctor
at Delft University of Technology,
by the authority of the Rector Magnificus Prof. dr. ir. T.H.J.J van der Hagen,
chair of the Board for Doctorates,
to be defended publicly on
Friday 22nd of February 2019 at 12:30 o'clock

by

Laura PALTRINIERI

Master of Science in Chemistry, University of Bologna, Italy
Born in Carpi (Modena), Italy

This dissertation has been approved by the promotor and the copromotor.

Composition of the doctoral committee:

Rector Magnificus	chairperson
Prof. dr. E.J.R. Sudhölter	Delft University of Technology, promotor
Dr. ir. L.C.P.M. de Smet	Delft University of Technology, copromotor

Independent members:

Prof. dr. ir. M.C.M. van Loosdrecht	Delft University of Technology
Prof. dr. S.J. Picken	Delft University of Technology
Prof. dr. ir. E.H.D.W. Roesink	University of Twente
Dr. W.A. Smith	Delft University of Technology

Other member:

Ir. W. van Baak	Water Future B.V.

The research was carried out at the Department of Chemical Engineering, Faculty of Applied Sciences, Delft University of Technology. The work was financially supported by Wetsus, Center of Excellence for Sustainable Water Technology. Wetsus is co-funded by the Dutch Ministry of Economic Affairs and Ministry of Infrastructure and Environment, the European Union Regional Development Fund, the Province of Fryslân, and the Northern Netherlands Provinces.

Cover Design
Patrizia D'Olivo
linkedin:/patrizia-d-olivo

Printed by
Ipskamp Printing
ISBN

Electronic version http://repository.tudelft.n

To my mum, Chiara
for all your support, love, and encouragement…

CONTENTS

30.973761 15

$3s^2 3p^3$

P

Melting point: 44.14° C
Boiling point: 280° C

PHOSPHORUS

CHAPTER 1

Introduction

Having a fresh fruit salad or a plate of colourful vegetables on a warm sunny day can be considered as a fast and simple meal prepared by most of the people I know. Less obvious is to realize and to quantify how much energy, water, and chemicals are needed to provide such refreshing food on a daily basis. A continuous production of fertilizers is required to guarantee a constant food supply to our ever-growing human population. Fertilizers for crop production are mostly composed of phosphorus (P)[1], which is a non-renewable and limited available, natural resource. P-containing ore is extracted from mines located in a limited number of countries (*e.g.,* Morocco and Western Sahara, Australia and China)[2], making most nations heavily dependent on P imports. Due to the high economic importance of P to the European Union combined with a high risk associated with it supply, the European Commission added phosphate rock to its revised list of Critical Raw Materials in 2014.[3]

In addition to the high demand of P, the uncontrolled discharge of P-containing products as present in aqueous streams from agricultural and cosmetic sectors[4,1] has increased the eutrophication processes, *i.e.,* the rapid growth of aquatic algae in lakes and rivers.[5,6] These processes have contributed to an unbalanced aquatic ecology and to a decrease of water quality. As a result, phosphate is considered to be one of the most critical contaminants present in wastewater. Therefore, the recovery and reuse of P from wastewater sources has been recognised as a strategic and sustainable solution to meet not only the constant high demand of water quality, but also to address the depletion of P resources the world is facing.[7,8]

Phosphate: pH and competing anions

P is normally found in wastewater as orthophosphate also known as phosphoric acid (H_3PO_4).[9] The type of orthophosphate present in water is depending on the pH value. A certain pH value is correlated with a specific phosphate speciation ratio, according to the following equilibrium reactions:

$$H_3PO_4 + H_2O \rightleftharpoons H_2PO_4^- + H_3O^+ \qquad pK_{a1} = 2.1 \qquad (1.1)$$

$$H_2PO_4^- + H_2O \rightleftharpoons HPO_4^{2-} + H_3O^+ \qquad pK_{a2} = 7.2 \qquad (1.2)$$

$$HPO_4^{2-} + H_2O \rightleftharpoons PO_4^{3-} + H_3O^+ \qquad pK_{a3} = 12.7 \qquad (1.3)$$

Based on the Equations 1.1, 1.2 and 1.3 it is easy to calculate the fraction of each species as a function of the pH of the solution (Figure 1.1). Given the fact that the pH of water streams in wastewater treatment plants is typically in the range of 6-8,[10,11] the phosphate ions found in wastewater are mostly monoanionic, and partly dianionic (pK_{a2} = 7.2).[12]

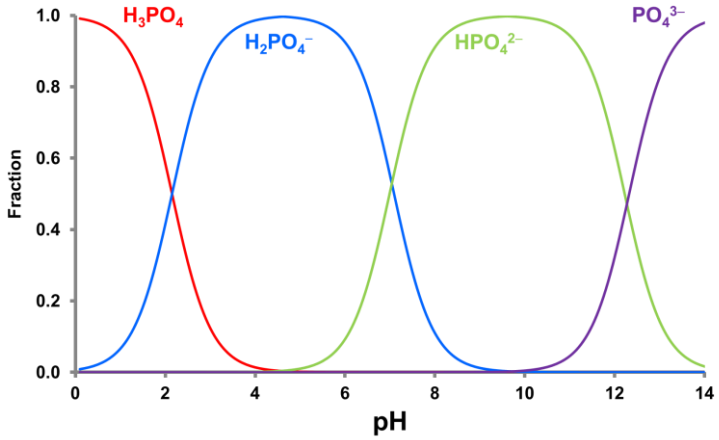

Figure 1.1 Phosphate speciation as a function of pH.

In addition to the pH-dependency of phosphoric acid (monovalent and divalent, or even trivalent), phosphate has a low diffusion coefficient and large ionic radius when compared to other anions present in wastewater (Table 1.1). These properties make the process of phosphate removal highly challenging; most of the conventional separation processes for phosphate removal (*i.e.,* precipitation, coagulation, flocculation, and biological treatment) are barely efficient in terms of recovery yields.[13] Over the past years, several research groups started to investigate alternative technologies to selectively recover

phosphate from various water sources. Such technologies have to guarantee high yields, economic feasibility, and most importantly, a high selectivity.

Table 1.1 Comparison of anions commonly present in wastewater and their related ionic conductivities (λ), diffusion coefficients (D), and Stokes radii (r_s).[14]

	λ (10^{-4} $m^2 \cdot S \cdot mol^{-1}$)	D (10^{-5} $cm^2 \cdot s^{-1}$)	r_s (Å)
Cl^-	76.3	2.032	1.2
NO_3^-	71.4	1.902	1.3
SO_4^{2-}	80.0	1.065	2.3
$H_2PO_4^-$	36.0	0.959	2.4
HPO_4^{2-}	57.0	0.759	2.6

Selectivity

Selectivity is part of nature. It plays an important role in various molecular systems and processes, including pheromone receptors, antigen-antibody interactions, enzyme-substrate complexes, and ligand-gated ion-channels. Selectivity is often searched for in water treatment to provide efficient and exclusive removal of the target elements. Clearly, high selectivities are required when the final goal is the recovery and reuse of desired components such as phosphate.

In order to design a phosphate-selective separation process, materials used during separation need to be combined with a specific phosphate-binder (receptor). Indeed, receptors play a key role in selective ion transport. For this specific purpose, the ideal receptor should provide a selective binding with phosphate, but also should allow its transport through the membrane, and its release at the permeate side. In other words, the binding should be reversible and tuneable. In a recent review of Wang *et al.*[15] an extensive overview is given of phosphate selective receptors used so far, and this is also depicted in Figure 1.2.

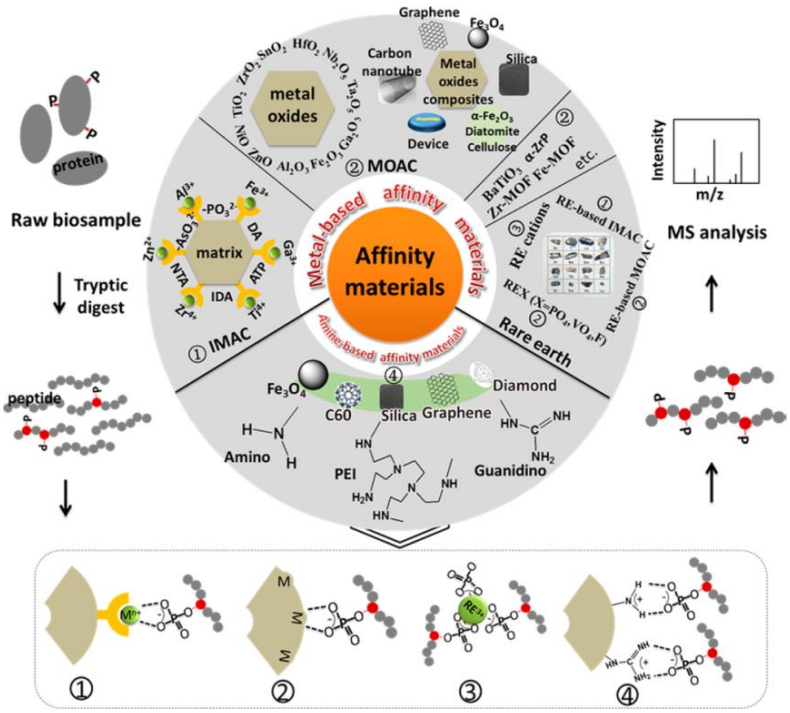

Figure 1.2 Illustration of different phosphate receptor units. Reprinted with permission from ACS Appl. Mater. Interfaces, 2015, 7 (16), pp 8377–8392. Copyright 2015 American Chemical Society.

While divalent, metal-based receptors have a strong binding towards phosphate, amino-based groups show weak (and thus tuneable) interactions. This is the reason why in this thesis, urea-type compounds were chosen as a receptor, to be specific the guanidinium (Gu) functionality. As described in several studies,[16–18] Gu is able to selectively bind phosphate through electrostatic and H-bond interactions. Again, the great advantage of this compound is its capability to form a 'reversible bond' able to remove and recover phosphate. Figure 1.3 is shown a schematic representation of the complex formation between guanidinium and phosphate monoanion.

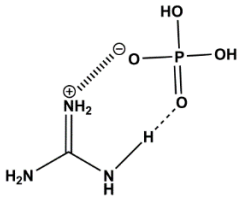

Figure 1.3 A schematic illustrating the interactions between Guanidinium and phosphate based on a H-bond (dotted line) and electrostatic forces (dashed line).

Gu is a versatile group and can be easily introduced into other chemical structures to be further employed in surface/bulk modifications of various substrates. In this thesis, Gu has been used in two different forms (Figure 1.4): *i)* in combination with a polyelectrolyte to obtain a guanidinium-functionalized poly(allylamine hydrochloride), so-called PAH-Gu, following the synthesis reported before by our group;[18] *ii)* as a guanidinium-modified acrylate monomer, used to form a polymer by UV initiation. The two Gu-based compounds have been applied in established advanced technologies to explore the possibility for phosphate recovery.

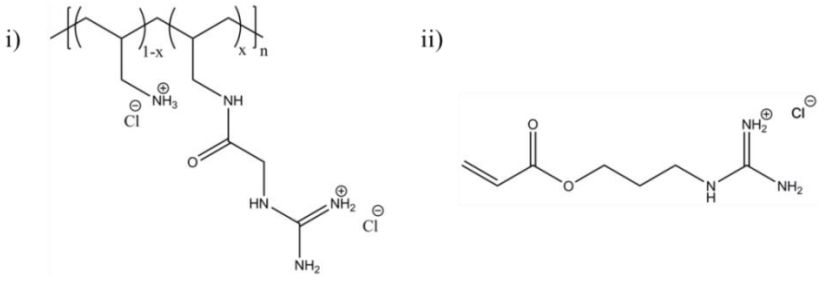

Figure 1.4 Chemical structures of Gu compounds used in this thesis: i) guanidinium functionalized poly(allylamine hydrochloride), x=0.3, (PAH-Gu); ii) guanidinium modified-acrylate monomer.

Materials and technologies for phosphate recovery

By now I made clear that the removal of phosphate from water comes with several challenges, mainly related to the pH-dependent speciation of phosphate and the presence of competing anions and cations. One approach is to start from established water treatment technologies and explore the integration of receptor groups to improve phosphate selectivity. The following paragraph will

explain the basic theory behind the advanced technologies used in this thesis. Several characteristics an advantages of each technology are briefly described as well as their combination with functionalized materials, in particular Gu-functionalized compounds.

Adsorption | Nanoparticles

Adsorption of target compounds to a surface is a straightforward and versatile process when it comes to water treatment. Over the last decades, the use of adsorption technology combined with functionalized particles has shown great potential, in terms of removal efficiency and being applicable for different wastewater streams.[19–21]

A good adsorbent is identified by, amongst others, the available specific adsorption area. Clearly, the smaller the size of the adsorbent material the larger the exposed area per weight or volume, and therefore the highest removal capacity is expected. For this reason, nano-sized adsorbents are considered to be highly promising. Iron oxide nanoparticles (Fe_3O_4 NPs) are of particular interest, not only because of their high-surface-area-to-volume ratio, but also for their magnetic properties, making easy separations possible by using external magnetic fields.[22–24]

Fe_3O_4 NPs can be used to treat phosphate-containing water with high yields.[25] This adsorption is dependent on the pH of the solution. Only under acidic conditions (pH < 7 = point of zero charge; PZC)[26] Fe_3O_4 NPs have a net positive charge and are, therefore, ready to adsorb phosphate anions. At higher pH values (pH >7) the surface charge of NPs turns to be negative, phosphate adsorption is unlikely to occur.

Extension of the pH-sensitive region of Fe_3O_4 NPs to adsorb phosphate can be expected by the introduction of functionalized polymers onto the NP surface and research in this direction has been extensively explored.[27–30] Therefore, the decoration of Fe_3O_4 NPs with PAH-Gu (Figure 1.4), our polyelectrolyte containing Gu receptor groups, has great potential due to the simplicity of the modification procedure, the adsorption properties, and most importantly, the removal of phosphate at higher pH-values. The latter is mainly related to the basicity of the

Gu groups that remain protonated at pH > 10[26] (because the pK_a of the Gu moiety is ~13)[18].

Electrodialysis | Anion-exchange membranes

Electrodialysis (ED) is an electrical-driven technology that can effectively remove ions from water by means of an applied electrical potential.[31] During ED, ions are transported from one compartment to another, allowing the recovery of compounds without any chemical regeneration process (which is, in contrast, necessary for adsorption technologies). Thus, the ED process shows specific advantages in terms of chemical consumption and operation time.[32]

The core of the ED process is the Ion-Exchange Membrane (IEM). Generally, a membrane is defined as a selective barrier that separates two phases/regions, allowing the exchange of matter and energy between the two regions. The separation process depends on specific features of the membrane, which includes the porosity, mechanical and thermal properties, permeability and chemical affinity.[33] In the case of an IEM, the selective barrier carries specific charged groups (fixed-charged groups) organized in a non-porous polymeric structure. The nature of the fixed-charged groups defines the type of IEM, generally categorized in two types: (1) *anion-exchange membranes* (AEMs) with fixed positively charged groups that permit only the exchange of anions (counter-ions) and the exclusion of cations (co-ions); and (2) *cation-exchange membranes* (CEMs) which contain fixed negatively charged groups and allow for the permeation of cations only.[33,34] The separation mechanism of an IEM is governed by the so-called Donnan exclusion principle[35], which defines the membrane capability to discriminate between anions and cations (*i.e.,* counter ions/co-ions). Figure 1.5 shows an illustration of the basic principle behind an anion-exchange membrane.

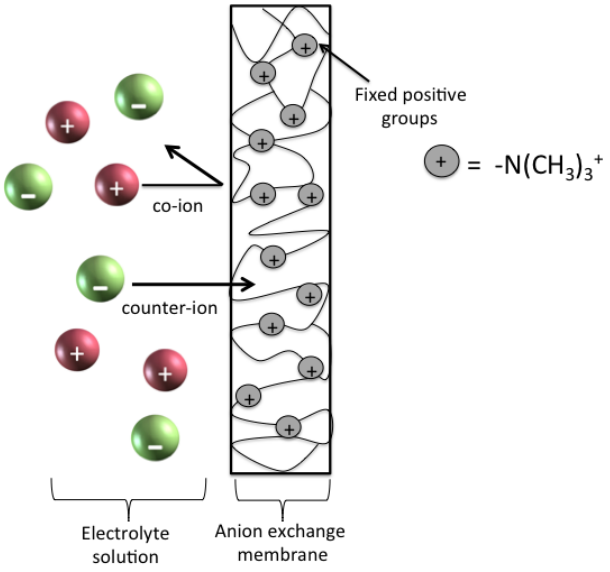

Figure 1.5 Illustration of the Donnan exclusion principle for an anion-exchange membrane having quaternary ammonium groups as fixed charges.

The mobility of counter-ions in the membrane depends mainly on the nature of the ion. Counter-ions with a small hydrated radius and high charge density would preferentially permeate the membrane compared to an ion with a large radius and low charge density.[36] For instance, the transport of phosphate, having a low diffusion coefficient and a high ionic radius (Table 1.1), would most likely be hindered by competing anions that are smaller and have a higher mobility like, *e.g.,* chloride.[36]

So far, research has been focused on new methodologies to change the membrane structure and to increase IEM selectivity. Often used are polyelectrolytes, which are generally deposited as polyelectrolyte multilayers on top of IEMs to improve the monovalent/divalent permeation selectivity. For example, the Bruening group[37] reported a CEM modified with PAH/PSS multilayers able to reach a K^+/Mg^{2+} selectivity as high as >1000; a similar multilayer configuration was also used by Mulyati *et al.*[38] to modify the surface of an AEM to obtain a Cl^-/SO_4^{2-} selectivity around 1.2 and improvements of membrane anti-fouling properties. Also used are monomers grafted onto membrane surfaces to reduce co-ion permeability[39] or to facilitate the

permeation of certain compounds, like urea[40]. While surface modification strategies have been used a lot to further tune the selectivity of IEMs, bulk modifications are still barely explored.[36] Modifications at the membrane surface are generally preferred because of their fast and easy realization. However, the deposition of thin films can present inhomogeneity, and the amount of deposited layers is limited by the available membrane surface area. While this can be solved to some extent by the addition of multiple layers on top of the membrane, the overall membrane thickness should not significantly increase to avoid undesired changes of some other membrane properties, *i.e.,* an increase of the membrane electrical resistance. Contrary to surface modifications, a change of the bulk structure can be complex and time-consuming. Nevertheless, the amount of selective functional groups can be adjusted during membrane formulation and the number of selective groups can be easily increased.

For these reasons in this thesis, Gu groups were organized in the bulk of the AEM, focussing on two different approaches: i) a Gu-functionalized polyelectrolyte as a component to prepare blended membranes and, ii) a Gu-acrylate monomer to form a membrane via UV polymerization.

Nanofiltration | Layer-by-Layer membranes

Nanofiltration (NF) is a pressure-driven technology that was introduced in the late 1980s, and was defined as "*a process intermediate between reverse osmosis and ultrafiltration that rejects molecules which have a size in the order of one nanometer*"[41]. In other words, NF combines the rejection of uncharged (> 1 nm) and charge molecules (mostly multivalent) based on size exclusion and charge repulsion. Thus, the rejection mechanism of NF membrane results from the combination of size exclusion effects and the Donnan exclusion mechanism.[42] As shown in Figure 1.1, phosphate at pH < pK_{a1} is present mostly as phosphoric acid (> 50%), an uncharged compound (radius < 1nm). Therefore, NF can be applied for the recovery of phosphoric acid from wastewater containing multivalent ions. Yet, commercially available NF membranes often show insufficient separation properties and/or low fluxes when it comes to fractionation of complex water streams.[43,44] The development of novel NF

membranes with improved selectivity is of interest to many scientists and in various fields of application.[45]

As mentioned previously, great attention has been given to the fast and low-cost procedures for membranes modification involving the use of polyelectrolytes.[46] Polyelectrolytes can be easily assembled in a layer on top of substrates having opposite charge. Polycations and polyanions can be alternatingly deposited onto (membrane) surfaces, by the so-called layer-by-layer (LbL) method, forming a polyelectrolyte multilayer. In literature, a lot of information can be found on the correlation between the LbL structures and their separation performance when applied as membranes.[47–49] Without going into details, we can generally state that LbLs deposited on porous membrane substrates can provide additional separation properties in terms of surface charge density, functionalities, and in their ability to reduce the pores size of membranes.

Modification of ultrafiltration (UF) hollow fiber membranes by LbL deposition can decrease the membrane porosity down to the NF scale, enabling such membranes to separate uncharged compounds (radius <1 nm) from multivalent ions.[47,49,50] Hollow fiber UF membranes modified with LbL, also known as LbL NF membranes to emphasize their separation features, are suitable candidates for the recovery of phosphoric acid from water containing multivalent ions. This is not only related to the separation mechanism (charged and size exclusion) but also to the geometry of the membrane. In more detail, all commercially available NFs are based on flat sheets and are generally arranged into spiral-wounded modules. This creates sometimes difficulties during the cleaning procedure due to the presence of the spacers which do limit the ion flux, therefore additional pre-treatments are often employed.[51] The geometry of hollow fiber LbL NF membranes allow high-pressure backwash approaches for cleaning purposes, and pre-treatments can be avoided, simplifying the overall separation process.[51] While LbL NF membranes show advantages in terms of expected performance (such as stability, permeability and retention performances)[50] and cost-reduction, their application for the recovery of phosphoric acid is still an unexplored area. NF technology has been largely employed in several industrial wastewater treatments plants and therefore the

use of LbL NF membranes for the phosphoric acid recovery can find an easy way for a direct industrial application.

Outline

The main objective of this thesis is to investigate Gu-based materials in combination with several advanced technologies for the removal of phosphate from water, at different pH conditions. Although the basic principles of the technologies used in this work are well known, as well as the chemical-physical properties of the Gu receptor groups, fundamental understanding of the precise interactions between Gu-based materials and phosphate in the presence of competing anions, is not straightforward. Especially, when the separation mechanism varies from electrical current, applied pressure and physical adsorption. The experimental chapters are organized in the following way.

In **Chapter 2** we investigated the phosphate adsorption properties of Fe_3O_4 NPs decorated with guanidinium modified-poly(allylamine hydrochloride) (PAH-Gu) containing 30% of Gu groups. The phosphate removal efficiency of the Fe_3O_4@PAH-Gu was investigated in a pH range between 5-10.

In **Chapter 3** a new polymeric blend was formulated by using the components of a commercial available AEM and different weight fractions of our PAH-Gu. The observed membrane surface and electrochemical impedance properties were correlated with the membrane phosphate-interaction properties in the presence of monovalent phosphate and divalent sulphate containing solution at pH = 5.

These modified AEMs were also investigated in **Chapter 4**. Here the loading of Gu groups was maximized by the use of a new Gu-acrylate monomer, synthesized in our lab, as a building block for the AEM fabrication. The resulting fully Gu-loaded AEM was employed for the electrodialysis of phosphate from a model dairy wastewater solution at pH = 7.

The removal of phosphate as phosphoric acid (pH = 1 < pK_{a1}) is described in **Chapter 5**. Three different polyelectrolytes (PAH-Gu, PAH and Polydiallyldimethylammonium chloride PDADMAC, a permanently charged

polycation) were employed in the membrane modification. The properties of LbL NF membranes were investigated in detail and correlated with the removal performance of phosphoric acid from a real leachate sewage sludge ash solution.

Finally, in **Chapter 6** the obtained knowledge from the previous chapters is summarized, and presented together with some future challenges and perspectives for the removal of phosphate from wastewater streams.

A schematic summary of all technologies and the employed materials used in each chapter given in Figure 1.6. Each technology is linked to the pH at which their effectiveness towards phosphate removal was maximized. In addition, the phosphate speciation mainly present at the indicated pH values is also displayed.

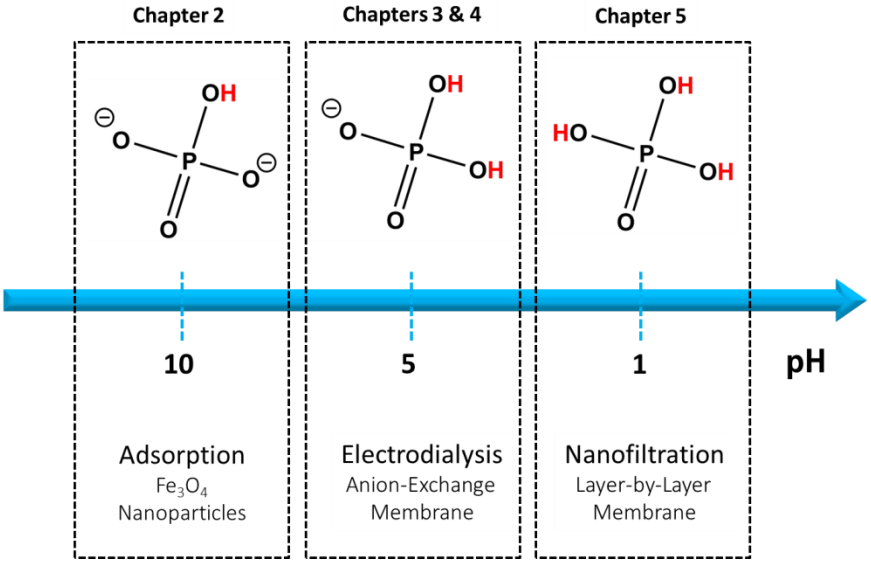

Figure 1.6 Schematic overview of the technologies and materials used in this dissertation, combined with the chosen pH and related phosphate speciation.

References

(1) FAO. *Current World Fertilizer Trends and Outlook to 2016*; 2012.

(2) Jasinski, S. M. Phosphate Rock. *U.S. Bur. Mines, Miner. Resour. Progr.* 2017, No. 703.

(3) European Commission. *On the Review of the List of Critical Raw Materials for the EU and the Implementation of the Raw Materials Initiative*; 2014.

(4) Schröder, J.; Cordell, D.; Smit, A. L.; Rosemarin, A. *Sustainable Use of Phosphorus*; 2010.

(5) Hudson, J. J.; Taylor, W. D.; Schindler, D. W. Phosphate Concentrations in Lakes. *Nature* 2000, *400*, 55–56.

(6) Conley, D. J. H. Paerl, W. Howarth, R. W. Boesch, D. F. Seitzinger, S. P. Havens, K. E.Lancelot, C. Likens, G. E. Controlling Eutrophication: Nitrogen and Phosphorus. *Science* 2009, *323*, 1014–1015.

(7) Van Vuuren, D. P.; Bouwman, A. F.; Beusen, A. H. W. Phosphorus Demand for the 1970-2100 Period: A Scenario Analysis of Resource Depletion. *Glob. Environ. Chang.* 2010, *20*, 428–439.

(8) Desmidt, E.; Ghyselbrecht, K.; Zhang, Y.; Pinoy, L.; Van der Bruggen, B.; Verstraete, W.; Rabaey, K.; Meesschaert, B. Global Phosphorus Scarcity and Full- Scale P-Recovery Techniques: A Review. *Crit. Rev. Environ. Sci. Technol.* 2015, *45*, 336–384.

(9) Egle, L.; Rechberger, H.; Krampe, J.; Zessner, M. Phosphorus Recovery from Municipal Wastewater: An Integrated Comparative Technological, Environmental and Economic Assessment of P Recovery Technologies. *Sci. Total Environ.* 2016, *571*, 522–542.

(10) Huang, H.; Yang, J.; Li, D. Recovery and Removal of Ammonia–nitrogen and Phosphate from Swine Wastewater by Internal Recycling of Struvite Chlorination Product. *Bioresour. Technol.* 2014, *172*, 253–259.

(11) Guaya, D.; Hermassi, M.; Valderrama, C.; Farran, A.; Cortina, J. L. Recovery of Ammonium and Phosphate from Treated Urban Wastewater by Using Potassium Clinoptilolite Impregnated Hydrated Metal Oxides as N-P-K Fertilizer. *J. Environ. Chem. Eng.* 2016, *4* (3), 3519–3526.

(12) Sarapulova, V.; Nevakshenova, E.; Pismenskaya, N.; Dammak, L.; Nikonenko, V. Unusual Concentration Dependence of Ion-Exchange Membrane Conductivity in Ampholyte-Containing Solutions: Effect of

Ampholyte Nature. *J. Memb. Sci.* 2015, *479*, 28–38.

(13) Tran, A. T. K.; Zhang, Y.; Lin, J.; Mondal, P.; Ye, W.; Meesschaert, B.; Pinoy, L.; Van der Bruggen, B. Phosphate Pre-Concentration from Municipal Wastewater by Selectrodialysis: Effect of Competing Components. *Sep. Purif. Technol.* 2015, *141*, 38–47.

(14) Lide, D. R. CRC Handbook of Chemistry and Physics, 84th Edition, 2003-2004. *Handb. Chem. Phys.* 2003, *53*, 2616.

(15) Wang, Z.-G.; Lv, N.; Bi, W.-Z.; Zhang, J.-L.; Ni, J.-Z. Development of the Affinity Materials for Phosphorylated Proteins/Peptides Enrichment in Phosphoproteomics Analysis. *ACS Appl. Mater. Interfaces* 2015, *7*, 8377–8392.

(16) Pantos, A.; Tsogas, I.; Paleos, C. M. Guanidinium Group: A Versatile Moiety Inducing Transport and Multicompartmentalization in Complementary Membranes. *Biochim. Biophys. Acta - Biomembr.* 2008, *1778*, 811–823.

(17) Paltrinieri, L.; Wang, M.; Sachdeva, S.; Besseling, N. A. M.; Sudholter, E. J. R.; de Smet, L. C. P. M. Fe3O4 Nanoparticles Coated with a Guanidinium-Functionalized Polyelectrolyte Extend the pH Range for Phosphate Binding. *J. Mater. Chem. A* 2017, *5*, 18476–18485.

(18) Cao, Z.; Gordiichuk, P. I.; Loos, K.; Sudholter, E. J. R.; de Smet, L. C. P. M. The Effect of Guanidinium Functionalization on the Structural Properties and Anion Affinity of Polyelectrolyte Multilayers. *Soft Matter* 2016, *12*, 1496–1505.

(19) Sen Gupta, S.; Bhattacharyya, K. G. Kinetics of Adsorption of Metal Ions on Inorganic Materials: A Review. *Adv. Colloid Interface Sci.* 2011, *162* (1–2), 39–58.

(20) Pan, B.; Han, F.; Nie, G.; Wu, B.; He, K.; Lu, L. New Strategy to Enhance Phosphate Removal from Water by Hydrous Manganese Oxide. *Environ. Sci. Technol.* 2014, *48*, 5101–5107.

(21) Blaney, L. M.; Cinar, S.; SenGupta, A. K. Hybrid Anion Exchanger for Trace Phosphate Removal from Water and Wastewater. *Water Res.* 2007, *41* (7), 1603–1613.

(22) Mandel, K.; Drenkova-Tuhtan, A.; Hutter, F.; Gellermann, C.; Steinmetz, H.; Sextl, G. Layered Double Hydroxide Ion Exchangers on Superparamagnetic Microparticles for Recovery of Phosphate from

Waste Water. *J. Mater. Chem. A* 2013, *1*, 1840–1848.

(23) Wilfert, P.; Suresh Kumar, P.; Korving, L.; Witkamp, G.-J.; Van Loosdrecht, M. C. M. The Relevance of Phosphorus and Iron Chemistry to the Recovery of Phosphorus from Wastewater: A Review. *Environ. Sci. Technol.* 2015, *49*, 9400–9414.

(24) Yavuz, C. T.; Mayo, J. T.; Yu, W. W.; Prakash, A.; Falkner, J. C.; Yean, S.; Cong, L.; Shipley, H. J.; Kan, A.; Tomson, M.; Natelson, D.; Colvin, V. L. Low-Field Magnetic Separation of Monodisperse Fe3O4 Nanocrystal. *Science* 2006, *314*, 964–967.

(25) Yoon, S. Y.; Lee, C. G.; Park, J. A.; Kim, J. H.; Kim, S. B.; Lee, S. H.; Choi, J. W. Kinetic, Equilibrium and Thermodynamic Studies for Phosphate Adsorption to Magnetic Iron Oxide Nanoparticles. *Chem. Eng. J.* 2014, *236*, 341–347.

(26) L. Paltrinieri, M.; Wang, S. Sachdeva, N. A. M. Besseling, E. J. S. and L. de S. Fe3O4 Nanoparticles Coated with a Guanidinium-Functionalized Polyelectrolyte Extend the pH Range for Phosphate Binding. *J. Mater. Chem. A* 2017, *5*, 18476–18485.

(27) Li, Y.; Xie, Q.; Hu, Q.; Li, C.; Huang, Z.; Yang, X.; Guo, H. Surface Modification of Hollow Magnetic Fe3O4@NH2-MIL-101(Fe) Derived from Metal-Organic Frameworks for Enhanced Selective Removal of Phosphates from Aqueous Solution. *Sci. Rep.* 2016, *6*, 1–11.

(28) Abo Markeb, A.; Alonso, A.; Dorado, A. D.; Sánchez, A.; Font, X. Phosphate Removal and Recovery from Water Using Nanocomposite of Immobilized Magnetite Nanoparticles on Cationic Polymer. *Environ. Technol.* 2016, *3330*, 1–14.

(29) Zhang, J.; Han, J.; Wang, M.; Guo, R. Fe3O4/PANI/MnO2 Core-Shell Hybrids as Advanced Adsorbents for Heavy Metal Ions. *J. Mater. Chem. A* 2017, *5*, 4058–4066.

(30) Tran, D. N. H.; Kabiri, S.; Wang, L.; Losic, D. Engineered Graphene–nanoparticle Aerogel Composites for Efficient Removal of Phosphate from Water. *J. Mater. Chem. A.* 2015, *3*, 6844–6852.

(31) Bernardes, A. M.; Rodrigues, M. a S. Electrodialysis and Water Reuse. *Electrodialysis Water Reuse Nov. Approaches* 2014, 63–75.

(32) Strathmann, H. Electrodialysis, a Mature Technology with a Multitude of New Applications. *Desalination* 2010, *264*, 268–288.

(33) Sata, T. *Ion Exchange Membranes Preparation, Characterization, Modification and Application*; RSC, 2004.

(34) Strathmann, H. Ion-Exchange Membrane Processes in Water Treatment. *Sustain. Sci. Eng. Elsevier* 2010, *2*, 141–199.

(35) Tanaka, Y. *Ion Exchange Membranes: Fundamentals and Application*; 2015.

(36) Luo, T.; Abdu, S.; Wessling, M. Selectivity of Ion Exchange Membranes: A Review. *J. Memb. Sci.* 2018, *555*, 429–454.

(37) White, N.; Misovich, M.; Yaroshchuk, A.; Bruening, M. L. Coating of Nafion Membranes with Polyelectrolyte Multilayers to Achieve High Monovalent/divalent Cation Electrodialysis Selectivities. *ACS Appl. Mater. Interfaces* 2015, *7* (12), 6620–6628.

(38) Kim, H.-C. High-Rate MIEX Filtration for Simultaneous Removal of Phosphorus and Membrane Foulants from Secondary Effluent. *Water Res.* 2015, *69*, 40–50.

(39) Kim, D. H.; Park, H. S.; Seo, S. J.; Park, J. S.; Moon, S. H.; Choi, Y. W.; Jiong, Y. S.; Kim, D. H.; Kang, M. S. Facile Surface Modification of Anion-Exchange Membranes for Improvement of Diffusion Dialysis Performance. *J. Colloid Interface Sci.* 2014, *416*, 19–24.

(40) Lee, W.; Saito, K.; Furusaki, S.; Sugo, T.; Makuuchi, K. Design of Urea-Permeable Anion-Exchange Membrane by Radiation-Induced Graft Polymerization. *J. Memb. Sci.* 1993, *81*, 295–306.

(41) Eriksson, P. Nanofiltration Extends the Range of Membrane Filtration. *Environ. Prog.* 1988, *7* (1), 58–62.

(42) Hilal, N.; Al-Zoubi, H.; Darwish, N. A.; Mohammad, A. W.; Abu Arabi, M. A Comprehensive Review of Nanofiltration Membranes: Treatment, Pretreatment, Modelling, and Atomic Force Microscopy. *Desalination* 2004, *170* (3), 281–308.

(43) Van der Bruggen, B.; Manttari, M.; Nystrom, M. Drawbacks of Applying Nanofiltration and How to Avoid Them: A Review. *Sep. Purif. Technol.* 2008, *63* (2), 251–263.

(44) Niewersch, C. Nanofiltration for Phosphorus Recycling from Sewage Sludge. *Ph.D. Diss. RWTH Aachen Univ.* 2013, 158.

(45) Mohammad, A. W.; Teow, Y. H.; Ang, W. L.; Chung, Y. T.; Oatley-Radcliffe, D. L.; Hilal, N. Nanofiltration Membranes Review: Recent Advances and

Future Prospects. *Desalination* 2015, *356*, 226–254.

(46) Menne, D.; Kamp, J.; Erik Wong, J.; Wessling, M. Precise Tuning of Salt Retention of Backwashable Polyelectrolyte Multilayer Hollow Fiber Nanofiltration Membranes. *J. Memb. Sci.* 2016, *499*, 396–405.

(47) de Grooth, J.; Haakmeester, B.; Wever, C.; Potreck, J.; de Vos, W. M.; Nijmeijer, K. Long Term Physical and Chemical Stability of Polyelectrolyte Multilayer Membranes. *J. Memb. Sci.* 2015, *489*, 153–159.

(48) Cheng, W.; Liu, C.; Tong, T.; Epsztein, R.; Sun, M.; Verduzco, R.; Ma, J.; Elimelech, M. Selective Removal of Divalent Cations by Polyelectrolyte Multilayer Nanofiltration Membrane: Role of Polyelectrolyte Charge, Ion Size, and Ionic Strength. *J. Memb. Sci.* 2018, *559*, 98–106.

(49) de Grooth, J.; Oborný, R.; Potreck, J.; Nijmeijer, K.; de Vos, W. M. The Role of Ionic Strength and Odd-Even Effects on the Properties of Polyelectrolyte Multilayer Nanofiltration Membranes. *J. Memb. Sci.* 2015, *475*, 311–319.

(50) Menne, D. Layer-by-Layer Design of Nanofiltration Membranes. *Layer-by-Layer Des. Nanofiltration Membr.* 2017.

(51) Vrouwenvelder, J. S.; Graf von der Schulenburg, D. A.; Kruithof, J. C.; Johns, M. L.; van Loosdrecht, M. C. M. Biofouling of Spiral-Wound Nanofiltration and Reverse Osmosis Membranes: A Feed Spacer Problem. *Water Res.* 2009, *43* (3), 583–594.

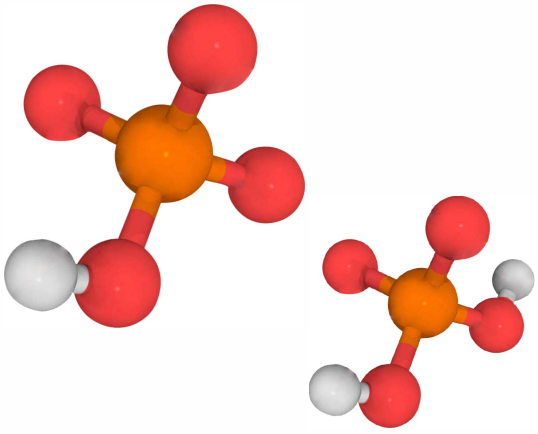

CHAPTER 2

Fe_3O_4 nanoparticles coated with a guanidinium-functionalized polyelectrolyte extend the pH range for phosphate binding

In this work commercially available Fe_3O_4 NPs were coated with polyallylamine hydrochloride (PAH) and PAH functionalized with guanidinium groups (PAH-Gu) for investigating the phosphate adsorption properties at alkaline conditions. The coating can be prepared easily and fast and results in Fe_3O_4 NPs with improved properties related to phosphate binding and colloidal stability. At a low initial phosphate concentration (2 mg/L), the novel Fe_3O_4@PAH-Gu material was able to remove phosphate rather independently of the pH condition (4.0, 3.6 and 3.7 mg/g at pH = 5, 8 and 10, respectively), whereas for the uncoated Fe_3O_4 NPs the amount of adsorbed phosphate drops with > 75% upon changing from acidic to alkaline conditions (0.84 mg/g at pH = 10). At alkaline conditions, the fastest adsorption was observed for Fe_3O_4@PAH-Gu followed by Fe_3O_4@PAH and Fe_3O_4, respectively. This can be related to the additional interaction forces due to the presence of primary amine groups (in PAH and PAH-Gu) and Gu groups (in PAH-Gu only) in coatings. This work will stimulate the design and preparation of functionalized polyelectrolytes for an extended area of applications, especially for the selective removal of target compounds from wastewater.

The content of this chapter has been published in:

Laura Paltrinieri, Min Wang, Sumit Sachdeva, Nicolaas A.M. Besseling, Ernst J.R. Sudhölter, Louis C.P.M. de Smet, *Journal of Material Chemistry A.*,5, **2017**, 18476-18458. (Front Cover Journal)

Introduction

The uncontrolled discharge of phosphate-containing products as present in aqueous streams from agricultural and cosmetic sectors[1,2] has increased eutrophication processes, *i.e.,* the rapid growth of aquatic algae in lakes and rivers.[3,4] These processes contribute to an unbalanced aquatic ecology and to a decrease of the water quality. Phosphate is therefore considered to be one of the most critical contaminants present in wastewater. Many countries have set a standard for the discharge of phosphate into water.[5] For instance, the European Union recently regulated a maximum value of 0.07 µg P/L for rivers and 100 µg P/L for lakes to reduce the risk of eutrophication.[6] In order to meet such strict requirements and to manage the high phosphorus demand at the same time,[7,8] the recovery of phosphorus from phosphate-contaminated aqueous media has been recognized as a challenging key strategy. For this purpose different technologies have been developed, including biological treatments,[9] membrane-based processes,[10,11] crystallization,[12,13] flotation,[14] and adsorption-based processes.[15] From this list of well-known techniques, adsorption processes have a high potential. This is mainly related to the low operational costs, high efficiency, low energy consumption and its versatility to be applicable in different wastewater sources.[15]

Among candidates for phosphate adsorbents, iron oxides are considered to be highly promising.[16] This is because of (1) their high selectivity to bind phosphate in the presence of competing anions, and (2) their easy introduction in municipal wastewater treatment plants (WWTs). Furthermore, a good adsorbent is identified by, amongst others, the available specific adsorption area. For this reason, a lot of attention is now paid to develop new nano-sized adsorbents, because of their high-surface-area-to-volume ratio.[17] Nanoparticles of iron oxide (Fe_3O_4 NPs) fulfil these conditions and even possess magnetic properties, making easy separations possible by using external magnetic fields.[18] Phosphate adsorption onto Fe_3O_4 NPs occurs through an inner-sphere complex, due to the presence of surface hydroxyl groups.[16,19] When the pH is lower than the point of zero charge (PZC), the surface of the iron oxide nanoparticles is positively charged which promotes binding and surface adsorption of phosphate anions. The lower the pH, the more charge on the surface and therefore a higher binding capacity.[20,21] However, at lower pH values the amount of phosphate anions decreases, as they are converted to phosphoric acid.[22] This becomes significant below pH < pK_{a1} = 2.1. The pH of water streams in WWTPs is typically 6-8,[23,24] *i.e.*, around the

PZC of the Fe_3O_4 NPs. At such pH values, the surface charge is slightly positive, neutral or slightly negative, which has a large negative impact on the phosphate anion binding capacity. In the mentioned pH range, the phosphates are monoanionic and partly di anionic (pK_{a2} = 7.2).[22] Moreover, at this pH range the NPs aggregate to precipitate, due to the decreased inter-particle electrostatic repulsions. Thus, for phosphate separation processes at pH values around the PZC of Fe_3O_4 NPs, there is room for improvement. For that reason, different types of chemical surface modification have been applied by the attachment of specific ligands, including amino groups,[25] metal organic frameworks (MOFs),[19] polymers,[26,27] layered double hydroxides (LDHs)[28] and graphene.[29] These examples illustrate well the effectiveness of surface functionalization in terms of controlling the affinity for a specific target species. Yet, it would be interesting to further employ these surface modification strategies in order to extend the use of iron oxide nanoparticles for phosphate anion binding at higher pH values, where unmodified iron oxide is otherwise less effective.

Receptor-functionalized polyelectrolytes (PEs) can bind to surfaces of opposite charge[30–32] and can contribute to nanoparticle stabilization,[33] while the receptor groups introduce selectivity for binding certain targets. Recent advances in this direction resulted in the availability of polyelectrolytes that were functionalized with, *e.g.*, biotin, fluorescent probes and guanidinium groups to address chelating and the selective capture of His-tagged proteins,[34,35] biosensing,[36] finger-mark visualization,[37] and ion selectivity,[38] respectively. Interestingly, polyelectrolyte functionalization and the subsequent modification of NPs do not require complicated chemical steps and can be performed fast in aqueous media.

In the current study, we present the concept of a simple surface modification of commercially available Fe_3O_4 NPs using polyelectrolytes functionalized with phosphate-receptors. For the receptor we have chosen the guanidinium moiety, which is able to coordinate phosphate ions in a wide range of pH values.[39,40] The Gu-functionalized polyelectrolyte was applied to modify the Fe_3O_4 NPs. The thus-obtained NPs are characterized in terms of morphology, thermal stability and surface properties. The effect of the pH on the phosphate adsorption is investigated in detail, as well as the kinetics of the process. The obtained results were compared with those of bare Fe_3O_4 NPs as well as Fe_3O_4 NPs coated with a non-functionalized polyelectrolyte.

Materials and Methods

Materials

Poly(allyamine hydrochloride) (PAH, M_w ~15,000 Da) guanidine acetic acid (GAA, 99%), 1-ethyl-3-(3-dimethylaminopropyl) carbodiimide (EDC, commercial grade) and N-hydroxysuccinimide (NHS, 98%) were purchased from Sigma-Aldrich and used without any further purification. 1 M of HCl and 1 M of NaOH (analytical reagent grade, obtained from Fluka, Germany) were used for pH adjustments. Sodium dihydrogen phosphate ($NaH_2PO_4.H_2O$, Acros Organic) was used in phosphate removal experiments. Commercial iron oxide nanoparticles (Fe_3O_4 NPs, 8 nm in diameter as determined by TEM) were purchased as a 3 wt % acidic aqueous dispersion from PlasmaChem GmbH (Germany) without any organic stabilizer. All aqueous solutions were prepared using Milli-Q water (Milli-Q Ultrapure Water System, Millipore 22 μm).

Preparation of PAH-Gu, Fe_3O_4@PAH and Fe_3O_4@PAH-Gu

PAH-Gu (Scheme 2.1, top right) was obtained by the reaction of GAA with part of the amino groups of PAH following the procedure published earlier by our group.[38] ^{1}H-NMR was used to confirm the chemical structure (Supporting Information, Figure S2.1) and to calculate the degree of amino group functionalization by guanidinium (Gu) moieties; it was found to be ~30 % for the batch used in the current work. In order to study the effect of present Gu groups, non-functionalized PAH was used as a reference.

Next, the Fe_3O_4 NPs were modified with PAH or PAH-Gu via the following procedure.[41] Aqueous solutions of PAH and PAH-Gu (2.5 g/L) were prepared by sonication using a probe sonicator (Cole-Parmer CPX750, 30% power, 750 watts) during 20 min and simultaneously cooling by placing the tube in ice. Similarly, a Fe_3O_4 NPs suspension (0.5 g/L) was prepared in MilliQ water and sonicated under the same conditions. After sonication, the pH of all solutions was adjusted to 9.5 by the addition of drops of concentrated HCl or NaOH (1 M). At this pH value the Fe_3O_4 NPs have a negative surface charge, while the polyelectrolytes are positively charged. The Fe_3O_4 NPs suspension was added drop-wise to the polyelectrolyte solutions and stirred during 24 h at room temperature (RT) to ensure complete adsorption at the Fe_3O_4 NPs surface. The functionalized NPs were separated from the excess of PEs by three cycles of centrifugation, decantation and washing using 3 cycles (Heraeus instrument D-

37520 Osterode, Germany) at 17,000 rpm (20 min at 20 °C). The product was finally re-dispersed in 40 mL of MilliQ water to maintain the initial concentration and then sonicated to obtain uniform solutions of Fe_3O_4@PAH and Fe_3O_4@PAH-Gu, respectively. A schematic overview of the coating procedure and the different types of Fe_3O_4 NPs are presented in Scheme 2.1.

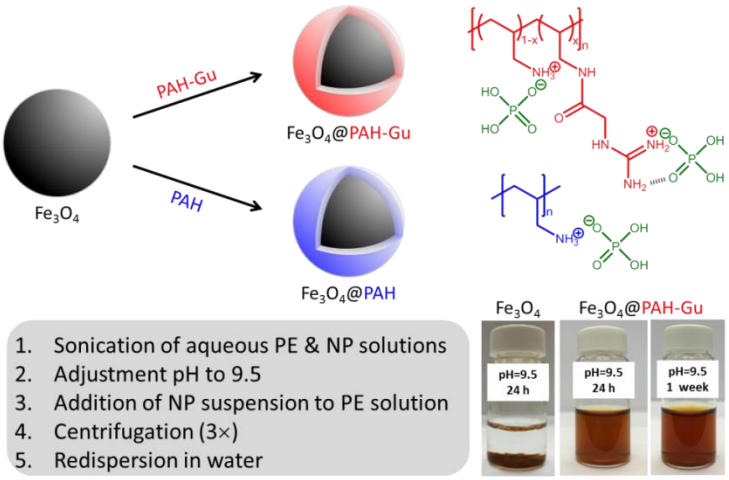

Scheme 2.1 A schematic showing the three different NPs (top left) and the interactions between amino-phosphate and guanidinium-phosphate, shown for the monovalent anion (top right). Brief, stepwise description of the coating process of Fe_3O_4 NPs with (functionalized) polyelectrolytes (in the grey-colored box, bottom left), and pictures of different NP suspensions at pH = 9.5 (bottom right).

Characterizations

^{1}H NMR spectrum of the PAH-Gu polymer was obtained using a Bruker AVANCE 400 NMR spectrometer with D_2O as solvent. Modified NPs were studied with Fourier Transform InfraRed (Nicolet 8700 FT-IR Spectrometer) by mixing the NPs with KBr and pressing pellets. The spectra range of FT-IR was from 4000 to 500 cm^{-1} with a resolution of 4 cm^{-1}. X-ray Photoelectron Spectroscopy (XPS, Thermo Fisher Scientific, K-Alpha model) was used to determine the atomic composition of the modified NP surfaces. In more detail, a monochromatic Al Kα

X-ray source was used with a spot size of 400 µm at a pressure of 10^{-7} mbar. A constant pass energy of 200 eV for the survey spectra and 50 eV for the detailed high-resolution spectra was used. The flood gun was turned on during the measurement to compensate for potential charging of the surface. The peak position was adjusted

based on the internal standard C1s peak at 284.8 eV, with an accuracy of ±0.05 eV. Avantage processing software was used to analyze all spectra.

ThermoGravimetric Analysis (TGA) measurements were performed with a Thermal Analysis (TA) Instruments from RT to 550 °C at a heating rate of 10 °C/min under continuous air purging. The size and morphology of the unmodified and modified NPs were studied by a Transmittance Electron Microscope (TEM, Jeol Jem-1400 Plus, USA) operated at 120 kV. A holey carbon support film (200 meshes, Quantifoil®) was dipped into the NPs-containing solution and then dried at room temperature overnight. TEM images were analyzed by using Image J software and the mean size values of each NPs system was calculated based on 20 separate determined diameters.

The hydrodynamic diameter (D_h) of NPs was determined at 25 °C by Dynamic Light Scattering (DLS) using a Zetasizer Nano ZS900 (Malvern, UK). The instrument was operated at a backscattering angle of 173° with a laser beam with a wavelength of 633 nm. The same instrument was used to measure ζ-potential at 25 °C for all samples and measurements were performed in triplicate. To this end, an aqueous suspension of Fe_3O_4 NPs (0.5 mg/mL) was prepared by adding 167 µL of the original concentrated NP solution into 10 mL MilliQ water. Samples for ζ-potential measurements were made by diluting 80 µL of the above-prepared NPs suspension (0.5 mg/mL) to 10 mL using MilliQ water. The solution was sonicated by probe sonicator (30%, 750 Watts, cooling in an ice bath, 6 min) to break the existing aggregates. In the last step, the pH was adjusted to the desired values by using 1 M NaOH and 1 M HCl. The same procedure was used to determine the ζ-potential of all NPs systems, as well for the pure PEs (PAH and PAH-Gu), where a solution of 0.5 mg/mL in MilliQ water was used. All the measurements were done 5 min after the sonication procedure to minimize possible differences due to colloidal instability.

Batch adsorption experiments

Phosphate adsorption experiments were performed for Fe_3O_4, Fe_3O_4@PAH, Fe_3O_4@PAH-Gu NPs. All desired phosphate solutions, including the standard known concentration of phosphate for calibration measurements, were prepared by diluting a stock solution (1000 mg/L of NaH_2PO_4 in 250 mL). The phosphate adsorption was studied as a function of time starting with an initial phosphate concentration of 2 mg/L, taken from the stock solution, and an adsorbent solution of 0.5 g/L in 30 mL. The

adsorbed amount was deduced from the reduction of the phosphate concentration according to the work optimized by Yoon *et al.*[42] In contrast to other studies,[42,43] we have decided to keep a fixed initial adsorbent concentration and to focus on the effect of pH in the adsorption process. In this study the pH conditions have a great impact not only on the stability of the NPs suspension and their surface charges, but also on the type of speciation of phosphate involved in the adsorption process. Before starting the experiments, the pH of both adsorbent solution and phosphate solution was adjusted to the desired value. Phosphate was added to NP solutions, followed by stirring at RT for 24 h. Samples were taken at different times and centrifuged (Eppendorf AG, Germany) at 13,000 rpm for 1 h. The phosphate adsorption efficiency was measured through UV-vis spectroscopy (UVIKON XL, Beun De Ronde) by using the ascorbic acid method.[44,45]

Results and Discussion

Given the importance of electrostatic interactions in the surface modification using polyelectrolytes,[33,46] we first present and discuss the ζ-potential data of the PAH and PAH-Gu separately, and Fe_3O_4 NPs as such. Next, FTIR, XPS, TGA and TEM data is given to characterize the bare and modified Fe_3O_4 NPs. The phosphate sorption studies of the NPs are split in two different topics: pH effects and a kinetic study.

ζ-potential investigation of PEs and Fe_3O_4 NPs

Figure 2.1 shows that the ζ-potential of bare Fe_3O_4 NPs as well as for PAH and PAH-Gu in aqueous solutions as a function of the solution pH. It is observed that for all cases the zeta potential becomes less positive with increasing pH value.

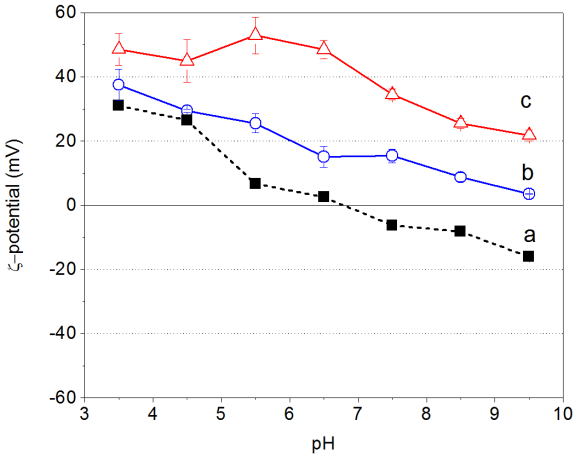

Figure 2.1 ζ-potential as a function of solution pH for (a) an aqueous suspension of unmodified Fe_3O_4 NPs (0.5 g/L, black squares), (b) an aqueous solution of 0.5 g PAH/L (blue circles), and (c) an aqueous solution of 0.5 g PAH-Gu/L (red squares).

For the unmodified Fe_3O_4 NPs the zeta potential changes from a positive ($Fe\text{-}OH_2^+$ groups are in excess) to a negative ($Fe\text{-}O^-$ groups are in excess) sign around pH 7, reflecting the PZC as has been reported in literature.[47]Differently, PAH and PAH-Gu polyelectrolyte solutions remain positive over the whole investigated pH region. PAH-Gu shows a higher positive surface charge compared to the (not functionalized) PAH. This can easily be understood in terms of their respective pK_a values, which is 8-9 for the primary amine of PAH[48,49]and 13 for the guanidinium group present in PAH-Gu.[50] Furthermore, for PAH-Gu the ζ-potential data at pH < 6.5 shows a plateau behaviour, which is absent for PAH and the Fe_3O_4 NPs in the studied pH window. This indicates that the overall surface-charge density of PAH-Gu at pH < 6 is constant. This difference may be associated to the differences in PZC of the respective materials, including a shift of the apparent dissociation constant of PAH (p$K_{a\,(app)}$) due to local changes of the electrostatic environment[51] and, for PAH-Gu a saturation of chargeable groups at acidic pH conditions.

To conclude this part, the results show that within the pH window of ~7 to ~9.5 the unmodified Fe_3O_4 NPs are negatively charged, while both PEs are positively charged. In addition, from literature it is known that Fe_3O_4 NPs are covered maximally by weak polyelectrolytes (like PAH) if the pH is similar to the polyelectrolyte pK_a value.[52] We have therefore chosen to perform our experiments at a pH of 9.5, the pK_a value of PAH, for both PAH and PAH-Gu modifications.

Characterization of coated Fe_3O_4 NPs

The FTIR spectra of bare Fe_3O_4 NPs, Fe_3O_4@PAH, Fe_3O_4@PAH-Gu as well as those of the pure PEs are shown in Figure 2.2. The data show that the modified NPs are covered with PAH or PAH-Gu. In all cases a large contribution between 3404 and 3017 cm^{-1} is observed, which can be associated with the O–H bond stretching. Its broadness originates from H-bridge formation with physically adsorbed water, which was used as a solvent and can be entrapped between the polymeric chains (see also TEM and TGA analysis; *vide intra*).[53] The presence of iron oxide is confirmed by the observed stretching of Fe–O at 577 cm^{-1} in the cases of Fe_3O_4 NPs (black), Fe_3O_4@PAH (pink) and Fe_3O_4@PAH-Gu (green).[54] The success of the PAH coating process becomes clear from the typical peaks at 2918 cm^{-1} and 2850 cm^{-1} that are associated to C–C stretching and two peaks at 1575 cm^{-1} and 1541 cm^{-1} of the C–N and N–H bending, which compare well with bands present in the FTIR spectrum of PAH (blue). Finally, the bands at 1604 cm^{-1} and 1506 cm^{-1} can be assigned to the bending vibration related to the amino group.[55]

Likewise, in agreement with the bare PAH-Gu spectrum (red), the coating of NPs with PAH-Gu is confirmed by the presence of two peaks at 2918 cm^{-1} and 2850 cm^{-1} for C-C stretching, a peak 1631 cm^{-1} assigned to the stretching of C=N bond from the Gu group and a peak at 1537 cm^{-1} of the N-H bending.[38,56] It should be mentioned that in both Fe_3O_4@PAH and Fe_3O_4@PAH-Gu, the position of characteristic peaks of primary amine and amide bond shift to some extent with respect to the corresponding bare PEs. This can be explained by interaction between iron ions and charged groups of PEs and the formation of amino compexes.[57]

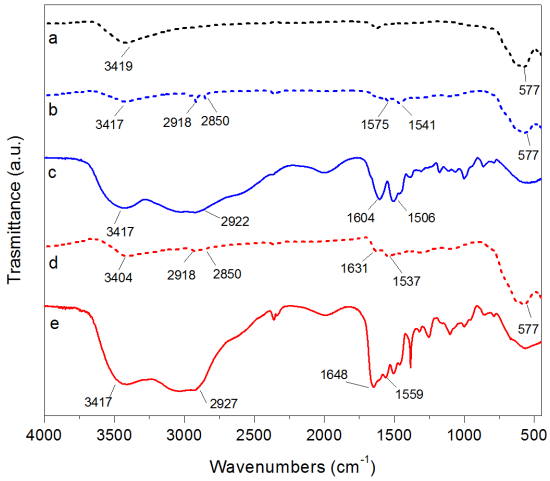

Figure 2.2 FTIR spectra of (a) bare Fe_3O_4 NPs (black, dashed), (b) Fe_3O_4@PAH (blue, dashed), (c) PAH polymer (blue, solid), (d) Fe_3O_4@PAH-Gu (red, dashed), (e) PAH-Gu polymer (red, solid).

XPS was used to further map the surface chemistry of NPs before and after modification (Table 2.1). The successful NPs functionalization is evident from the N/Fe ratio that increases upon the preparation of the coating from 0 (bare Fe_3O_4 NPs) to 0.30 and 0.60 for Fe_3O_4@PAH and Fe_3O_4@PAH-Gu, respectively. Moreover, with respect to the bare NPs, the C/Fe ratio is higher in the presence of the PEs and this can be associated to the alkyl polymer backbone and methylene groups in the side chains. Oxygen is measured in all samples, which is can be related to OH groups present at the Fe_3O_4 NPs surface and the C=O in the Fe_3O_4@PAH-Gu system.

Carbon is detected in Fe_3O_4 as well, and this can be related to hydrocarbon surface contamination often observed on surfaces.[58] While the C/Fe ratio of Fe_3O_4@PAH is higher than the one of Fe_3O_4@PAH-Gu, the contribution of carbon contamination makes it hard to draw any conclusions on the degree of coverage based on C/Fe. An indication of the amount of PEs bound to the NPs surface can be deduced from the N/Fe ratio. Taking into account a degree of Gu group substitution of 30 % (see chemical structure reported in Scheme 2.1), the calculated amount of N per repeating unit in PAH-Gu is 1.9 times higher than for PAH (considering 0.3×4(N) + 0.7×1(N)). From XPS analysis a ratio of (0.60/0.30) = 2 was observed, indicating that a similar amount of both polyelectrolytes is bound to the NPs.

Table 2.1 XPS elemental ratios of bare and polyelectrolyte-modified NPs.

	C/Fe	O/Fe	N/Fe
Fe_3O_4	1.67	1.64	-
Fe_3O_4@PAH	6.02	4.69	0.30
Fe_3O_4@PAH-Gu	2.44	2.52	0.60

Additional evidence of the changed surface chemistry of the NPs was obtained from TGA analysis (Figure 2.3). Bare Fe_3O_4 (line a) showed hardly any weight loss for the indicated temperature range (residual of 98%). This small weight reduction can be attributed to the loss of water physically adsorbed at NPs surface combined with the loss of hydrate condensed groups at temperatures higher than 100 °C.[59] Differently, two degradation steps clearly appear for Fe_3O_4@PAH (line b) and Fe_3O_4@PAH-Gu (line c). The first step at 30-120 °C refers to the loss of water. The presence of water is due both to physically adsorbed water at modified NPs particles surfaces and to the hydration shell of ions (ammonium and chlorine) of the polyelectrolytes chains, which is found to be almost the same for both systems (in accordance with FTIR spectra). The second weight loss at 250-400 °C can be related to the breakdown of the PEs. The residuals of Fe_3O_4@PAH and Fe_3O_4@PAH-Gu overall drop to 87% and 84%, respectively. The weight drop can be attributed to the bonded polyelectrolyte at the NP surface. The difference between the drop for Fe_3O_4@PAH and Fe_3O_4@PAH-Gu is due to the Gu modification, considering that the average mass per monomer unit is larger for PAH-Gu than for PAH.

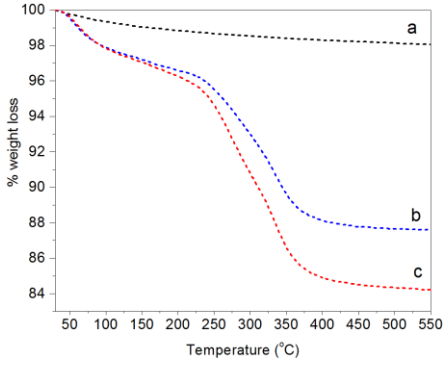

Figure 2.3 TGA curves showing the fractional weight loss of (a) bare Fe_3O_4 (black), (b) Fe_3O_4@PAH (blue), (c) Fe_3O_4@PAH-Gu (red).

The morphology of NPs was examined with TEM; images of Fe_3O_4 NPs, Fe_3O_4@PAH, and Fe_3O_4@PAH-Gu are shown in Figure 2.4. In the absence of a polymeric coating, Fe_3O_4 NPs show a typical spherical shape.[60] The same spherical shape can also be observed in images (b) and (c); in addition, a smooth and transparent layer is seen around the NPs, likely due to the presence of the polymeric coating (c).[61] Table 2.2 lists the mean diameters of the NPs as obtained from TEM analysis. Fe_3O_4 NPs were found to have a diameter of 8 ± 2 nm, confirming the specifications given by the supplier. The diameters of Fe_3O_4@PAH and Fe_3O_4@PAH-Gu, including the additional smooth layer, are 11 ± 2 nm, indicating an adsorbed polyelectrolyte layer thickness of ca. 3 nm.[62]

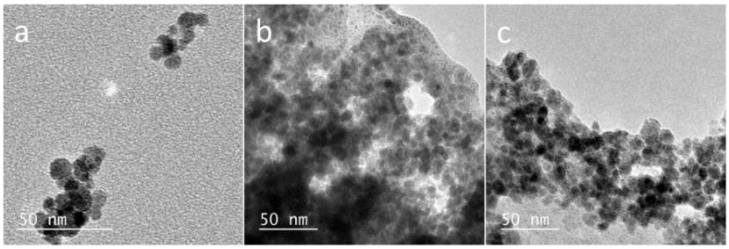

Figure 2.4 TEM images of (a) bare Fe_3O_4, (b) Fe_3O_4@PAH NPs, (c) Fe_3O_4@PAH-Gu NPs.

Table 2.2 summarizes the size data of our investigated NPs as obtained from TEM and DLS (hydrodynamic diameters) and zeta potential measurements. At pH = 9.5, the unmodified and polyelectrolyte-modified NPs have hydrodynamic diameters much larger than the sizes of single particles observed by TEM. This is due to the agglomeration of these NPs in solution. This agglomeration is reduced for the NPs modified with a polyelectrolyte: 86 nm observed for the unmodified Fe_3O_4 NPs, compared to 65 nm and 41 nm for the Fe_3O_4@PAH and Fe_3O_4@PAH-Gu, respectively. The difference is related to the colloidal stability which is increased for polyelectrolyte-modified NPs, thus preventing aggregation.[29,30,58] We also observed a stable suspension for both PE-modified NPs, while the unmodified Fe_3O_4 NPs precipitated after 24 h, at pH = 9.5. (Scheme 2.1, bottom left and Supporting Information Figs. S2.2 and S2.3).

The stability of the NP suspension at pH 9.5 as observed from DLS was confirmed with ζ-potential measurements (final column in Table 2.2). The ζ-potential of bare Fe_3O_4 NPs is –16.7 mV, which changes sign upon modification to +26 and +32 mV for the PAH and PAH-Gu coatings, respectively. The positive ζ-potential values strongly confirm the presence of polycations at NPs surface.[61] Moreover, it should be noticed

that the magnitute of the surface potential reflects the level of electrostatic repulsion between NPs. A higher zeta potential, gives more repulsion and therefore a more stable suspension. From these zeta potential measurements it is now clearly understood why the Fe_3O_4 NPs start to agglomerate, while the PE-modified NPs are still stable. From the results obtained, it is evident that the addition of a Gu moiety altered the Fe_3O_4 properties; this is not only in terms of reversing the surface charge to a positive value (as it is for Gu-free PAH), but also by increasing the absolute charge density, leading to an increased colloidal stability. Again, this can be explained by the differences in PZC between the amino-PAH and Gu moiety.[65] Images of the NPs suspension at different pH values after 24h and Fe_3O_4@PAH-Gu after 1 week are reported in Figs. S2.2 and S2.3 in the Supporting Information.

Table 2.2 Sizes and zeta potentials of our investigated NPs.

Type of NPs	TEM diameter	D_h (nm)[a,b]	ζ-potential (mV)[b]
Fe_3O_4	8 ± 2	86 (PDI 0.7)	-16.7 ± 0.7
Fe_3O_4@PAH	11 ± 2	65 (PDI 0.5)	26.0 ± 1.2
Fe_3O_4@PAH-Gu	11 ± 2	41 (PDI 0.3)	32.0 ± 1.7

[a] From DLS; [b] pH = 9.5

Phosphate adsorption: effect of pH

In order to map the pH-dependency of phosphate adsorption at our (modified) NPs, three pH values were chosen for the adsorption experiments: pH = 5, pH = 8 and pH = 10. Within the pH window from 5 to 10 the degree of dissociation of phosphoric acid decreases accordingly, thus at pH = 5 $H_2PO_4^-$ is predominant, at pH = 8 $H_2PO_4^-$ and HPO_4^{2-} are equally present, while at pH = 10 mostly HPO_4^{2-} can be expected.[22] The adsorption experiments were performed at a fixed concentration of 0.5 g (modified) NP/L and 2 mg NaH_2PO_4/L; thus there is always an excess of adsorbent. Figure 2.5 shows the results of the phosphate adsorption as function of pH for Fe_3O_4 NPs, Fe_3O_4@PAH and Fe_3O_4@PAH-Gu after equilibration during 24h at RT and was determined by the ascorbic acid/UV method.[45]

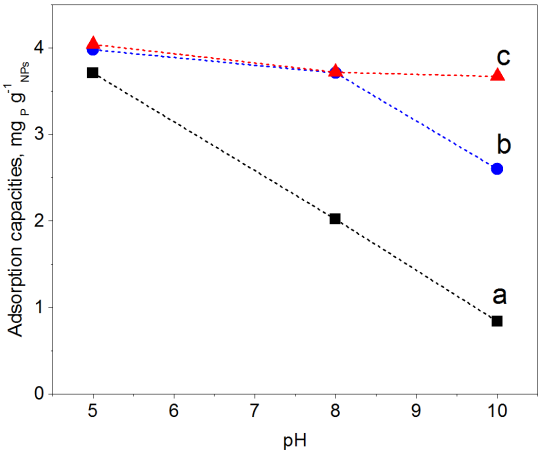

Figure 2.5 Amount of phosphate adsorbed ($mg_{PO4\text{-}P}/g_{NPs}$) after equilibration during 24h at RT for (a) Fe_3O_4 NPs (black), (b) Fe_3O_4@PAH (blue), (c) Fe_3O_4@PAH-Gu NPs (red). The dashed lines serve as a guide to the eye. Measurements were done in triplicate and all errors were found to be lower the 0.05%.

At pH = 5 all NPs show a similar amount of phosphate adsorbed. At these conditions, the phosphate is predominantly present as the monoanion (pK_{a1} = 2.1 and pK_{a2} = 7.2) and the Fe_3O_4 NPs are below their PZC and therefore will have a net positive charge. For the PAH and PAH-Gu modified Fe_3O_4 NPs also the net surface charge is positive. The phosphate mono-anion will therefore bind, to the unmodified Fe_3O_4 NPs, as reported in literature.[19] Since there is hardly any extra effect of the PAH and PAH-Gu modifications on the adsorbed phosphate amount it is suggested that the Fe_3O_4 NPs surface is determining the adsorption under these conditions. Despite the positive charges at the Fe_3O_4 NP surface, the stability of the PE coating at this pH condition can be related to the presence of neutral amino groups in the PAH and PAH-Gu chains. It is likely that both positive charges and neutral hydroxyl groups present on the Fe_3O_4 NP surface interact with the unprotonated amino groups of PEs.

Increasing the pH from 5 to 8 and 10 shows a reduction of phosphate adsorption by the unmodified Fe_3O_4 NPs of 46% and 77%, respectively. At these pH values, the surface charge has turned to negative value and adsorption of phosphate monoanion or di anion is suppressed by electrostatic repulsion. Yet, at pH = 10 the phosphate adsorption is not reduced to 0; instead, it is still 0.85 mg/g. Thus, the adsorption of phosphate onto iron-oxide surfaces occurs both by electrostatic interactions, absent at pH = 10, and by a chemisorption process.[66,67] The latter involves the formation of Fe-O-

P bonds through ligand exchange reaction between OH groups at NP surface and phosphate oxygen. This may explain the P adsorption detected at pH = 10.

A very clear difference is observed for pH = 8 and pH = 10, if PAH or PAH-Gu are present. The amount of adsorbed phosphate is now higher than observed for unmodified Fe_3O_4 NPs and more or less similar to the adsorbed amount observed at pH 5 for the three investigated NPs. Clearly, the reduced affinity of the (unmodified) Fe_3O_4 NPs surface at pH = 8 is compensated nearly completely by the PAH and PAH-Gu modifications. For pH = 10, it is seen that the phosphate adsorption for PAH is decreased compared to the PAH-Gu modified surface. For PAH-Gu still a phosphate adsorption of 3.67 mg/g is observed. This difference reflects nicely the difference of the pK_a values of PAH (8-9) and PAH-Gu (Gu groups pK_a = 13) due to which the latter has a higher positive charge density at pH = 10.

In addition, the increased stability of the colloidal suspension may contribute to the uptake of phosphate, because a higher contact area is available compared to the aggregated state. Increased colloidal stability is supported by ζ-potential measurements: at pH = 10 a zeta potential of +21.1 mV and +3.8 mV is found for Fe_3O_4@PAH-Gu and Fe_3O_4@PAH, respectively. As mentioned previously, adsorption of phosphate slightly decreases upon increasing pH. At alkaline conditions, OH^- groups are abundant and they might compete with phosphate in the adsorption process.[19,28]

Effect of contact time, adsorption kinetics

Phosphate adsorption was monitored as the decrease of the phosphate concentration over time at pH values of 5, 8 and 10 (Figure 2.6). At pH = 5 all NPs show a very fast adsorption behaviour. Equilibrium was reached within 5 min. Due to our experimental set up we are not able to monitor accurately the adsorption increase within that time frame. However, it is clear that at pH = 8 and pH = 10 the adsorption process is slower, making monitoring of the adsorption increase possible. Equilibrium is now obtained within 1h. This is similar to observations made by others.[29,68] The monitored increase of phosphate adsorption as function of time can be nicely fitted with a pseudo-second-order kinetic equation.[70]

$$\frac{dq_t}{dt} = k_2 (q_e - q_t)^2 \qquad (2.1)$$

where q_e is the amount of phosphate adsorbed at the equilibrium, q_t is the phosphate adsorbed during the time t and k_2 is the pseudo-second-order rate constant. The equation describes the increased amount of adsorbed phosphate in time as function of the difference between q_e and q_t. Although other kinetic models are reported in literature to describe adsorption processes (*i.e.*, pseudo-first-order, Elovich), the pseudo-second-order is widely recognized as the best model particularly at low initial solution concentration.[71] The fit is shown for the linearized form of eq. 2.1, which is given by eq. 2.2 (fitting plots are reported in Figure S2.4, while the non-linear curve fitting parameters are listed in Table S2.1):

$$\frac{t}{q_t} = \frac{1}{k_2 q_e^2} + \frac{1}{q_e} t \qquad (2.2)$$

In Table 2.3 the results of the fitting q_e and k_2 are compiled together with the calculated value of the initial rate at $t \rightarrow 0$ (h in mg/g/min),

$$h = k_2 q_e^2 \qquad (2.3)$$

and the coefficient of determination (R^2), reflecting the quality of the fit.

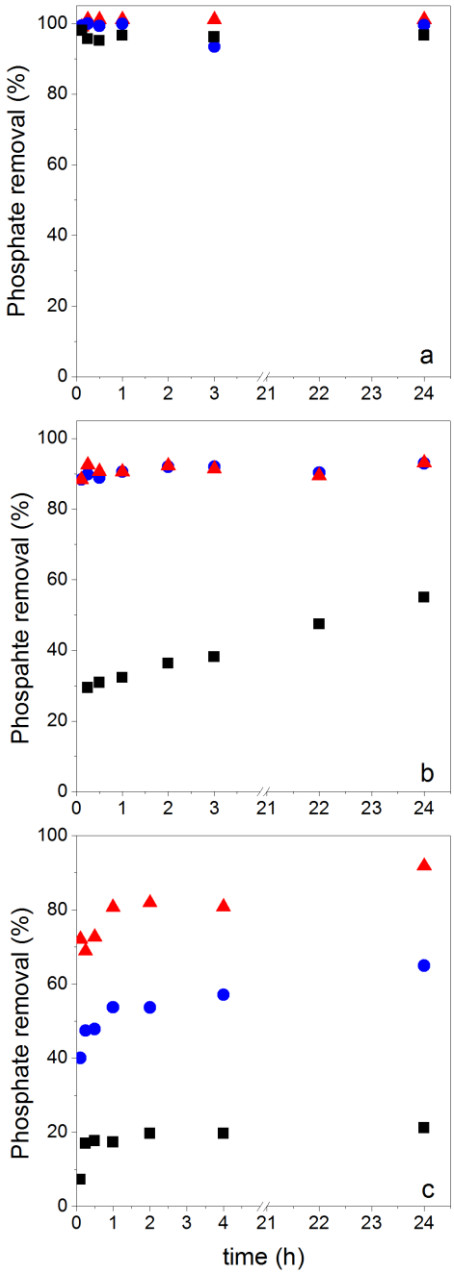

Figure 2.6 Phosphate adsorption in time at (a) pH = 5, (b) pH = 8 and (c) pH = 10. Data were collected for bare Fe_3O_4 (black squares), Fe_3O_4@PAH (blue spheres) and Fe_3O_4@PAH-Gu (red triangle). Measurements were done in triplicate and all errors were found to be lower the 0.05%.

As said, under conditions of pH = 5 the process is too fast for monitoring adsorption increase data and therefore we only report here experimental values of q_e. For conditions at pH = 8 and 10 the monitored data of increased adsorption fitted very well with the second-order kinetic equation as deduced from the obtained coefficients of determination close to unity. The observed second order behaviour is a net result of the combination of adsorption and desorption processes occurring simultaneously.[71] While it is realized that the pseudo-second-order kinetics is often ascribed to a double-site interaction[42,70], we point to the derivation of the pseudo-second-order rate equation from the Langmuir kinetics as described by Liu and Shen.[71] Double-site adsorption would be a correct physical interpretation, only if the binding sites involved can move independently over the surface and need to be close in order to bind one phosphate. However, the work of Liu and Shen[71] demonstrates that the combination of the simultaneous adsorption and desorption process also leads to apparent second-order kinetics when the total amount of binding sites per unit of volume is larger than both the initial concentration of adsorbate and the inverse of the equilibrium binding constant. The fact that we observe second-order kinetics implies that these conditions are met.

No physical meaning can be attributed to k_2,[72] but the values for the initial a desorption rate (h) and the amount of adsorbed phosphate at equilibrium (q_e) can be interpreted. At both pH = 8 and 10, h increases from Fe_3O_4 to Fe_3O_4@PAH to Fe_3O_4@PAH-Gu. At pH = 10, q_e also increases in this order. Differently, at pH = 8 Fe_3O_4@PAH to Fe_3O_4@PAH-Gu a similar order of q_e is observed, that is higher than Fe_3O_4. It is suggested therefore that at pH = 8 the adsorption capacity for the two investigated polyelectrolytes is similar. The difference between the two polyelectrolytes becomes visible at pH = 10, in favour for Fe_3O_4@PAH-Gu, showing a pH-independent value of q_e. This is likely due to the differences in pK_a of the PAH and PAH-Gu PEs; the Gu moieties are still protonated at pH = 10, while for PAH the degree of protonation is reduced compared to the situation at pH 8. From the results shown in Table 2.3, it is also clearly seen that at pH = 8 and pH = 10 the phosphate adsorption is dictated by the present PEs and that the dominant role observed for Fe_3O_4 at pH = 5 in now tempered. An additional difference between Fe_3O_4@PAH to Fe_3O_4@PAH-Gu (not shown here) is the selectivity for phosphate binding for the Gu containing polyelectrolytes, which we have shown in our previous study.[38]

Table 2.3 Kinetic model parameters (q_e - mg/g; k_2 – mg/g/min; h – mg/g/min; R^2) obtained from pseudo-second-order model fitting to experimental time-dependent adsorption data for phosphate on Fe_3O_4, Fe_3O_4@PAH, and Fe_3O_4@PAH-Gu at pH = 5, 8 and 10. For completeness the q_e values experimentally determined at 24h (q_e *exp mg/g*) are included.

	pH 5	**pH 8**					**pH 10**				
	q_e exp	**q_e exp**	**q_e**	**k_2**	**h**	**R^2**	**q_e exp**	**q_e**	**k_2**	**h**	**R^2**
Fe_3O_4	3.7	2.0	1.5	0.28	0.63	0.99	0.84	0.82	0.15	0.10	0.99
Fe_3O_4@ PAH	4.0	3.7	3.7	0.52	7.0	0.99	2.6	2.3	0.13	0.68	0.99
Fe_3O_4@ PAH-Gu	4.0	3.7	3.6	2.2	29	0.99	3.7	3.7	0.20	2.1	0.99

Conclusions

While several nanomaterials have been investigated for the removal of phosphate from aqueous (wastewater) streams, it remains a challenge to develop new systems operable under alkaline conditions. This study shows the results of a simple surface modification method applied to commercially available Fe_3O_4 NPs by using a polyelectrolyte functionalized with guanidimium groups for phosphate anion binding. The surface modification was confirmed by thermal, morphological and surface analysis measurements (FTIR, XPS and ζ-potential analysis). The PAH-Gu modified Fe_3O_4 NPs showed good phosphate adsorption (3.7 mg/g) up to pH = 10, where the phosphate adsorption ability of the PAH-modified Fe_3O_4 (2.3 mg/g) and unmodified Fe_3O_4 (0.82 mg/g) is reduced. The initial rate of phosphate adsorption increased from 2.1 to 29 mg/g/min for PAH-Gu coated Fe_3O_4 NP upon switching the pH from 10 to 8. The observed second-order adsorption kinetics can be explained as the net result of simultaneous adsorption and desorption processes at the NPs surface. At the same time colloidal stability was enhanced upon coating the NPs with polyelectrolytes.

Supporting Information

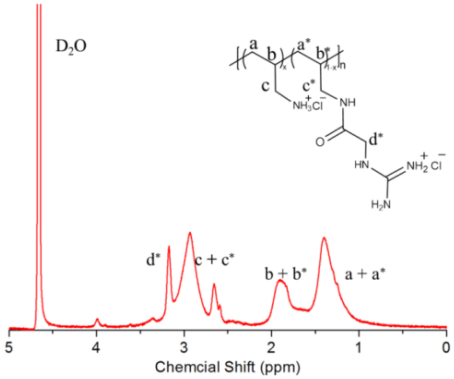

Figure S2.1 H^1-NMR spectrum of polyallylamine hydrochloride functionalized with Gu moiety.

The synthesis was done according to the work of Cao *et al.*[38] The substitution degree of PAH-Gu was 30% as estimated by the H^1-NMR spectrum and the reaction yield was found to be 39% after dialysis.

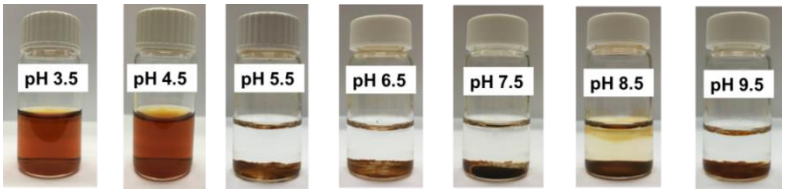

Figure S2.2 Images of vials containing an aqueous Fe_3O_4 suspension (0.5 g/L) taken 24 h after preparation at pH range from 3.5 to 9.5.

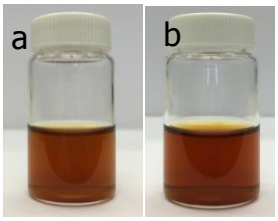

Figure S2.3 Images of a suspension of 0.5 g/L of Fe_3O_4@PAH-Gu at pH 9.5 taken after a) 24h and b) one week. Compared to Fe_3O_4 NPs at pH 9.5, Fe_3O_4@PAH-Gu maintains a stable colloidal suspension for months.

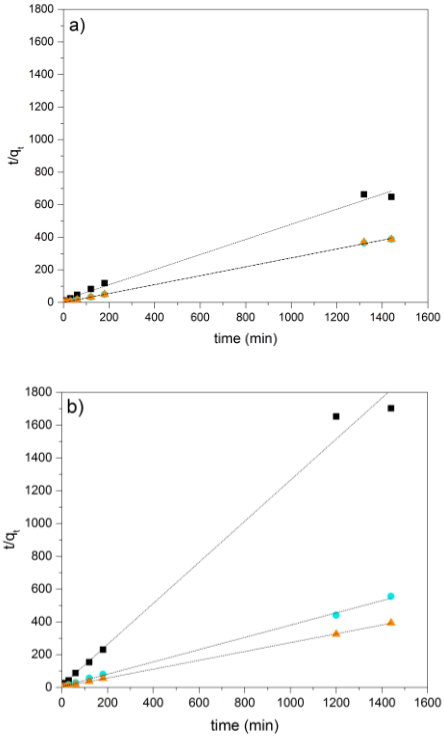

Figure S2.4 Pseudo second-order linear fitting curves Fe_3O_4 (black) Fe_3O_4@PAH (light blue) and Fe_3O_4@PAH-Gu (orange) at a) pH 8 and b) pH 10.

Table S2.1 Pseudo second-order non-linear curve fitting parameters, based on equation 1.

	pH 8			**pH 10**		
	q_e mg g^{-1}	**k_2 mg g^{-1} min^{-1}**	**R^2**	**q_e mg g^{-1}**	**k_2 mg g^{-1} min^{-1}**	**R^2**
Fe_3O_4	2.00	0.0196	0.867	0.814	0.175	0.919
Fe_3O_4@PAH	3.65	1.03	0.999	2.45	0.083	0.949
Fe_3O_4@PAH-Gu	3.66	1.45	0.998	3.42	0.126	0.958

References

(1) FAO. *Current World Fertilizer Trends and Outlook to 2016*; 2012.

(2) Schröder, J.; Cordell, D.; Smit, A. L.; Rosemarin, A. *Sustainable Use of Phosphorus*; 2010.

(3) Hudson, J. J.; Taylor, W. D.; Schindler, D. W. Phosphate Concentrations in Lakes. *Nature* 2000, *400*, 55–56.

(4) Conley, D. J. H. Paerl, W. Howarth, R. W. Boesch, D. F. Seitzinger, S. P. Havens, K. E.Lancelot, C. Likens, G. E. Controlling Eutrophication: Nitrogen and Phosphorus. *Science* 2009, *323*, 1014–1015.

(5) Levlin, E.; Löwén, M.; Stark, K. Hultman, B. Effects of Phosphorus Recovery Requirements on Swedish Sludge Management. *Water Sci. Technol.* 2002, *46*, 435–440.

(6) European Commission. *Common Implementation Strategy for the Water Framework Directive (200/60/EC)*; 2009.

(7) Desmidt, E.; Ghyselbrecht, K.; Zhang, Y.; Pinoy, L.; Van der Bruggen, B.; Verstraete, W.; Rabaey, K.; Meesschaert, B. Global Phosphorus Scarcity and Full- Scale P-Recovery Techniques: A Review. *Crit. Rev. Environ. Sci. Technol.* 2015, *45*, 336–384.

(8) Van Vuuren, D. P.; Bouwman, A. F.; Beusen, A. H. W. Phosphorus Demand for the 1970-2100 Period: A Scenario Analysis of Resource Depletion. *Glob. Environ. Chang.* 2010, *20*, 428–439.

(9) Mino, T.; Van Loosdrecht, M. C. M.; Heijnen, J. J. Microbiology and Biochemistry of the Enhanced Biological Phosphate Removal Process. *Water Res.* 1998, *32*, 3193–3207.

(10) Zhang, Y.; Van der Bruggen, B.; Pinoy, L.; Meesschaert, B. Separation of Nutrient Ions and Organic Compounds from Salts in RO Concentrates by Standard and Monovalent Selective Ion-Exchange Membranes Used in Electrodialysis. *J. Memb. Sci.* 2009, *332*, 104–112.

(11) Hong, S. U.; Ouyang, L.; Bruening, M. L. Recovery of Phosphate Using Multilayer Polyelectrolyte Nanofiltration Membranes. *J. Memb. Sci.* 2009, *327*, 2–5.

(12) Tran, Anh T KTran, A. T. K., Zhang, Y., De Corte, D., Hannes, J. B., Ye, W., Mondal, P., Van Der Bruggen, B. P-Recovery as Calcium Phosphate from Wastewater Using an Integrated Selectrodialysis/crystallization Process. *J. Clean. Prod.* 2014, *77*, 140–151.

(13) Hao, X.; Wang, C.; Van Loosdrecht, M. C. M.; Hu, Y. Looking beyond Struvite for

P-Recovery. *Environ. Sci. Technol.* 2013, *47*, 4965–4966.

(14) Karageorgiou, K.; Paschalis, M.; Anastassakis, G. N. Removal of Phosphate Species from Solution by Adsorption onto Calcite Used as Natural Adsorbent. *J. Hazard. Mater.* 2007, *139* (3), 447–452.

(15) Sen Gupta, S.; Bhattacharyya, K. G. Kinetics of Adsorption of Metal Ions on Inorganic Materials: A Review. *Adv. Colloid Interface Sci.* 2011, *162* (1–2), 39–58.

(16) Wilfert, P.; Suresh Kumar, P.; Korving, L.; Witkamp, G.-J.; Van Loosdrecht, M. C. M. The Relevance of Phosphorus and Iron Chemistry to the Recovery of Phosphorus from Wastewater: A Review. *Environ. Sci. Technol.* 2015, *49*, 9400–9414.

(17) Yavuz, C. T.; Mayo, J. T.; Yu, W. W.; Prakash, A.; Falkner, J. C.; Yean, S.; Cong, L.; Shipley, H. J.; Kan, A.; Tomson, M.; Natelson, D.; Colvin, V. L. Low-Field Magnetic Separation of Monodisperse Fe3O4 Nanocrystal. *Science* 2006, *314*, 964–967.

(18) Mandel, K.; Drenkova-Tuhtan, A.; Hutter, F.; Gellermann, C.; Steinmetz, H.; Sextl, G. Layered Double Hydroxide Ion Exchangers on Superparamagnetic Microparticles for Recovery of Phosphate from Waste Water. *J. Mater. Chem. A* 2013, *1*, 1840–1848.

(19) Li, Y.; Xie, Q.; Hu, Q.; Li, C.; Huang, Z.; Yang, X.; Guo, H. Surface Modification of Hollow Magnetic Fe3O4@NH2-MIL-101(Fe) Derived from Metal-Organic Frameworks for Enhanced Selective Removal of Phosphates from Aqueous Solution. *Sci. Rep.* 2016, *6*, 1–11.

(20) Qu, H.; Caruntu, D.; Liu, H.; O'Connor, C. J. Water-Dispersible Iron Oxide Magnetic Nanoparticles with Versatile Surface Functionalities. *Langmuir* 2011, *27* (6), 2271–2278.

(21) Sun, Y. P.; Li, X. Q.; Zhang, W. X.; Wang, H. P. A Method for the Preparation of Stable Dispersion of Zero-Valent Iron Nanoparticles. *Colloids Surfaces A Physicochem. Eng. Asp.* 2007, *308*, 60–66.

(22) Sarapulova, V.; Nevakshenova, E.; Pismenskaya, N.; Dammak, L.; Nikonenko, V. Unusual Concentration Dependence of Ion-Exchange Membrane Conductivity in Ampholyte-Containing Solutions: Effect of Ampholyte Nature. *J. Memb. Sci.* 2015, *479*, 28–38.

(23) Huang, H.; Yang, J.; Li, D. Recovery and Removal of Ammonia–nitrogen and Phosphate from Swine Wastewater by Internal Recycling of Struvite Chlorination Product. *Bioresour. Technol.* 2014, *172*, 253–259.

(24) Guaya, D.; Hermassi, M.; Valderrama, C.; Farran, A.; Cortina, J. L. Recovery of Ammonium and Phosphate from Treated Urban Wastewater by Using Potassium Clinoptilolite Impregnated Hydrated Metal Oxides as N-P-K Fertilizer. *J. Environ. Chem. Eng.* 2016, *4* (3), 3519–3526.

(25) Wang, H.; Xu, X.; Fei, R.; Gao, B. Removal of Phosphate and Chromium (VI) from Liquids by Amine-Crosslinked Nano-Fe3O4 Biosorbent Derived from Corn Straw. *RSC Adv.* 2016, *6*, 47237–47248.

(26) Abo Markeb, A.; Alonso, A.; Dorado, A. D.; Sánchez, A.; Font, X. Phosphate Removal and Recovery from Water Using Nanocomposite of Immobilized Magnetite Nanoparticles on Cationic Polymer. *Environ. Technol.* 2016, *3330*, 1–14.

(27) Zhang, J.; Han, J.; Wang, M.; Guo, R. Fe3O4/PANI/MnO2 Core-Shell Hybrids as Advanced Adsorbents for Heavy Metal Ions. *J. Mater. Chem. A* 2017, *5*, 4058–4066.

(28) Yan, L. guo; Yang, K.; Shan, R.; Yan, T.; Wei, J.; Yu, S. jun; Yu, H. qin; Du, B. Kinetic, Isotherm and Thermodynamic Investigations of Phosphate Adsorption onto Core-Shell Fe3O4@LDHs Composites with Easy Magnetic Separation Assistance. *J. Colloid Interface Sci.* 2015, *448*, 508–516.

(29) Tran, D. N. H.; Kabiri, S.; Wang, L.; Losic, D. Engineered Graphene–nanoparticle Aerogel Composites for Efficient Removal of Phosphate from Water. *J. Mater. Chem. A.* 2015, *3*, 6844–6852.

(30) Richardson, J. J.; Bjornmalm, M.; Caruso, F. Technology-Driven Layer-by-Layer Assembly of Nanofilms. *Science* 2015, *348*, 1–11.

(31) Femmer, R.; Mani, A.; Wessling, M. Ion Transport through Electrolyte/polyelectrolyte Multi-Layers. *Sci. Rep.* 2015, *5*, 1–12.

(32) Caruso, F. Nanoengineering of Particle Surfaces. *Adv. Mater.* 2001, *13* (1), 11–22.

(33) Choi, Y.-W.; Lee, H.; Song, Y.; Sohn, D. Colloidal Stability of Iron Oxide Nanoparticles with Multivalent Polymer Surfactants. *J. Colloid Interface Sci.* 2015, *443* (0), 8–12.

(34) Wijeratne, S.; Bruening, M. L.; Baker, G. L. Layer-by-Layer Assembly of Thick, Cu2+ Chelating Films. *Langmuir* 2013, *29*, 12720–12729.

(35) Wijeratne, S.; Liu, W.; Dong, J.; Ning, W.; Ratnayake, N. D.; Walker, K. D.; Bruening, M. L. Layer-by-Layer Deposition with Polymers Containing Nitrilotriacetate, A Convenient Route to Fabricate Metal- and Protein-Binding Films. *Appl. Mater. Interfaces* 2016, *8*, 10164–10173.

(36) Ullien, D.; Harmsma, P. J.; Abdulla, S. M. C.; de Boer, B. M.; Bosma, D.; Sudhölter, E. J. R.; de Smet, L. C. P. M.; Jager, W. F. Protein Detection on Biotin-Derivatized Polyallylamine by Optical Microring Resonators. *Opt. Express* 2014, *22*, 16585–16594.

(37) Van der Mee, L.; Chow, E. S. Y.; de Smet, L. C. P. M.; de Puit, M.; Sudholter, E. J. R.; Jager, W. F. Fluorescent Polyelectrolyte for the Visualization of Fingermarks. *Anal. Methods* 2015, *7*, 10121–10124.

(38) Cao, Z.; Gordiichuk, P. I.; Loos, K.; Sudholter, E. J. R.; de Smet, L. C. P. M. The Effect of Guanidinium Functionalization on the Structural Properties and Anion Affinity of Polyelectrolyte Multilayers. *Soft Matter* 2016, *12*, 1496–1505.

(39) Schug, K.; Lindner, W. Noncovalent Binding between Guanidinium and Anionic Groups: Focus on Biological- and Synthetic-Based Arginine/guanidinium Interactions with Phosph[on]ate and Sulf[on]ate Residues. *Chem. Rev.* 2005, *105*, 67–114.

(40) Xiong, Z.; Chen, Y.; Zhang, L.; Ren, J.; Zhang, Q.; Ye, M.; Zhang, W.; Zou, H. Facile Synthesis of Guanidyl-Functionalized Magnetic Polymer Microspheres for Tunable and Specific Capture of Global Phosphopeptides or Only Multiphosphopeptides. *ACS Appl. Mater. Interfaces* 2014, *6*, 22743–22750.

(41) Caruso, F. Hollow Capsule Processing through Colloidal Templating and Self-Assembly. *Chem. - A Eur. J.* 2000, *6* (3), 413–419.

(42) Yoon, S. Y.; Lee, C. G.; Park, J. A.; Kim, J. H.; Kim, S. B.; Lee, S. H.; Choi, J. W. Kinetic, Equilibrium and Thermodynamic Studies for Phosphate Adsorption to Magnetic Iron Oxide Nanoparticles. *Chem. Eng. J.* 2014, *236*, 341–347.

(43) Eljamal, O.; Khalil, A. M. E.; Sugihara, Y.; Matsunaga, N. Phosphorus Removal from Aqueous Solution by Nanoscale Zero Valent Iron in the Presence of Copper Chloride. *Chem. Eng. J.* 2016, *293*, 225–231.

(44) Laboratory Research in Environmental Engineering. *Phosphorus Determination Using the Colorimetric Ascorbic Acid Technique*; 2001.

(45) Water Environment Federation. *Standard Methods for the Examination of Water and Wastewater*; 1999.

(46) Szilagyi, I.; Trefalt, G.; Tiraferri, A.; Maroni, P.; Borkovec, M. Polyelectrolyte Adsorption, Interparticle Forces, and Colloidal Aggregation. *Soft Matter* 2014, *10*, 2479–2502.

(47) Lamanna, G.; Kueny-Stotz, M.; Mamlouk-Chaouachi, H.; Ghobril, C.; Basly, B.; Bertin, A.; Miladi, I.; Billotey, C.; Pourroy, G.; Begin-Colin, S.; Felder-Flesch, D. Dendronized Iron Oxide Nanoparticles for Multimodal Imaging. *Biomaterials*

2011, *32* (33), 8562–8573.

(48) Choi, J.; Rubner, M. F. Influence of the Degree of Ionization on Weak Polyelectrolyte Multilayer Assembly. *Macromolecules* 2005, *38* (1), 116–124.

(49) Jachimska, B.; Jasiski, T.; Warszyski, P.; Adamczyk, Z. Conformations of Poly(allylamine Hydrochloride) in Electrolyte Solutions: Experimental Measurements and Theoretical Modeling. *Colloids Surfaces A Physicochem. Eng. Asp.* 2010, *355* (1–3), 7–15.

(50) Pantos, A.; Tsogas, I.; Paleos, C. M. Guanidinium Group: A Versatile Moiety Inducing Transport and Multicompartmentalization in Complementary Membranes. *Biochim. Biophys. Acta - Biomembr.* 2008, *1778*, 811–823.

(51) Burke, S. E.; Barrett, C. J. Acid - Base Equilibria of Weak Polyelectrolytes in Multilayer Thin Films. *Langmuir* 2003, *19*, 3297–3303.

(52) Maroni, P.; Montes Ruiz-Cabello, F. J.; Cardoso, C.; Tiraferri, A. Adsorbed Mass of Polymers on Self-Assembled Monolayers: Effect of Surface Chemistry and Polymer Charge. *Langmuir* 2015, *31* (22), 6045–6054.

(53) Wong, J. E.; Gaharwar, A. K.; Müller-Schulte, D.; Bahadur, D.; Richtering, W. Magnetic Nanoparticle-Polyelectrolyte Interaction: A Layered Approach for Biomedical Applications. *J. Nanosci. Nanotechnol.* 2008, *8* (8), 4033–4040.

(54) Wang, T.; Zhang, L.; Wang, H.; Yang, W.; Fu, Y.; Zhou, W.; Yu, W.; Xiang, K.; Su, Z.; Dai, S.; Chai, L. Controllable Synthesis of Hierarchical Porous Fe3O4 Particles Mediated by Poly(diallyldimethylammonium Chloride) and Their Application in Arsenic Removal. *ACS Appl. Mater. Interfaces* 2013, *5* (23), 12449–12459.

(55) Tristán, F.; Palestino, G.; Menchaca, J.-L.; Pérez, E.; Atmani, H.; Cuisinier, F.; Ladam, G. Tunable Protein-Resistance of Polycation-Terminated Polyelectrolyte Multilayers. *Biomacromolecules* 2009, *10* (8), 2275–2283.

(56) Lin, X.; Wu, L.; Liu, Y.; Ong, A. L.; Poynton, S. D.; Varcoe, J. R.; Xu, T. Alkali Resistant and Conductive Guanidinium-Based Anion-Exchange Membranes for Alkaline Polymer Electrolyte Fuel Cells. *J. Power Sources* 2012, *217*, 373–380.

(57) Szpak, A.; Kania, G.; Skorka, T.; Tokarz, W.; Zapotoczny, S.; Nowakowska, M. Stable Aqueous Dispersion of Superparamagnetic Iron Oxide Nanoparticles Protected by Charged Chitosan Derivatives. *J Nanopart Res* 2013, *15* (1), 1372.

(58) Stevens, J. S.; De Luca, A. C.; Pelendritis, M.; Terenghi, G.; Downes, S.; Schroeder, S. L. M. Quantitative Analysis of Complex Amino Acids and RGD Peptides by X-Ray Photoelectron Spectroscopy (XPS). *Surf. Interface Anal.* 2013, *45*, 1238–1246.

(59) Li, L.; Zheng, S. Poly(ε-Caprolactone)-Grafted Fe3O4 Nanoparticles: Preparation

and Superparamagnetic Nanocomposites with Epoxy Thermosets. *Ind. Eng. Chem. Res.* 2015, *54*, 171–180.

(60) Lai, Y.; Yin, W.; Liu, J.; Xi, R.; Zhan, J. One-Pot Green Synthesis and Bioapplication Ofl-Arginine-Capped Superparamagnetic Fe3O4 Nanoparticles. *Nanoscale Res. Lett.* 2009, *5*, 302–307.

(61) Zhang, L.; Zhou, N.; Wang, B.; Liu, C.; Zhu, G. Fabrication of Fe3O4/PAH/PSS@Pd Core–shell Microspheres by Layer-by-Layer Assembly and Application in Catalysis. *J. Colloid Interface Sci.* 2014, *421*, 1–5.

(62) Liu, P.; Li, X.; Mu, B.; Du, P.; Zhao, X.; Zhong, Z. Aggregation-Resistant Superparamagnetic Noncovalent Hybrid Multilayer Hollow Microcapsules in High Ionic Strength Media. *Ind. Eng. Chem. Res.* 2012, *51*, 13875–13881.

(63) Wilcox, D. L.; Berg, M. Microsphere Fabrication and Applications: An Overview. *MRS Proc.* 1994, *372*, 3.

(64) Davies, R.; Schurr, G. A.; Meenan, P.; Nelson, R. D.; Bergna, H. E.; Brevett, C. A. S.; Goldbaum, R. H. Engineered Particle Surfaces. *Adv. Mater.* 1998, *10* (15), 1264–1270.

(65) Sajjad, S. D.; Hong, Y.; Liu, F. Synthesis of Guanidinium-Based Anion Exchange Membranes and Their Stability Assessment. *Polym. Adv. Technol.* 2014, *25*, 108–116.

(66) Chitrakar, R.; Tezuka, S.; Sonoda, A.; Sakane, K.; Ooi, K.; Hirotsu, T. Phosphate Adsorption on Synthetic Goethite and Akaganeite. *J. Colloid Interface Sci.* 2006, *298*, 602–608.

(67) Environ, E.; Kim, J.; Li, W.; Philips, L.; Grey, C. P. Phosphate Adsorption on the Iron Oxyhydroxides Goethite (a-FeOOH), Akaganeite (B-FeOOH), and Lepidocrocite (G-FeOOH): A 31 P NMR Study. *Energy Environ. Sci.* 2011, *4*, 4298–4305.

(68) Zhu, Z.; Zeng, H.; Zhu, Y.; Yang, F.; Zhu, H.; Qin, H.; Wei, W. Kinetics and Thermodynamic Study of Phosphate Adsorption on the Porous Biomorph-Genetic Composite of Fe2O3/Fe 3O4/C with Eucalyptus Wood Microstructure. *Sep. Purif. Technol.* 2013, *117*, 124–130.

(69) Robati, D. Pseudo-Second-Order Kinetic Equations for Modeling Adsorption Systems for Removal of Lead Ions Using Multi-Walled Carbon Nanotube. *J. Nanostructure Chem.* 2013, *3* (1), 1–6.

(70) Ho, Y. Review of Second-Order Models for Adsorption Systems. *J. Hazard. Mater.* 2006, *B136*, 681–689.

(71) Liu, Y.; Shen, L. From Langmuir Kinetics to First-and Second-Order Rate

Equations for Adsorption. *Langmuir* 2008, *24*, 11625–11630.

(72) Miyake, Y.; Ishida, H.; Tanaka, S.; Kolev, S. D. Theoretical Analysis of the Pseudo-Second Order Kinetic Model of Adsorption . Application to the Adsorption of Ag (I) to Mesoporous Silica Microspheres Functionalized with Thiol Groups. *Chem. Eng. J.* 2013, *218*, 350–357.

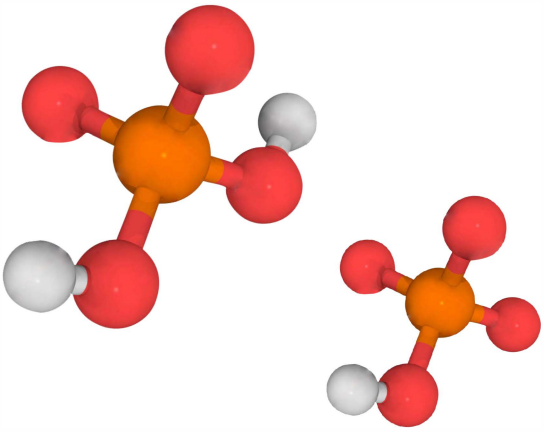

CHAPTER 3

Hybrid polyelectrolyte-anion exchange membrane and its interaction with phosphate

We have investigated in detail properties of hybrid polyelectrolyte-anion exchange membranes (AEMs) having different amounts of a guanidinium-modified poly(allylamine hydrochloride) (PAH-Gu) derivative (2, 5, and 8 wt%). The presence of guanidinium groups at the membrane surface was confirmed by XPS. For 2 and 5 wt% the blended membranes are homogeneous, while at 8 wt% segregation is observed by AFM. The membrane permselectivity and ionic electrical resistance for phosphate reduce upon incorporation of the PAH-Gu in the membrane, reflecting an increased co-ion (H^+ and Na^+) permeation. We conclude that PAH-Gu loaded in the AEM favours an interaction with phosphate. In electrodialysis, using sodium sulfate and sodium dihydrogen phosphate at equal concentrations in the source phase a slight preference for phosphate was observed. Our work shows that this facile membrane fabrication procedure shows great potential in terms of tuning the membrane properties. One way to boost selective ion transport could be by increasing the number of functional groups in the membrane.

The content of this chapter has been published in:

Laura Paltrinieri, Lukasz Poltorak, Liangyong Chu, Theo Puts, Willem van Baak, Ernst J.R. Sudhölter, Louis C.P.M. de Smet, Reactive and Fucntional Polymers*, 133*, **2018**, 126-135.

Introduction

Over the past decades, phosphorous (P)-containing compounds have been extensively discharged to environmental water due to increasing human activities, especially in the agricultural sector[1,2]. As a consequence, eutrophication processes in lakes and rivers expedited[3,4] and resulted in a decrease of water quality. For this reason, P species are considered as one of the most critical contaminants present in wastewater. The recovery of P from wastewater sources has been recognised as a strategic and sustainable solution to meet not only the constant high demand of water quality, but also to address the depletion of P resources the world is facing [5,6]. Several technologies have been developed to treat wastewater with the aim of P recovery, *e.g.,* adsorption processes[7,8], struvite crystallization[9] and, more recently, nanofiltration[10] and electro-membrane processes[11–13].

Currently, electro-membrane technology is largely applied in desalination applications[14] as well as wastewater treatments[13]. While adsorption and crystallization technologies require extensive use of chemicals due to regeneration processes or, in case of nanofiltration, additional costs due to the required high pressure; electro-membrane technology guarantees a continuos process with a limited amount of chemicals and high versatitily[12,15]. Ion-exchange membranes (IEMs) are the core of all electro-membrane based technologies. An IEM relies on the ability to form a selective barrier where anions are only transported by an anion-exchange membrane (AEM) and cations by a cation-exchange membrane (CEM) [16–18]. The biggest limitation of currently available IEMs is their scarce selectivity for ions with similar characteristics, preventing their use in emerging and more demanding applications.[19]

Improving the membrane selectivity towards specific target ions remains a great challenge[20–22]. Several factors influence membrane selectivity, *i.e.*, the nature of ion of interest (diffusion coefficient, charge, ionic radii, (de)hydration enthalpy)[21,23], the chemical composition of the membrane, the solution concentration, the applied electrical current density, the temperature and a few other minor parameters. Of great importance is the type of interaction between the fixed charged groups of the membrane and the exchanging ions [24], which is

mainly determined by the physico-chemical properties of the membrane. For instance, a dense membrane structure, characterized by a high cross-linking degree, hinders the passage of larger ions and facilitates the transport of relatively small ions.[25] However, this concept is not applicable in the case of ions that have similar sizes, *e.g.*, phosphate and sulfate.

The use of selective anchor groups,[26] in sensor concepts often referred to as receptors, is a possible way to address the selective uptake of ions.[27,28] Important progress in the field was achieved through the modification of IEMs with active compounds, *e.g.*, incorporation of nano-fillers during the membrane fabrication [29] to obtain hybrid membranes or the deposition of a polymer coating on the membrane surface[30–32], including surface modification with polyelectrolyte species[33]. In this context, polyelectrolytes can be easily functionalized with specific moieties, *e.g.*, biotin[34–36], fluorescent probes[37], graphene[38] and guanidinium groups[39] to address a wide range of specific applications. Recently, we have presented the use of poly(allylamine hydrochloride) functionalized with guanidinium groups (PAH-Gu) for the coating of Fe_3O_4 nanoparticles to improve the reversible adsorption of phosphate under alkaline conditions (Chapter 2).[40] We conclude that both the selectivity of PAH-Gu and the reversibility of the process exhibit great potential in the recovery of phosphate, which stimulated us to explore the use of functionalized polyelectrolytes in combination with AEM-based separations.

Most of the research in the field of membrane modification has been performed on CEMs[41,42], leaving AEM functionalization approaches tangential. To the best of our knowledge, polyelectrolytes have only been applied as a multilayer to modify the AEM surface to impart selectivity towards multivalent *vs.* monovalent anions.[32,43] Based on a high loading of selective functional groups, in this work we used PAH-Gu as an AEM modifier. Following this approach, we have investigated the effect of the polyelectrolyte on the membrane morphology and its effect on the transport properties of phosphate ions. In more detail, we hypothesized that the incorporation of PAH-Gu in the membrane would maintain a high density of positively charged sites and the presence of Gu groups would improve an uptake of phosphate.

In this work, PAH-Gu was mixed with the AEM building blocks before starting a UV polymerization to obtain an AEM polymer matrix with physically entangled PAH-Gu. The initial part of this study covers the characterization of the membrane doped with PAH-Gu, surface analysis (XPS and AFM) and membrane properties (water content and ion-exchange capacity). Next, diffusion experiments (permselectivity) and electrochemical characterizations (electrochemical impedance spectroscopy) were performed to better understand the interactions between the blended AEM and phosphate. The last part includes the comparison between phosphate and sulfate electrodialysis of the blended AEMs. To study the effects of PAH-Gu doping, the standard grade AEM from Fujifilm was used as a reference in all experiments.

Materials and Methods

Materials

Poly(allylamine hydrochloride) (PAH, M_w ~ 15,000 Da), guanidine acetic acid (GAA, 99%), 1-ethyl-3-(3-dimethylaminopropyl) carbodiimide (EDC, commercial grade) and n-hydroxysuccinimide (NHS, 98 wt%) were all purchased from Sigma-Aldrich and used to synthesize poly(allyamine hydrochloride) functionalized with guanidine groups (PAH-Gu), according to the procedure we reported earlier[39]. This way we obtained a 30% degree of functionalization as determined by ^{1}H-Nuclear Magnetic Resonance (H-NMR).[39] All purchased chemicals were used without any further purification. Sodium phosphate monobasic monohydrate (purity, $NaH_2PO_4 \cdot H_2O$, Acros Organic) and sodium sulfate (purity, Na_2SO_4, Sigma) were used to prepare the salt solutions at pH ~ 4.5. A standard grade Anion-Exchange Membrane (Fuji_AEM) from Fujifilm Manufacturing Europe BV (The Netherlands, hereafter Fuji) was selected as a reference, having quaternary ammonium as fixed charged groups. Also, others standard-grade type 1 and type 2 CEMs and AEMs, used to build the electrodialysis set-up, were provided by Fujifilm. To obtain a PAH-Gu doped membrane we used a water-soluble crosslinking agent provided by Fujifilm, and 2-hydroxy-2-methyl-1-phenyl-1-propane (Darocure1173, Ciba Specialty Chemicals) as the free-radical photo-initiator, TEGO® Glide (Evonik) as an inhibitor and a charged quaternary ammonium monomer (Fuji) as an additional compound to reinforce the

membrane structure during the UV polymerization. Milli-Q water (Millipore, 18.2 MΩ cm^2, T = 24.5°C) was used as a solvent for the synthesis of PAH-Gu, while Demi water was used for membrane fabrication. PAH-Gu was added to the mixture of monomers forming the Fuji_AEM in different amounts: 2 wt%, 5 wt% and 8 wt% before polymerization was initiated (*vide infra*). The resulting PAH-Gu doped membranes are labelled as 2 wt% PAH-Gu, 5 wt% PAH-Gu and 8 wt% PAH-Gu

Membrane fabrication

PAH-Gu blended AEMs were made via a UV-induced photopolymerization reaction initiated by free-radicals from the active double bonds of the Darocure1173 photo-initiator. The water-soluble cross-linker, the charged quaternary ammonium monomer (provided by Fuji) and the PAH-Gu polyelectrolyte were mixed together before the photo-polymerization was started. In more detail, 5 wt% of quaternary ammonium monomer (Fuji) and crosslinker (2 wt%) were added to 2 mL of water at 30°C and mixed until a clear solution was formed. Next, 1 wt% of TEGO® Glide and 0.05 wt% of Darocure1173 were added to the mixture. To obtain the final composition, 2 wt%, 5 wt% or 8 wt% of PAH-Gu was added to three separated solutions. Each solution was stirred at room temperature for one hour to obtain a clear solution. The mixture was cast into films by coating a non-woven fibrous polypropylene substrate with a 12 µm wire-wound coating bar. Each membrane was exposed to UV irradiation (240 W/cm) through a bench-top conveyor system (Heraeus Noblelight Fusion UV inc. USA). A mercury H-bulb (240-280 nm) working at 100% intensity was used, and the conveyor speed was 30 m/min with a single pass.

Ion-exchange capacity and water uptake

Water uptake and ion-exchange capacity (IEC) are important parameters to evaluate the membrane performance. Their values depend on membrane-intrinsic properties, such as hydrophobicity, the amount of fixed charged groups, the degree of crosslinking and type of testing solution. In general, an AEM with high IEC and high water uptake and low cross-linkage have an high electrical conductivity.[17] The membrane IEC was determined through a titration (Metrohm

auto-titration), following the method described elsewhere.[17,18] The membranes were dried at 50°C for 48 h before the dry weights were obtained. The IEC (meq./g) was calculated as:

$$IEC = \frac{C_{\mathrm{tot}}}{m_{\mathrm{dry}}} \qquad \text{[meq./g]} \qquad (3.1)$$

where C_{tot} is the total charge (meq.) and m_{dry} the mass (g) of the dry membrane. Measurements were done in triplicate. Samples were discarded after the drying process.

Water uptake (w_{uptake}) was determined by the following equation:[17]

$$w_{\mathrm{uptake}} = \frac{m_{\mathrm{wet}} - m_{\mathrm{dry}}}{m_{\mathrm{wet}}} \qquad [\%] \qquad (3.2)$$

where m_{wet} and m_{dry} are the membrane masses in the wet and dry state, respectively. The wet mass was obtained after immersing the membrane in Milli-Q water for 48 h. The excess of the water on the membrane surface was quickly removed using laboratory wipes. For the dry mass, samples were dried in a vacuum oven at 50°C for 48 h. The w_{uptake} is reported as an average of the measurements for three different membranes. After the drying process samples were discarded.

Imaging, adhesion force measurements and x-ray spectroscopy

A SOLVER NEXT AFM instrument from NT-MDT was used in all AFM experiments. A NSG03 silicon tip, purchased from NT-MDT, with a nominal value of the tip radius of 7 nm (guaranteed < 10 nm) and a nominal spring constant of 0.4 - 2.7 N/m was used in the height imaging and adhesive force measurements. The actual value of the spring constant was measured to be 0.87 N/m using the thermal noise method.[44] In scanning the surface morphology, 512 × 512 points are recorded in a 1 µm × 1 µm area. For height images, samples were all scanned with a rate of 0.3 Hz. For each sample, force-distance curves were obtained repeatedly for more than 25 times at different locations. Prior to the analysis, membranes were fixed with a double-sided tape to an aluminium substrate in order to maintain a flat surface during the analysis. The relative humidity of the

room was maintained constant at 48 %. The adhesion force measurements were done by performing standard force-displacement curves using AFM.[45] For all the force-displacement curves, the piezo displacement ranges from -50 nm to +300 nm, where 0 nm corresponds to the position when the normal load force is 0 nN.

Elemental composition X-ray Photoelectron Spectroscopy (XPS, Thermo Fisher Scientific, K-Alpha model) was used to determine the atomic composition of all membranes under investigation. In detail, a monochromatic Al Kα X-ray source with a spot size of 400 µm at a pressure of 10^{-7} mbar, a constant pass energy of 400 eV for the survey spectra and 50 eV for the detailed high-resolution spectra were used. The flood gun was turned on during the measurement to compensate for potential charging of the surface. The peak position was adjusted based on the internal standard C1s peak at 284.8 eV, with an accuracy of ±0.05 eV. Avantage processing software was used to analyze all spectra.

Permselectivity

Membrane permselectivity (PS) was determined with a two-compartment cell,[23] (custom-made by STT Products, The Netherlands), as illustrated in Figure S3.1 which is given in the supporting data. The membrane was placed in the sample holder with an effective cross-sectional area of 8.14 cm^2 separating two solutions having a concentration of 0.05 M NaH_2PO_4 and 0.5 M NaH_2PO_4 pH ~ 4.5 for phosphate PS and 0.05 M NaCl and 0.5 M NaCl pH ~ 6 for chloride PS. The potential difference between two Ag/AgCl double-junction reference electrodes (Metrohm, the Netherlands) separated with a membrane under investigation (E_x) was measured with the digital multimeter (Digimess). The potential was read after reaching stabilization (typically after 3-5 min). For each membrane, at least three measurements were performed and the number-averaged value was tabulated. The potential drop across the membrane (E_m) was then calculated by subtracting the offset potential (E_{offset}) of the electrodes measured in 3 M KCl solutions [23,26]:

$$E_{\mathrm{m}} = E_{\mathrm{x}} - E_{\mathrm{offset}} \qquad [\mathrm{mV}] \qquad (3.3)$$

The final value of permselectivity (%*PS*) was calculated as the ratio between E_m and the theoretical Nernst potential (E_{Nernst}) [23,26]

$$\%PS = \frac{E_m}{E_{Nernst}} \quad [\%] \quad (3.4)$$

E_{Nernst} was calculated using the following formula:

$$E_{Nernst} = \frac{RT}{nF} ln \frac{C_1 \gamma_1}{C_2 \gamma_2} \quad [mV] \quad (3.5)$$

where R is the gas constant, T is the temperature in K, F is the Faraday constant, n is the valency of the transferring ion and C_1, γ_1 and C_2, γ_2 are the concentrations and activity coefficient of the transferring anion in the diluted and the concentrate compartment, respectively. The electrolyte solutions were continuously recirculated by using two peristaltic pumps (Masterflex Peristaltic pumps, model L/S Economy Pump System with Easy-Load II pump head 230 VAC, the Netherlands) keeping a constant flow rate of 110 mL/min in each compartment. A thermal bath (Thermo Fisher Scientific Inc, USA) was used to maintain a constant temperature of 20°C.

Electrochemical measurements

Ion transport across the membrane can be directly measured with several electrochemical techniques.[46–48] One of the most important electrical parameters of the membrane is the Ohmic resistance, which describes the opposition to the flow of ionic currents. Intuitively, a perfect AEM should have an infinitely low resistance towards the transfer of anions and an infinitely large resistance for the transfer of cations. The overall membrane resistance can be, for instance, easily measured by applying a direct current (lower than the limiting current given by the concentration polarization region)[49] and measuring the resulting potential drop followed by straightforward scrutiny given by Ohm's law. In this work, the electrochemical properties of the membrane were investigated using electrochemical impedance spectroscopy (EIS).[50] This method has the ability to distinguish between a number of electrical parameters that all together give the overall impedance of a membrane [50]: the resistance of a pure membrane (R_m); the resistance (R_{edl}) and capacitance (C_{edl}) of the electrical

double layer; and the resistance (R_{dbl}) and capacitance (C_{dbl}) of diffusion boundary layer. A schematic representation of the different contributions is shown in Figure 3.1a and the equivalent circuit is displayed in Figure 3.1b.

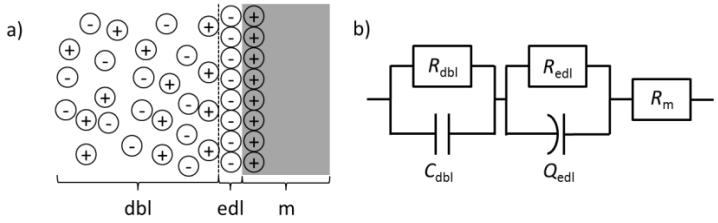

Figure 3.1 a) Schematic representation of the membrane (m), electric double layer (edl) and diffusion boundary layer (dbl) with b) corresponding equivalent circuit used to fit impedance spectra. *R* stands for resistance, *C* for capacitance and *Q* is the constant phase element.

Since the membrane surface can be considered as being porous, the current distribution is non-uniform, and hence the EDL can be treated as an imperfect capacitor. For this reason, the capacitance of the EDL is replaced with a constant phase element (CPE)[50,51] of which the impedance is given by:

$$Z_{\mathrm{CPE}} = \frac{1}{Y_0(i\omega)^N} \qquad [\mathrm{Fcm^{-2}S^{N-1}}] \qquad (3.6)$$

where Y_0 is the CPE parameter with a unit of $\mathrm{Fcm^{-2}S^{N-1}}$, *i* the complex number, $\omega = 2\pi f$ the angular frequency and *N* the constant phase exponent that can be found in the range from 0 (for a pure resistor) to 1 (for a pure capacitor). The pseudo-capacitance of a CPE can be calculated using the following equation:

$$C_{\mathrm{CPE}} = Y_0^{\frac{1}{N}} R_{\mathrm{CPE}}^{\frac{(1-N)}{N}} \qquad [\mathrm{F}] \qquad (3.7)$$

where R_{CPE} corresponds to the resistance connected in parallel to the CPE. EIS spectra were recorded in the frequency range from 1 Hz down to 0.001 Hz with an alternating current perturbation of 0.5 mA. No superimposed direct current was applied. An Autolab, potentiostat/galvanostat (PGSTAT302N) equipped with a frequency response analyzer was used to perform all impedance measurements. In order to distinguish between different membrane contributions (R_M, R_{EDL}, C_{EDL}, R_{DBL} and C_{DBL}) we fitted experimental data to the equivalent circuit from Figure 3.1b. Fitting was performed with ZView software.

Membrane impedance measurements were performed in a conventional six-compartment cell (custom-made by STT Products, the Netherlands) with appropriate membranes configuration as schematically illustrated in Figure 3.2.[18,49]

Compartments containing the anode (compartment 1) and the cathode (compartment 6) were filled with 0.5 M Na_2SO_4 solution, while compartments 2 and 5 were filled with 0.5 M NaH_2PO_4. The concentration of NaH_2PO_4 in compartment 3 and 4 was varied and the values are indicated where necessary. The pH in compartment 2, 3, 4 and 5 was ~ 4-5. Electrolyte solutions were circulated individually at the same flow rate of 110 mL/min and the temperature was maintained at 25°C by a thermal bath (Thermo Fisher Scientific Inc, USA). The potential drop across the membrane was measured with two Ag/AgCl reference electrodes positioned on both sides of the membrane with the help of Luggin capillaries.

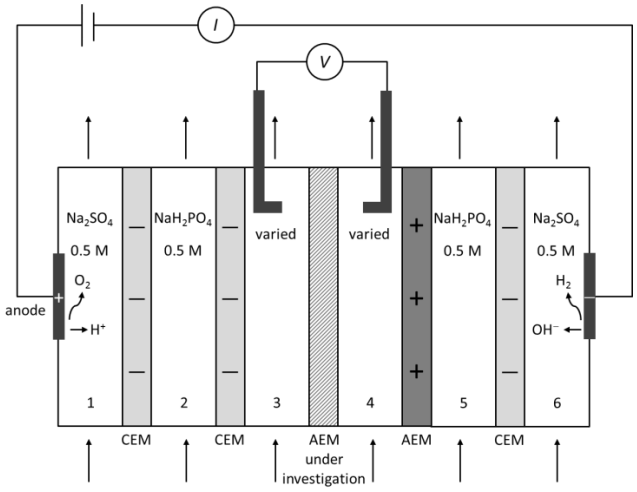

Figure 3.2 Scheme of the set-up used to perform electrochemical impedance spectroscopy and electrodialysis experiments. CEM and AEM stand for cation- and anion-exchange, standard-grade membranes, respectively. The membrane under investigation was positioned between compartment 3 and 4. The current was supplied from two counter electrodes positioned in compartment 1 (anode) and compartment 6 (cathode).

Ion flux, transport number and selectivity

Electrodialysis was performed on a 5 wt% PAH-Gu membrane and the standard-grade AEM (Fuji_AEM) to study the transport of phosphate and sulfate. The set-up shown in Figure 3.2 was used for the experiment. A solution of 0.01 M NaH_2PO_4 and 0.01 M Na_2SO_4 was placed in compartment 3 (feed) and 4 (receiving) of the electrodialysis set-up (Figure 3.2); compartment 2 and 5 were filled with 0.5 M NaH_2PO_4, while a solution of 0.5 M Na_2SO_4 was circulated through the compartments containing the cathode and anode electrodes (1 and 6). All solutions were continuously pumped at 110 mL/min at a fixed temperature of 25°C by using the peristaltic pump and the thermostatic bath described in the electrochemical measurement section. During the electrodialysis experiments, a constant direct current of 0.06 A was applied (current density 7.1×10^{-3} A/cm^2) and every 30 minutes aliquots of the solution (5 mL) were collected from both receiving and feed compartments. Collected samples were analysed by ion chromatography (930 Compact IC Flex, 150 mm A Supp 5 column, Metrohm).

In order to evaluate the phosphate selectivity over sulfate, the flux of the corresponding anion through the membrane (J_{ion}) was calculated using the following equation [32]:

$$J_{\mathrm{ion}} = \frac{V \frac{\mathrm{d}C_{\mathrm{ion}}}{\mathrm{d}t}}{A} \qquad [\mathrm{mol/cm^2\ s}] \qquad (3.8)$$

where V is the volume of receiving solution (cm^3), C_{ion} the concentration (mol/cm^3) of anion at time t (sec) and A the surface area of the membrane (cm^2). This corresponds to the slope of the ion concentration plotted as function of time, divided by the membrane area exposed to the electrolyte solutions. The membrane selectivity for phosphate over sulfate is simply calculated by the ratios of the ion fluxes.[52] Since the ratio of phosphate to sulfate concentration in compartment 4 (source side) hardly changed during our experiments, no corrections for this were applied. The ion transport number was calculate as (t_{ion})[53]:

$$t_{\text{ion}} = \frac{nF\,V\,\frac{\mathrm{d}C_{\text{ion}}}{\mathrm{d}t}}{iA} = \frac{n\,F\,J_{\text{ion}}}{i} \qquad [-] \qquad (3.9)$$

in this equation, F is the Faraday constant (96485 C mol^{-1} = 96485 A sec mol^{-1}), i is the current density (A cm^{-2}), and n is the valency of the ion. The t_{ion} thus relates the ion flux J_{ion} to the current density divided by the Faraday constant (i/nF). In this way the dimension of the current density is converted from A/cm^2 = C/sec.cm^2 to mol/sec.cm^2). For permeating divalent ions (n = 2), the current is twice compared to the one of monovalent ions (n = 1).

Results and Discussion

Surface characterization: XPS and AFM

XPS was used to map the elemental composition and the type of chemical bonds at the membrane surface. We focused on nitrogen, a key element to detect the presence of Gu groups. Figure 3.3 shows the high-resolution N1s region spectra of all investigated membranes. For Fuji_AEM (Figure 3.3a), as expected, two contributions are observed: one points to C-N^+, originating from the fixed charged groups and the other one at lower binding energy can be associated to C-N from the uncharged N groups of the membrane components.[32] For the PAH-Gu doped membranes (Figure 3.3 b, c and d) an additional peak was observed around 401 eV, which can be associated with N1s of both the guanidinium charged groups and the amide groups (O=C-N)[54], originating from the reaction of the PAH primary amine with guanidine acetic acid.

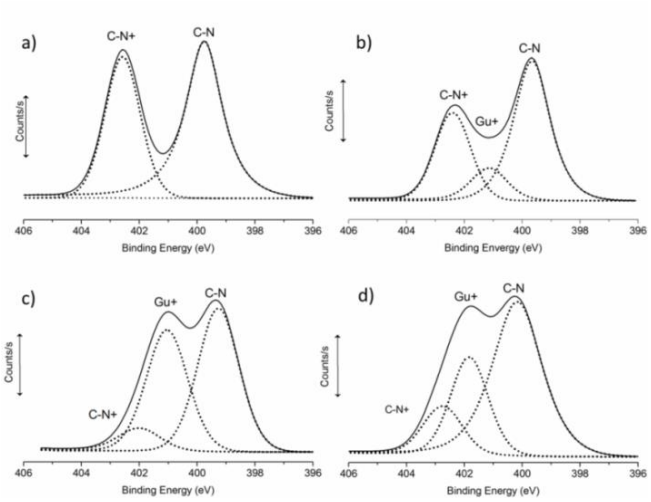

Figure 3.3 High-resolution XPS N1s region spectra (solid lines) and corresponding fitting (dotted lines) for a) Fuji_AEM, b) 2 wt% PAH-Gu c) 5 wt% PAH-Gu and d) 8 wt% PAH-Gu.

Next to the binding energies and peak assignments, the relative contribution (%) of the indicated groups to the surface composition of the investigated AEMs were determined for the XPS region spectra (Table 3.1). The percentages observed for Fuji_AEM and for the composition containing 2 wt% and 5 wt% PAH-Gu can be understood; the relative amount of O=C-N/Gu^+ increases and, at the same time, the relative amount of C-N^+ decreases upon increasing loading. Positions of the charged monomer from Fuji at the membrane surface are being replaced by the added PAH-Gu. The added PAH-Gu is clearly present at the top ~10 nm of the membrane surface. It is remarkable that for 8 wt% PAH-Gu the observed trend is broken since XPS shows a value of O=C-N/Gu^+ and C-N^+ in between the other two compositions. This is possibly due to phase segregation and inhomogeneities in the spotted areas. Among the three studied membrane compositions, we found that the 5 wt% PAH-Gu loading gives the highest amount of Gu groups located at the surface, which is around 3 times higher than found for the 2 wt% PAH-Gu loaded membrane, very close to expectation (*i.e.*, 2.5 times higher). This result indirectly indicates that, within the studied range, the 5 wt% PAH-Gu membrane contains the highest amount of phosphate-receptors at the surface as measured by XPS.

Table 3.1. Binding energies (BEs) of the assigned elements and relative contribution (%) from high-resolution XPS analysis and mathematical fitting.

	C-N		O=C-N / Gu^+		$C\text{-}N^+$	
	BE (eV)	**%**	**BE (eV)**	**%**	**BE (eV)**	**%**
Fuji_AEM	399.8	59.1	-	-	402.6	40.9
2 wt% PAH-Gu	399.7	53.6	401.1	14.0	402.2	32.4
5 wt% PAH-Gu	399.3	48.3	401.1	41.8	402.0	9.9
8 wt% PAH-Gu	399.8	59.8	401.4	26.4	402.3	13.8

In Figure 3.4 the calculated N/C ratios from the compositions of the starting mixtures are compared with the experimental N/C ratios, obtained from XPS for the four AEMs. As expected, more N is found upon increasing the amount of added PAH-Gu. The discrepancy between theoretical and experimental values can be explained as (i) the XPS gives the elemental composition of the only top-layer of a membrane equal to around 10 nm; (ii) some inhomogeneities at the membrane surface (phase separation) can locally affect the membrane composition and (iii) hydrocarbon contamination, often observed at the membrane top layer[54], which decreases the overall ratio.

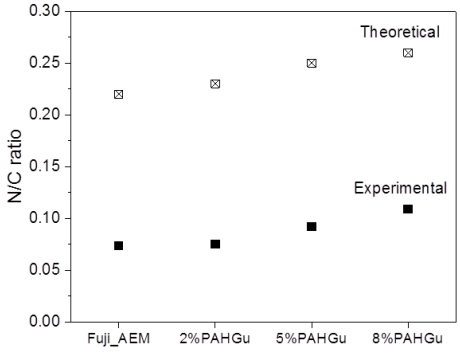

Figure 3.4 Theoretically and experimentally determined N/C ratios for Fuji_AEM, 2 wt% PAH-Gu, 5 wt% PAH-Gu and 8 wt% PAH-Gu. Data obtained from XPS analysis (solid squares) are compared with the theoretical atomic ratio calculated based on the monomers (open squares).

In Figure 3.5 the morphology of the Fuji_AEM and the three PAH-Gu membranes was investigated by height imaging AFM and adhesion force measurements on different locations. The height image of the Fuji_AEM membranes (Figure 3.5a) reveals a wide valley area (dark coloured) and high-hill regions (light coloured). This can be attributed to an irregular distribution of the fibres of the non-woven polypropylene reinforcement material.[32] The PAH-Gu modified membranes show different surface properties. Besides the appearance of the hilly and valley structures, also elongated pillars are observed, giving the impression of a rough surface. The number and the distribution of the regions where the pillars were observed are dependent on the percentage of the polyelectrolyte present and are homogeneously distributed for 2 wt% PAH-Gu, homogeneously distributed with some local separation for 5 wt% PAH-Gu and clearly arranged in 'island-like' regions for 8 wt% PAH-Gu (Figure 3.5b-d). This separation, which starts already for 5 wt% PAH-Gu and is very prominent for 8 wt% PAH-Gu, affects the local visco-elastic properties. This is especially visible in Figure 5d, where spike-like structures are concentrated in well-defined areas, and which likely originate from the interaction of the AFM tip with the highly concentrated region of the polyelectrolyte. In order to get a better insight into the differences between spotted areas, we also measured the adhesion forces for the Fuji_AEM (F) and PAH-Gu modified membranes. We discriminated between the adhesion forces for flat areas (F_{fl}) and the spike-like (F_s) regions in case of modified membranes. It is observed that the incorporation of more PAH-Gu in the membrane results in an increase of adhesion force for both the inspected flat areas and the spike-like region, see Figure 3.5a-d, inserts. This is due to the stronger electrostatic interaction between the AFM tip (negatively charged in the presence of some physically adsorbed water) and the positively charged PAH-Gu that is present. The adhesion force is larger for the flat areas compared to the spiky areas. Generally, the amount of adsorbed water is higher in dense polyelectrolytes regions[47,55] (spiky areas) resulting in a smaller adhesion force.[48] Herein we can confirm that the surface topology of PAH-Gu modified membranes is clearly different compared to Fuji_AEM and that for the 8 wt% PAH-Gu AFM points to phase separation. The lowest adhesion force measured for the Fuji_AEM indicates that its surface is less hydrophilic as compared to flat regions of membranes doped with PAH-Gu.[56,57] This indicates, that also here

some polyelectrolytes species (at much lower concentrations than in the spike-domains) might be present.

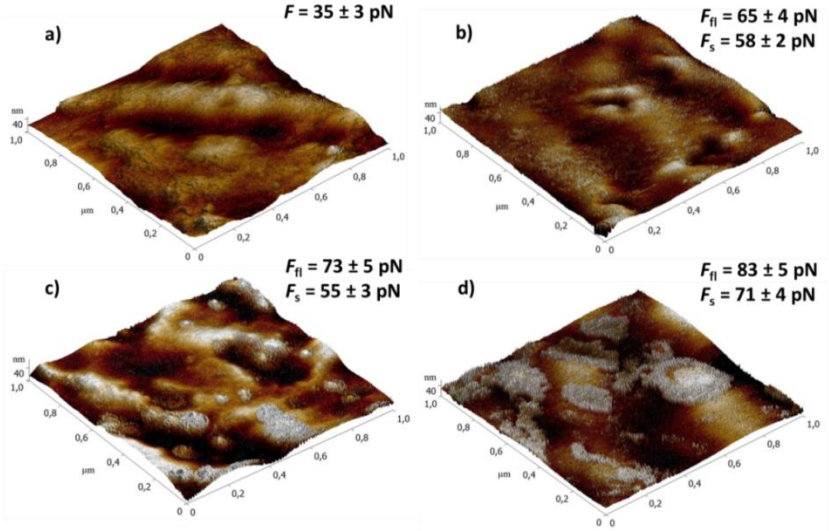

Figure 3.5 AFM 3D height images of a) Fuji_AEM, b) 2 wt% PAH-Gu, c) 5 wt% PAH-Gu and d) 8 wt% PAH-Gu. The analyzed area was 1 µm × 1 µm in size. Measurements were performed at room temperature with 48 % relative humidity. The values in the inserts correspond to adhesion forces measured for all surfaces (F) in the case of Fuji_AEM (a) and for flat (F_{fl}) and spike-like (F_s) regions for the modified membranes (b-d).

Water uptake, ion-exchange capacity and permselectivity of NaH_2PO_4

The measured water uptakes, ion-exchange capacity (IEC) values, permselectivity (PS), and surface-bound phosphate for the Fuji_AEM and PAH-Gu modified membranes are listed in Table 3.2. The water uptake of the Fuji_AEM (1.0 wt%) slightly increases with PAH-Gu content, reaching a maximum value of 1.3 wt% for the 8 wt% PAH-Gu membrane. Due to the hygroscopic behaviour, the presence of the polyelectrolyte contributes to a higher membrane hydrophilicity, resulting in a more open structure of the polymeric network.[17,58–60]

Generally, the IEC values were found to be slightly higher for PAH-Gu compositions with respect to the Fuji_AEM (Table 3.2), indicating a higher charged density after PAH-Gu incorporation. Considering associated errors, we

notice that the IEC of the first two compositions (2 wt% and 5 wt% PAH-Gu) are rather at the same level, whereas for 8 wt% PAH-Gu the IEC value slightly drops. The highest studied polyelectrolyte loading again deviates from the expected trend (higher concentration, higher charged density). In good agreement with previously discussed XPS and AFM data, we attribute this deviation to inhomogeneities within the 8 wt% modified membrane.

Table 3.2 Water uptake, ion-exchange capacity, permselectivity and surface-bound phosphate for Fuji_AEM and PAH-Gu doped AEMs.

	Water uptake (wt.%)	**IEC (meq/g_{dry})**	**PS NaCl*** **(%)**	**PS NaH_2PO_4**** **(%)**	**Phosphate after PS***** **(%)**
Fuji_AEM	0.98 ± 0.00	2.37 ± 0.57	90.7 ± 0.1	73.4 ± 0.2	1.3 ± 0.1
2 wt% PAH-Gu	1.16 ± 0.01	3.61 ± 0.57	90.5 ± 1.7	76.5 ± 1.3	2.2 ± 0.2
5 wt% PAH-Gu	1.18 ± 0.02	3.30 ± 0.82	88.1 ± 0.6	52.6 ± 5.9	2.4 ± 0.2
8 wt% PAH-Gu	1.29 ± 0.03	3.01 ± 0.31	88.6 ± 0.2	43.6 ± 4.0	2.2 ± 0.1

*0.05/0.5 M of NaCl at pH≈6, **0.05/0.5 M of NaH_2PO_4 at pH≈4.5, see Experimental section; ***measured by XPS.

The permselectivity (PS) has been determined for NaCl, as a common reference anion at pH around 6, and for NaH_2PO_4 solutions at pH around 4-5, by applying eq. 3.4 (Table 3.2). For NaCl transport, these membranes show a similar PS of as high as around 90%. Clearly, minor differences observed for IEC and water uptake have no influence on the permselectivity values. Moreover, having similar PS value in NaCl, PAH-Gu shows no specific interaction with chloride anion. The PS for the standard grade Fuji_AEM recorded in the presence of NaH_2PO_4 is only 73% being lower than that observed for NaCl, which can be associated with an increase of co-ion transport. Considering the associated error, there is no significant difference between Fuj_AEM and 2 wt% PAH-Gu; while addition of PAH-Gu >5 wt% shows a further reduction of PS to 43%, thus a further increase of co-ion transport. This increased co-ion transport can be explained by phosphate dianions (HPO_4^{2-}) being present in the membrane, which is an ampholyte electrolyte having different speciation depending on the local pH (pK_{a1} = 2.12, pK_{a2} = 7.12 and pK_{a3} = 12.34).[61] HPO_4^{2-} ions have an interaction with

the anion-exchanging sites in the membrane and have also a second dissociated OH group, giving an (additional) anionic group for the interaction with sodium co-ions. The dissociation of the second OH group arises probably from the increased acidity of that OH group if phosphate is bound to the quaternary ammonium sites, and/or by the presence of hydroxide anions in the membrane.[62] For the PAH-Gu modified membranes this effect is clearly more enhanced by the specific stronger binding interactions of monovalent phosphate ($H_2PO_4^-$) with the present guanidinium moieties[63–66] Finally, inhomogeneities in the membrane, as was found for 8 wt% PAH-Gu, can form non-conductive areas (intra-gel phases)[67] able to limit ion transport and the binding affinity of phosphate to the guanidinium group.[68] The amount of phosphate residing on the membrane surface after the permselectivity experiments was measured by XPS (Table 3.2). On average, the amount of phosphate doubled upon blending with PAH-Gu. This difference can be attributed to a higher amount of exchange sites at the membrane surface in the presence of PAH-Gu, as the N peak analysis from XPS measurements in Table 3.1 and the IEC data suggested.

Electrochemical characterization

Electrochemical impedance was used to investigate the resistance of the membranes to ion transport. During the measurement, compartments 3 and 4 were flushed with 0.1 M NaH_2PO_4 at a rate of 110 mL/min. All other compartments were filled as shown in Figure 3.2. The R_m values of all four membranes as obtained from the best fit of the EIS spectra (Bode and Nyquist plots of the impedance measurement are shown in Figure S3.2 of the supporting data) using the equivalent circuit presented in Figure 3.2c are given in Figure 3.6. This analysis reveals an initial decrease of the membrane resistance upon increasing PAH-Gu loading. A slight increase of R_m was observed when the amount of PAH-Gu was raised from 5 wt% to 8 wt% and again this can be associated with the inhomogeneous distribution of polyelectrolyte in the membrane. A lower membrane resistance most probably arises from the increasing amount of fixed charges, which enhances the facilitated ion transport[69] across the membrane, and from an increase in the water content as observed previously. We also cannot exclude an increased flux of the co-ions, this are Na^+ and H^+, as indicated by the PS data (*vide supra*).

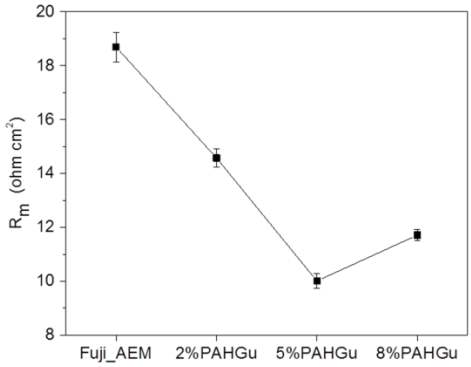

Figure 3.6 Membrane resistance obtained from electrochemical impedance spectroscopy measurements in electrodialysis setup (Figure 3.2) The line is a guide to the eye.

Table 3.3 summarizes the electrical parameters of the electrical double layer (edl) and the diffusion boundary layer (dbl) as obtained from the fitting of impedance measurements. Low χ^2 values indicate very good fitting to experimental impedance values. The R_{dbl} and C_{dbl} were shown to be independent of the membrane composition, which is understood, as these parameters can only be influenced by the bulk concentration of the supporting electrolyte or adjacent solution convection flow rates.[50] The determined pseudo-capacitance, C_{edl}, calculated according to Eq. 3.7, is within the experimental error constant for all investigated membranes. This indicates that the corresponding thickness of the electrical double-layer capacitor (given by the Debye length) remained constant with increasing amounts of added PAH-Gu to the membrane. Interestingly, R_{edl} increased from 15.6 Ωcm^2 for Fuji_AEM to 20.4 Ωcm^2 for 5 wt% PAH-Gu or 20.9 Ωcm^2 for 8 wt% PAH-Gu loaded membrane. This observation can only be related to the change in ionic composition or depletion of the ionic charge carriers within the nanometer-thick layer adjacent to the membrane surface. For the latter, we can speculate that the presence of PAH-Gu improves the uptake of phosphate anions into the membrane, which can deplete the electrical double layer from ions and consequently increase its resistance.

Table 3.3 Obtained resistance (*R*) and capacitance (*C*) values of the electrical double layer (edl) and the diffusion boundary layer (dbl) obtained from electrochemical impedance spectroscopy.

	R_{edl} Ohm cm^2	C_{edl} F cm^{-2}	R_{dbl} Ohm cm^2	C_{dbl} F cm^{-2}	χ^2 (10^{-5})
Fuji_AEM	15.6 ± 1.3	10.3 ± 0.7	0.7 ± 0.2	0.9 ± 0.1	6.55·
2 wt% PAH-Gu	18.1 ± 2.9	9.5 ± 3.5	0.7 ± 0.3	1.3 ± 0.4	3.88·
5 wt% PAH-Gu	20.4 ± 1.8	11.3 ± 0.9	0.7 ± 0.1	1.1 ± 0.1	7.36·
8 wt% PAH-Gu	20.9 ± 1.6	11.1 ± 2.0	0.6 ± 0.2	0.9 ± 0.2	5.28·

So far, electrochemical and permselectivity characterizations point towards a specific interaction between Gu groups and phosphate, most likely leading to partitioning. Therefore, we expect that the transport of phosphate across the modified AEM is facilitated by the presence of the Gu groups and hence lowers the energy needed to cross the membrane – feed solution interface, as compared to the bare AEM. After partitioning to the functional ion-exchange groups of the PAH-Gu AEM, ion transport will be governed by a hopping mechanism, likely the limiting step of the overall separation process

Selectivity in phosphate and sulfate electrodialysis

We have performed electrodialysis experiments with the set-up as illustrated in Figure 3.2 having the compartments 3 and 4 both filled with a mixed solution of ~10 mM NaH_2PO_4 and ~10 mM Na_2SO_4 at a pH around 4.5. Other compartments were filled as shown in Figure 3.2. The experiment was performed for both the Fuji_AEM and the 5 wt% PAH-Gu membrane, which showed the best performance so far. The increase of the SO_4^{2-} and $H_2PO_4^-$ concentrations (mmol/L) in the receiving phase (compartment 3) were monitored during 120 min. at intervals of 30 min. Collected aliquots of the solutions were analysed by ion chromatography. The experiments were done under a constant current density of 7.1 mA cm^{-2}. Sulfate was chosen as a competitive ion because it has an ion size and a diffusion coefficient (Stokes radius = 0.231 nm; and D_i = 1.05 × 10^{-5} cm^2 s^{-1}) similar to those of monovalent phosphate (Stokes radius = 0.260 nm; and D_i = 0.958 × 10^{-5} cm^2 s^{-1}).[61] Due to

structural similarities, any size exclusion effect on discrimination between these two anions can be neglected. The major differences are the anion valency at a pH~4.5, phosphate is monovalent while sulfate is bivalent.

The concentration (mmol/L) of both anions at function of time are reported in the supporting information in Fig S3.3. The slope of each curve gives ion fluxes (mol/cm^2 s), applying Eq. 3.8, and corresponding data are listed in Table 4 together with the transport numbers obtained using Eq. 3.9. To our surprise, Fuji_AEM shows a permeation of SO_4^{2-} almost equal to $H_2PO_4^-$, as ion fluxes equal 2.0 × 10^{-8} mol/cm^2 s and 1.9 × 10^{-8} mol/cm^2 s, respectively. Based on the difference in valency at pH 4.5, we had expected in our electrodialysis experiment that sulfate would be transported slower than phosphate.[70] If dehydration plays a role, this would benefit phosphate compared to sulfate as the dehydration energies $\Delta G_{hydration}$ are -465 kJ mol^{-1} and -1080 kJ mol^{-1} respectively.[70] The observed similar transport numbers of phosphate and sulfate can be best explained by the presence of phosphate dianions (HPO_4^{2-}), instead of phosphate monoanions ($H_2PO_4^-$), in the AEM. This is not only supported by the reported increased local basicity in AEMs,[62] but also by the calculated transport numbers (Table 3.4) for the phosphate dianion and sulfate. The sum of both transport numbers equals ~1; if phosphate would cross the membrane as monoanion, the sum of transport numbers would be only 0.79 (= 0.5 × 0.51 + 0.53). The presence of phosphate dianions is also in agreement with calculated the PS values available in the Table 3.2.

Addition of 5 wt% PAH-Gu to the Fuji membrane shows hardly any effect on the phosphate transport, and although the error bars are significant, the sulfate transport is slightly decreased. This reduced transport is also reflected in a lower transport number for sulfate. Since the sum of transport numbers for phosphate (dianion) and sulfate for 5 wt% PAH-Gu is 0.90, it indicates that another anion is also permeating. This is most likely the hydroxide anion.[71,72] Considering the related errors caused by the variation on the linearity of the plots in Figure S3.3, we conclude that the desired selectivity of phosphate transport over sulfate, in the presence of Gu groups, is far from expected values. We do, however, see a reduced sulfate permeation in the 5 wt% PAH-Gu membrane, and this may indicate that sulfate is somewhat stronger bound to the PAH-Gu receptors in the

membrane compared to phosphate, and this might favor phosphate permeation. Yet, previous PS and ER characterizations on PAH-Gu loaded AEM point towards a high interaction of phosphate anions compared to Fuji_AEM. Nevertheless the presence of quaternary charged groups together with Gu-groups in the membrane might interfere during the selective permeation. Future work to improve selectivity and to better control the transport properties is directed to increase the amount and distribution of receptors within the membrane as well as to engineer the membrane at the nanometer level, *e.g.,* by the formation of aligned nanodomains/channels to intensify mass transport.

Table 3.4 Ion-flux values (*J*) for phosphate and sulfate and relative anion selectivity (*S*) calculated over 120 min for mixed solution ~10 mM NaH_2PO_4 and ~10 mM Na_2SO_4 at pH around 4.5.

	$J_{H_2PO_4^-}10^{-8}$ mol/cm^2 s	$J_{SO_4^{2-}}10^{-8}$ mol/cm^2 s	$t^*(HPO_4^{2-})$	$t^*(SO_4^{2-})$	$S_{SO_4^{2-}}^{H_2PO_4^-}$
Fuji_AEM	1.9 ± 0.06.	2.0 ± 0.03	0.51 ± 0.02	0.53 ± 0.01	0.9 ± 0.01
5 wt% PAH-Gu	1.8 ± 0.3	1.5 ± 0.3	0.48 ± 0.05	0.42 ± 0.08	1.2 ± 0.03

*calculated as it is expected in the membrane

Conclusions

We have successfully fabricated a hybrid polyelectrolyte-anion exchange membrane having different amounts (2, 5 and 8 wt%) of a 30% functionalized guanidinium poly(allylamine hydrochloride) (PAH-Gu). XPS analysis confirmed that PAH-Gu was present at the membrane surface for all studied loadings, and AFM showed a morphological segregation in 'island-like' domain of the PAH-Gu, being most prominent for 8 wt%. We noticed that the PAH-Gu modified AEMs has a low value of permselectivity and electrical resistance in NaH_2PO_4 compared to a standard grade Fuji_AEM. We can attribute this to 1) differences in membrane properties (high ion-exchange capacity and high water uptake); 2) the deprotonation of the second OH group of dihydrogen phosphate, acting as a site for co-ions (sodium or protons) permeation. Electrodialysis experiments were performed on 5 wt% PAH-Gu, which was the optimum configuration, in equal concentrations of sodium sulfate and sodium dihydrogen phosphate in the source phase. Differences in the transport among anions were minor for both

Fuji_AEM and 5 wt% PAH-Gu AEM, although a slight preference for phosphate was observed. In future, we plan to increase the concentration of Gu-active sites and study its effect on the transport of different ions.

Supporting Information

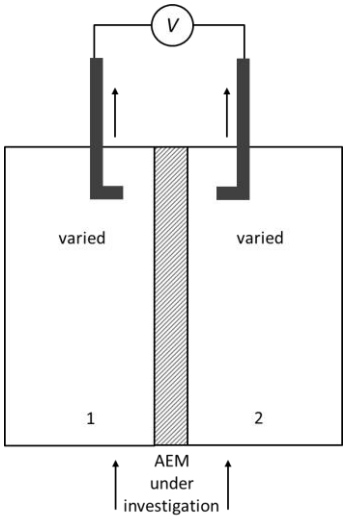

Figure S3.1 Scheme of the setup used to study the permselectivty of the membranes (shaded area in the middle). Two Ag/AgCl reference electrode (ref) were symmetrically positioned close to the membrane (few mm) with the help of Luggin capillaries.

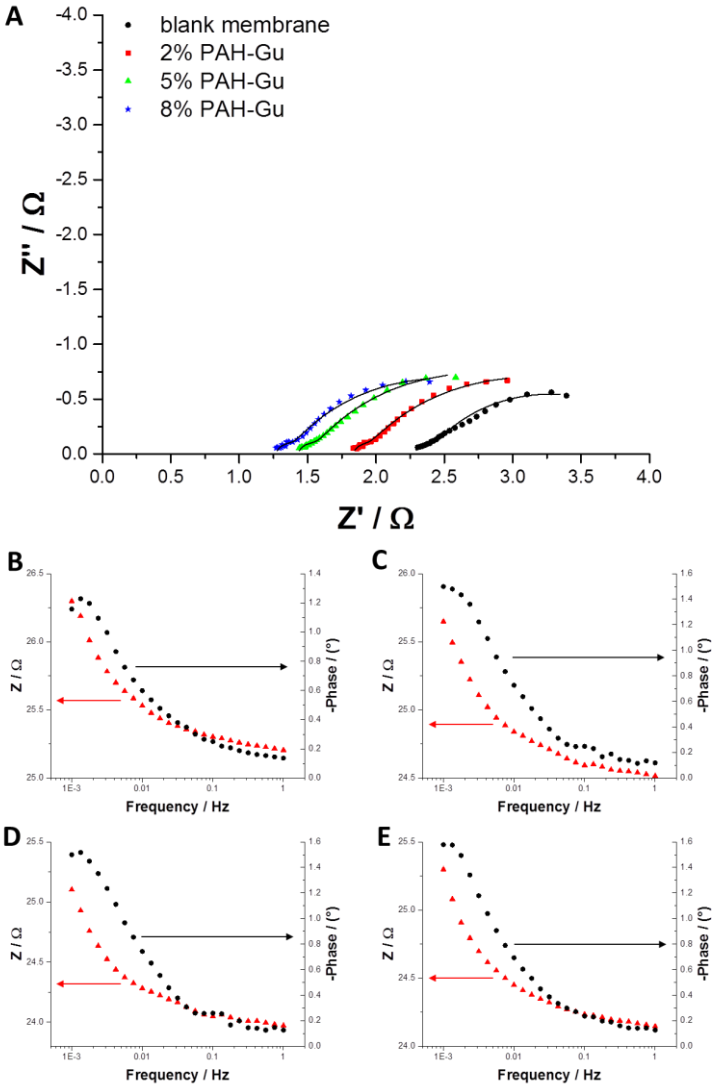

Figure S3.2 Nyquist plots recorded in the electrodialysis set-up (see Figure 3.2 in Chapter 3) containing 0.1 M NaH_2PO_4 in compartments 3 and 4; 0.5 M NaH_2PO_4 in compartments 2 and 5 after background resistance subtraction. Black lines correspond to best fit using the equivalent circuit shown in Figure A, B, C, D and E are the Bode modulus/phase plots for blank, 2 wt% PAH-Gu, 5 wt% PAH-Gu and 8 wt% PAH-Gu membranes respectively.

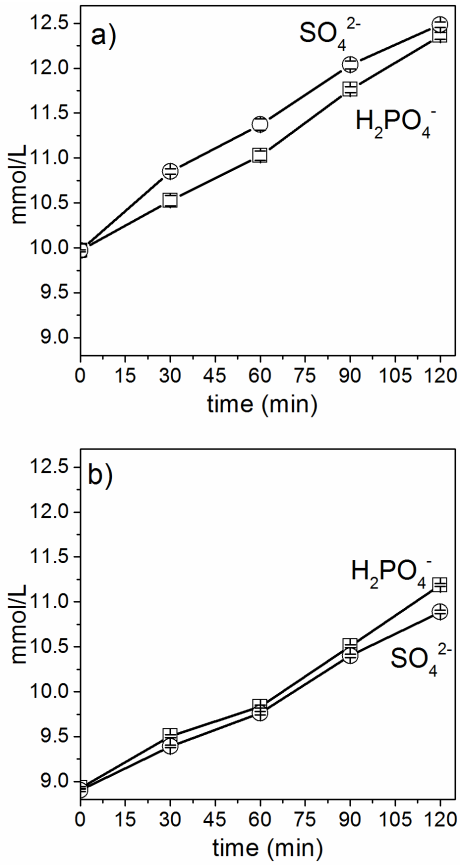

Figure S3.3 Electrodialysis data showing the increase of dihydrogen monophosphate (squares) and sulfate concentration (circles) in the receiving phase (compartment 3) as a function of time for a) Fuji_AEM and b) 5 wt% PAH-Gu.

References

(1) Schröder, J.; Cordell, D.; Smit, A. L.; Rosemarin, A. *Sustainable Use of Phosphorus*; 2010.

(2) FAO. *Current World Fertilizer Trends and Outlook to 2016*; 2012.

(3) Conley, D. J. H. Paerl, W. Howarth, R. W. Boesch, D. F. Seitzinger, S. P. Havens, K. E.Lancelot, C. Likens, G. E. Controlling Eutrophication: Nitrogen and Phosphorus. *Science* 2009, *323*, 1014–1015.

(4) Hudson, J. J.; Taylor, W. D.; Schindler, D. W. Phosphate Concentrations in Lakes. *Nature* 2000, *400*, 55–56.

(5) Van Vuuren, D. P.; Bouwman, A. F.; Beusen, A. H. W. Phosphorus Demand for the 1970-2100 Period: A Scenario Analysis of Resource Depletion. *Glob. Environ. Chang.* 2010, *20*, 428–439.

(6) Desmidt, E.; Ghyselbrecht, K.; Zhang, Y.; Pinoy, L.; Van der Bruggen, B.; Verstraete, W.; Rabaey, K.; Meesschaert, B. Global Phosphorus Scarcity and Full- Scale P-Recovery Techniques: A Review. *Crit. Rev. Environ. Sci. Technol.* 2015, *45*, 336–384.

(7) Wilfert, P.; Suresh Kumar, P.; Korving, L.; Witkamp, G.-J.; Van Loosdrecht, M. C. M. The Relevance of Phosphorus and Iron Chemistry to the Recovery of Phosphorus from Wastewater: A Review. *Environ. Sci. Technol.* 2015, *49*, 9400–9414.

(8) Huang, H.; Yang, J.; Li, D. Recovery and Removal of Ammonia–nitrogen and Phosphate from Swine Wastewater by Internal Recycling of Struvite Chlorination Product. *Bioresour. Technol.* 2014, *172*, 253–259.

(9) Hao, X.; Wang, C.; Van Loosdrecht, M. C. M.; Hu, Y. Looking beyond Struvite for P-Recovery. *Environ. Sci. Technol.* 2013, *47*, 4965–4966.

(10) Niewersch, C.; Battaglia Bloch, A. L.; Yüce, S.; Melin, T.; Wessling, M. Nanofiltration for the Recovery of Phosphorus - Development of a Mass Transport Model. *Desalination* 2014, *346*, 70–78.

(11) Tran, A. T. K., Zhang, Y., De Corte, D., Hannes, J. B., Ye, W., Mondal, P., Van Der Bruggen, B. P-Recovery as Calcium Phosphate from Wastewater Using an Integrated Selectrodialysis/crystallization Process. *J. Clean. Prod.* 2014, *77*, 140–151.

(12) Zhang, Y.; Desmidt, E.; Van Looveren, A.; Pinoy, L.; Meesschaert, B.; Van Der Bruggen, B. Phosphate Separation and Recovery from Wastewater

by Novel Electrodialysis. *Environ. Sci. Technol.* 2013, *47* (11), 5888–5895.

(13) Wang, X.; Wang, Y.; Zhang, X.; Feng, H.; Li, C.; Xu, T. Phosphate Recovery from Excess Sludge by Conventional Electrodialysis (CED) and Electrodialysis with Bipolar Membranes (EDBM). *Ind. Eng. Chem. Res.* 2013, *52* (45), 15896–15904.

(14) Hamad, J. Z.; Ha, C.; Kennedy, M. D.; Amy, G. L. Application of Ceramic Membranes for Seawater Reverse Osmosis (SWRO) Pre-Treatment. *Desalin. Water Treat.* 2013, *51*, 4881–4891.

(15) Chen, G. Electrochemical Technologies in Wastewater Treatment. *Sep. Purif. Technol.* 2004, *38*, 11–41.

(16) Strathmann, H. Ion-Exchange Membrane Processes in Water Treatment. *Sustain. Sci. Eng. Elsevier* 2010, *2*, 141–199.

(17) Sata, T. *Ion Exchange Membranes Preparation, Characterization, Modification and Application*; RSC, 2004.

(18) Dlugolecki, P.; Nijmeijer, K.; Metz, S.; Wessling, M. Current Status of Ion Exchange Membranes for Power Generation from Salinity Gradients. *J. Memb. Sci.* 2008, *319*, 214–222.

(19) Park, H. B.; Kamcev, J.; Robeson, L. M.; Elimelech, M.; Freeman, B. D. Maximizing the Right Stuff: The Trade-off between Membrane Permeability and Selectivity. *Science* 2017, *356*, 1–10.

(20) Zeng, J.; Zhang, Z.; Dong, Z.; Ren, P.; Li, Y.; Liu, X. Fabrication and Characterization of an Ion-Imprinted Membrane via Blending Poly(methyl Methacrylate-Co-2-Hydroxyethyl Methacrylate) with Polyvinylidene Fluoride for Selective Adsorption of Ru(III). *React. Funct. Polym.* 2017, *115*, 1–9.

(21) Luo, T.; Abdu, S.; Wessling, M. Selectivity of Ion Exchange Membranes: A Review. *J. Memb. Sci.* 2018, *555* (December 2017), 429–454.

(22) Jiang, Y.; Liao, J.; Yang, S.; Li, J.; Xu, Y.; Ruan, H.; Sotto, A.; Van der Bruggen, B.; Shen, J. Stable Cycloaliphatic Quaternary Ammonium-Tethered Anion Exchange Membranes for Electrodialysis. *React. Funct. Polym.* 2018, *130*, 61–69.

(23) Geise, G. M.; Cassady, H. J.; Paul, D. R.; Logan, B. E.; Hickner, M. A.; Logan, E.; Hickner, M. A. Specific Ion Effects on Membrane Potential and the Permselectivity of Ion Exchange Membranes. *Phys. Chem. Chem. Phys.* 2014, *16* (39), 21673–21681.

(24) Takata, K.; Yamamoto, Y.; Sata, T. Modification of Transport Properties of Ion Exchange Membranes XIV . Effect of Molecular Weight of Polyethyleneimine Bonded to the Surface of Cation Exchange Membranes by Acid – Amide Bonding on Electrochemical Properties of the Membranes. *J. Memb. Sci.* 2000, *179*, 101–107.

(25) Chapotot, A.; Lopez, V.; Lindheimer, A.; Aouad, N.; Gavach, C. Electrodialysis of Acid Solutions with Metallic Divalent Salts: Cation-Exchange Membranes with Improved Permeability to Protons. *Desalination* 1995, *101*, 141–153.

(26) Cassady, H. J.; Cimino, E. C.; Kumar, M.; Hickner, M. A. Specific Ion Effects on the Permselectivity of Sulfonated Poly(ether Sulfone) Cation Exchange Membranes. *J. Memb. Sci.* 2016, *508*, 146–152.

(27) Nasef, M. M.; Nallappan, M.; Ujang, Z. Polymer-Based Chelating Adsorbents for the Selective Removal of Boron from Water and Wastewater: A Review. *React. Funct. Polym.* 2014, *85*, 54–68.

(28) Branger, C.; Meouche, W.; Margaillan, A. Recent Advances on Ion-Imprinted Polymers. *React. Funct. Polym.* 2013, *73*, 859–875.

(29) Hosseini, S. M.; Nemati, M.; Jeddi, F.; Salehi, E.; Khodabakhshi, R.; Madaeni, S. S. Fabrication of Mixed Matrix Heterogeneous Cation Exchange Membrane Modified by Titanium Dioxide Nanoparticles: Mono/bivalent Ionic Transport Property in Desalination. *Desalination* 2015, *359*, 167–175.

(30) Farrokhzad, H.; Moghbeli, M. R.; Van Gerven, T.; Van der Bruggen, B. Surface Modification of Composite Ion Exchange Membranes by Polyaniline. *React. Funct. Polym.* 2015, *86*, 161–167.

(31) Vaselbehagh, M.; Karkhanechi, H.; Takagi, R.; Matsuyama, H. Surface Modification of an Anion Exchange Membrane to Improve the Selectivity for Monovalent Anions in Electrodialysis - Experimental Verification of Theoretical Predictions. *J. Memb. Sci.* 2015, *490*, 301–310.

(32) Güler, E.; van Baak, W.; Saakes, M.; Nijmeijer, K. Monovalent-Ion-Selective Membranes for Reverse Electrodialysis. *J. Memb. Sci.* 2014, *455*, 254–270.

(33) Femmer, R.; Mani, A.; Wessling, M. Ion Transport through Electrolyte/polyelectrolyte Multi-Layers. *Sci. Rep.* 2015, *5*, 1–12.

(34) Wijeratne, S.; Bruening, M. L.; Baker, G. L. Layer-by-Layer Assembly of

Thick, Cu^{2+} Chelating Films. *Langmuir* 2013, *29*, 12720–12729.

(35) Wijeratne, S.; Liu, W.; Dong, J.; Ning, W.; Ratnayake, N. D.; Walker, K. D.; Bruening, M. L. Layer-by-Layer Deposition with Polymers Containing Nitrilotriacetate, A Convenient Route to Fabricate Metal- and Protein-Binding Films. *Appl. Mater. Interfaces* 2016, *8*, 10164–10173.

(36) Ullien, D.; Harmsma, P. J.; Abdulla, S. M. C.; de Boer, B. M.; Bosma, D.; Sudhölter, E. J. R.; de Smet, L. C. P. M.; Jager, W. F. Protein Detection on Biotin-Derivatized Polyallylamine by Optical Microring Resonators. *Opt. Express* 2014, *22*, 16585–16594.

(37) Van der Mee, L.; Chow, E. S. Y.; de Smet, L. C. P. M.; de Puit, M.; Sudhölter, E. J. R.; Jager, W. F. Fluorescent Polyelectrolyte for the Visualization of Fingermarks. *Anal. Methods* 2015, *7*, 10121–10124.

(38) Wang, S.; Yu, D.; Dai, L.; Chang, D. W.; Baek, J.-B. Polyelectrolyte-Functionalized Graphene as Metal-Free Electrocatalysts for Oxygen Reduction. *ACS Nano* 2011, *5*, 6202–6209.

(39) Cao, Z.; Gordiichuk, P. I.; Loos, K.; Sudhölter, E. J. R.; de Smet, L. C. P. M. The Effect of Guanidinium Functionalization on the Structural Properties and Anion Affinity of Polyelectrolyte Multilayers. *Soft Matter* 2016, *12*, 1496–1505.

(40) Paltrinieri, L.; Wang, M.; Sachdeva, S.; Besseling, N. A. M.; Sudhölter, E. J. R.; de Smet, L. C. P. M. Fe_3O_4 Nanoparticles Coated with a Guanidinium-Functionalized Polyelectrolyte Extend the pH Range for Phosphate Binding. *J. Mater. Chem. A* 2017, *5*, 18476–18485.

(41) Abdu, S.; Marti-Calatayud, M.-C.; Wong, J. E.; Garcia-Gabaldon, M.; Wessling, M. Layer-by-Layer Modification of Cation Exchange Membranes Controls Ion Selectivity and Water Splitting. *Appl. Mater. Interfaces* 2014, *6*, 1843–1854.

(42) Vyas, P. V.; Shah, B. G.; Trivedi, G. S.; Ray, P.; Adhikary, S. K.; Rangarajan, R. Studies on Heterogeneous Cation-Exchange Membranes. *React. Funct. Polym.* 2000, *44* (2), 101–110.

(43) Mulyati, S.; Takagi, R.; Fujii, A.; Ohmukai, Y.; Matsuyama, H. Simultaneous Improvement of the Monovalent Anion Selectivity and Antifouling Properties of an Anion Exchange Membrane in an Electrodialysis Process, Using Polyelectrolyte Multilayer Deposition. *J. Memb. Sci.* 2013, *431*, 113–120.

(44) Hutter, J. L.; Bechhoefer, J. Calibration of Atomic-Force Microscope Tips. *Rev. Sci. Instrum.* 1993, *64*, 1868–1873.

(45) Cappella, B.; Dietler, G. Force-Distance Curves by Atomic Force Microscopy. *Surf. Sci. Rep.* 1999, *34*, 1–104.

(46) Ho, J. S.; Low, J. H.; Sim, L. N.; Webster, R. D.; Rice, S. A.; Fane, A. G.; Coster, H. G. L. In-Situ Monitoring of Biofouling on Reverse Osmosis Membranes: Detection and Mechanistic Study Using Electrical Impedance Spectroscopy. *J. Memb. Sci.* 2016, *518*, 229–242.

(47) Pismenskaia, N.; Sistat, P.; Huguet, P.; Nikonenko, V.; Pourcelly, G. Chronopotentiometry Applied to the Study of Ion Transfer through Anion Exchange Membranes. *J. Memb. Sci.* 2004, *228*, 65–76.

(48) Zhang, W.; Wang, P.; Ma, J.; Wang, Z.; Liu, H. Investigations on Electrochemical Properties of Membrane Systems in Ion-Exchange Membrane Transport Processes by Electrochemical Impedance Spectroscopy and Direct Current Measurements. *Electrochim. Acta* 2016, *216*, 110–119.

(49) Krol, J. J.; Wessling, M.; Strathmann, H. Concentration Polarization with Monopolar Ion Exchange Membranes: Current-Voltage Curves and Water Dissociation. *J. Memb. Sci.* 1999, *162*, 145–154.

(50) Dlugolecki, P.; Ogonowski, P.; Metz, S. J.; Saakes, M.; Nijmeijer, K.; Wessling, M. On the Resistances of Membrane, Diffusion Boundary Layer and Double Layer in Ion Exchange Membrane Transport. *J. Memb. Sci.* 2010, *349*, 369–379.

(51) Zhang, W.; Wang, P.; Ma, J.; Wang, Z.; Liu, H. Investigations on Electrochemical Properties of Membrane Systems in Ion-Exchange Membrane Transport Processes by Electrochemical Impedance Spectroscopy and Direct Current Measurements. *Electrochim. Acta* 2016, *216*, 110–119.

(52) Zhu, Y.; Ahmad, M.; Yang, L.; Misovich, M.; Yaroshchuk, A.; Bruening, M. L. Adsorption of Polyelectrolyte Multilayers Imparts High Monovalent/divalent Cation Selectivity to Aliphatic Polyamide Cation-Exchange Membranes. *J. Memb. Sci.* 2017, *537*, 177–185.

(53) Sata, T. Studies on Anion Exchange Membranes Having Permselectivity for Specific Anions in Electrodialysis - Effect of Hydrophilicity of Anion Exchange Membranes on Permselectivity of Anions. *J. Memb. Sci.* 2000,

167, 1–31.

(54) Stevens, J. S.; De Luca, A. C.; Pelendritis, M.; Terenghi, G.; Downes, S.; Schroeder, S. L. M. Quantitative Analysis of Complex Amino Acids and RGD Peptides by X-Ray Photoelectron Spectroscopy (XPS). *Surf. Interface Anal.* 2013, *45*, 1238–1246.

(55) Richardson, J. J.; Bjornmalm, M.; Caruso, F. Technology-Driven Layer-by-Layer Assembly of Nanofilms. *Science* 2015, *348*, 1–11.

(56) Kim, S. H.; Opdahl, A.; Marmo, C.; Somorjai, G. A. AFM and SFG Studies of pHEMA-Based Hydrogel Contact Lens Surfaces in Saline Solution: Adhesion, Friction, and the Presence of Non-Crosslinked Polymer Chains at the Surface. *Biomaterials* 2002, *23* (7), 1657–1666.

(57) Jones, R.; Pollock, H. M.; Cleaver, J. A. S.; Hodges, C. S. Adhesion Forces between Glass and Silicon Surfaces in Air Studied by AFM: Effects of Relative Humidity, Particle Size, Roughness, and Surface Treatment. *Langmuir* 2002, *18* (21), 8045–8055.

(58) Geise, G. M.; Hickner, M. A.; Logan, B. E. Ionic Resistance and Permselectivity Tradeoffs in Anion Exchange Membranes. *ACS Appl. Mater. Interfaces* 2013, *5*, 10294–10301.

(59) Tanaka, Y. Ion Exchange Membranes: Fundamentals and Application; *Elsevier*, 2015.

(60) Geise, G. M.; Paul, D. R.; Freeman, B. D. Fundamental Water and Salt Transport Properties of Polymeric Materials. *Prog. Polym. Sci.* 2014, *39*, 1–24.

(61) Lide, D. R. CRC Handbook of Chemistry and Physics, 84th Edition, 2003-2004. *Handb. Chem. Phys.* 2003, *53*, 2616.

(62) Sarapulova, V.; Nevakshenova, E.; Pismenskaya, N.; Dammak, L.; Nikonenko, V. Unusual Concentration Dependence of Ion-Exchange Membrane Conductivity in Ampholyte-Containing Solutions: Effect of Ampholyte Nature. *J. Memb. Sci.* 2015, *479*, 28–38.

(63) Belashova, E. D.; Pismenskaya, N. D.; Nikonenko, V. V; Sistat, P.; Pourcelly, G. Current-Voltage Characteristic of Anion-Exchange Membrane in Monosodium Phosphate Solution . Modelling and Experiment. *J. Memb. Sci.* 2017, *542*, 177–185.

(64) Franck-Lacaze, L.; Sistat, P.; Huguet, P. Determination of the pKa of Poly (4-Vinylpyridine)-Based Weak Anion Exchange Membranes for the

Investigation of the Side Proton Leakage. *J. Memb. Sci.* 2009, *326*, 650–658.

(65) Fibbioli, M.; Berger, M.; Schmidtchen, F. P.; Pretsch, E. Polymeric Membrane Electrodes for Monohydrogen Phosphate and Sulfate. *Anal. Chem.* 2000, *72*, 156–160.

(66) Chaniotakis, N. a; Jurkschat, K.; Ruehlemann, A. Potentiometric Phosphate Selective Electrode Based on a Multidentate-tin(IV) Carrier. *Anal. Chim. Acta* 1993, *282*, 345–352.

(67) Galama, A. H.; Vermaas, D. A.; Veerman, J.; Saakes, M.; Rijnaarts, H. H. M.; Post, J. W.; Nijmeijer, K. Membrane Resistance: The Effect of Salinity Gradients over a Cation Exchange Membrane. *J. Memb. Sci.* 2014, *467*, 279–291.

(68) Pantos, A.; Tsogas, I.; Paleos, C. M. Guanidinium Group: A Versatile Moiety Inducing Transport and Multicompartmentalization in Complementary Membranes. *Biochim. Biophys. Acta - Biomembr.* 2008, *1778*, 811–823.

(69) Kivlehan, F.; Mace, W. J.; Moynihan, H. A.; Arrigan, D. W. M. Study of Electrochemical Phosphate Sensing Systems: Spectrometric, Potentiometric and Voltammetric Evaluation. *Electrochim. Acta* 2009, *54*, 1919–1924.

(70) Steed, J. W.; Atwood, J. L. *Supramolecular Chemistry 2nd Ed.*; 2009.

(71) Liu, L.; Li, Q.; Dai, J.; Wang, H.; Jin, B.; Bai, R. A Facile Strategy for the Synthesis of Guanidinium-Functionalized Polymer as Alkaline Anion Exchange Membrane with Improved Alkaline Stability. *J. Memb. Sci.* 2014, *453*, 52–60.

(72) Sajjad, S. D.; Hong, Y.; Liu, F. Synthesis of Guanidinium-Based Anion Exchange Membranes and Their Stability Assessment. *Polym. Adv. Technol.* 2014, *25*, 108–116.

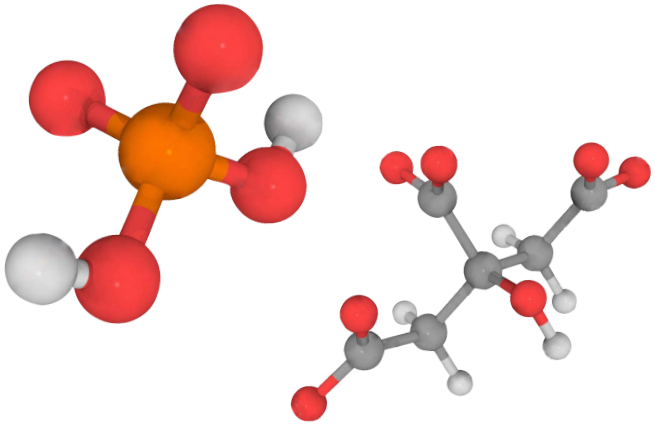

CHAPTER 4

Functionalized anion exchange membrane facilitates electrodialysis of citrate and phosphate from model diary wastewater

In this study, the preparation of a new, functional anion-exchange membrane (AEM), containing guanidinium groups as the anion-exchanging sites (Gu-100), is described as well as the membrane characterization by XPS, water uptake, permselectivities, and electrical resistances. The functional membrane was also employed in pH-dependent electrodialysis experiments using model dairy wastewater streams. The properties of the new membrane are compared to those of a commercially available anion-exchange membrane bearing the conventional quaternary ammonium groups (Gu-0). Guanidinium was chosen for its specific binding properties towards oxyanions, *e.g.,* phosphate. This functional moiety was covalently coupled to an acrylate monomer via a facile two-step synthesis to yield bulk-modified membranes upon polymerization. Significant differences were observed in the electrodialysis experiments for Gu-0 and Gu-100 at pH =7, showing an enhanced phosphate and citrate transport for Gu-100 compared to Gu-0. At pH = 10 the difference is much more pronounced: for Gu-0 membranes almost no phosphate and citrate transport could be detected, while the Gu-100 membranes transported both ions significantly. We conclude that having guanidinium groups as anionic-exchange sites improve the selectivity of AEMs. As the presented monomer synthesis strategy is modular, we consider the implementation of functional groups into polymer-based membrane via the synthesis of tailor-made monomers as an important step toward selective ion transport, which is relevant for various field including water treatment processes and fuel cells.

The content of this chapter has been published in :

Laura Paltrinieri, Elisa Huerta, Theo Puts, Willem van Baak, Albert B. Verver, Ernst J. R. Sudhölter, Louis C. P. M. de Smet, *Journal of Environmental Science and Technology,* **2019**

Introduction

Providing innovative separation technologies for a sustainable water supply is a key challenge facing society.[1,2] Electrical-driven based technologies such as electrodialysis (ED),[3] membrane capacitive deionization (MCDI)[4,5], reverse electrodialysis (RED)[6] are efficient and versatile systems for water treatment that can effectively overcome the global need for the supply and reuse of water. Mentioned technologies rely on the use of Ion-Exchange Membranes (IEMs) as the core of the separation process. Under applied current or potential, cations can cross Cation-Exchange Membranes (CEMs) while anions can permeate through Anion-Exchange Membranes (AEMs), resulting in an alternating concentrated and depleted compartment. IEMs have been employed extensively in several sectors such as brine concentration[7], wastewater treatment[8], nutrient recovery[9], organic compound separation[10], mineral production from acids and bases[11], and acid production[12]. Most recently, IEMs have been used for the ED of dairy industrial effluents as advanced food processing technology.[13] The process has been applied for the separation of various ions, including lactate[14], citrate[15], potassium[16], magnesium[16], sodium[17], chloride[17] and phosphate[18]. Thus, ED effectively removes ions from various feed streams, but typically IEMs exhibit a low selectivity when exposed to complex matrix solutions. High selectivities towards specific ions are required when the final goal is the recovery and reuse of the target compounds. Although variations of operational parameters (*e.g.,* current density, flow rate, stacks design) can provide a certain control over ion-transport, tuning the (perm)selectivity properties of IEMs by synthetic approaches is becoming of increasing interest and importance[19].

Over the past years, several research groups started investigating the fabrication and/or modification of IEMs to increase their selectivity. Often used are polyelectrolytes, which are deposited as multilayers on top of IEMs to improve monovalent/divalent selectivity, for example K^+/Mg^{2+}, Cl^-/SO_4^{2-} or Cl^-/Ca^{2+} [20–22]. Other methods involve the use of monomers grafted at membrane surfaces to reduce co-ion permeability [23] or to facilitate permeation of certain compounds, like urea[24]. Recently nanoparticles have been incorporated in the IEM to improve Na^+/Ba^{2+} transport[25]. While these studies nicely show the potential of functionalizing membranes to tune selectivity, most of the experiments are carried out with solutions containing only two different salts, reflecting a strong simplification of industrially relevant conditions.

In this study, we developed a new AEM exclusively composed of receptor-groups and we examined the ion-selective properties, in comparison with a commercial AEM, when being exposed to a complex model dairy solution. In more detail, to improve the membrane ion-transport performances, we synthesized an acrylate monomer containing the guanidinium receptor(Gu) as a building block for the AEM fabrication via UV-polymerization. Gu can form preferential bonds with oxyanions[26–28], which are abundant in dairy effluents. In addition, Gu is a versatile group which can be easily functionalized with specific chemical groups, in this case an acrylate. Gu has been already combined with AEM to enhance alkaline stability[29–31] or to increase membrane conductivity[32]. However, research on the integration of functional groups, like Gu, with membranes aiming to improve ion selectivity is at its infancy. Recently, we blended a Gu-based polyelectrolyte with AEM building blocks to prepare a functionalized AEM aiming to facilitate $H_2PO_4^-/SO_4^{2-}$ transport.[33] The addition of 8 wt % of functionalized polyelectrolyte resulted in an increased permeation of phosphate over sulfate when applied in electrodialysis. In the current study, the electrochemical properties of a Gu-functionalized AEM of which the fixed charges are exclusively due to the presence of the covalently linked Gu groups were investigated in detail and correlated with the observed membrane selectivity performances. The membranes were investigated using a model dairy wastewater composition.

Materials and Methods

Materials

All chemicals listed in this section were used are received, unless stated otherwise. 3-Amino-1-propanol, 2-ethyl-2-thiopseudourea, acryloyl chloride and triethylamine were purchased from Sigma-Aldrich and used for the synthesis of the guanidinium acrylate monomer. Acetonitrile (anhydrous, 99.8 %, Sigma), ethylacetate (anhydrous, 99.8%, Sigma), ethanol (BioUltra > 99.8%, Sigma), methanol (anhydrous, 99.8%, Sigma) and MilliQ water (Millipore, 18.2 MΩ cm^2, T = 24.5°C) were used as solvent during the synthetic steps. A standard grade AEM, having quaternary ammonium as fixed charged groups, from Fujifilm Manufacturing Europe BV (the Netherlands, hereafter Fuji) was selected as a reference membrane. To obtain a guanidinium acrylate based membrane we used N,N-methylene-*bis*-(acrylamide) (99% Sigma) as cross-linker, 2-hydroxy-2-methyl-1-phenyl-1-propane (Darocure1173, Ciba Specialty Chemicals) as the free-radical photo-initiator, TEGO® Glide (Evonik) as surfactant, Hydroquinone monomethyl

ether (MEHQ) as an inhibitor, and a polypropylene non-woven material was used as substrate for the membrane formation during the UV polymerization. Demi water and *iso*-propanol (Sigma) were used as solvents during membrane fabrication. Sodium phosphate monobasic monohydrate (>98%, $NaH_2PO_4 \cdot H_2O$, Across Organic), sodium phosphate dibasic (Na_2HPO_4, 99.95%, Sigma), sodium sulfate (>99%, Na_2SO_4, Sigma), sodium chloride (NaCl, 99.5%, Sigma), sodium citrate tribasic hydrate (ReagentPlus, >99%, Sigma) and sodium L-lactate (98%, Sigma) were used to prepare the model aqueous dairy solutions.

Monomer synthesis

Scheme 4.1 shows the two-step synthesis developed to obtain the guanidinium acrylate monomer. Guanidinopropanol (**1**) was synthesized according to Funhoff et al.[34] In detail, 8.54 mMol of 3-aminopropanol was slowly added to 8.54 mMol of 2-ethyl-2-thiopseudourea hydrobromide in a 100 mL flask. Subsequently, 2 mL of MilliQ was added. The solution was stirred overnight at room temperature (RT). Next, water was removed under reduced pressure to obtain a viscous transparent liquid (yield 16.47 mMol, 96%). For the synthesis of guanidinium acrylate monomer (**2**), compound (**1**) (1.67 g = 8.43 mMol) was stirred in acetonitrile (5 mL) at RT for 1 h. Freshly activated molecular sieves (4 Å, Sigma) were added to the solution in order to remove residual amounts of water. Triethylamine (0.85 mL = 8.43 mMol) was added dropwise, followed by the dropwise addition of 0.76 mL (8.43 mMol) of acryloyl chloride. The solution was stirred for 24 h and kept in an ice bath to avoid pre-polymerization. The acetonitrile was removed under vacuum. The product (**2**) was washed with EtAc:EtOH (1:1) to remove any unreacted Et_3N and filtered to remove the molecular sieves. Purification was done by column chromatography using MeOH:EtAc (20:80) as eluent. ^{1}H NMR spectra were recorded using a Bruker AVANCE 400 NMR spectrometer with D_2O as solvent. For (**2**) the following ^{1}H NMR (CD_3OD) was obtained δ (ppm): 7.4 (s, 1H, NH), 6.8 (s, 1H, NH), 6.4 (d, 1H, CH, J = 17.2 Hz), 5.8 (d, 1H, CH, J = 10.5 Hz), 6.1 (m, 1H, CH, J = 27.7 Hz), 4.2 (t, 2H, CH_2, J = 12 Hz), 3.2 (t, 2H, CH_2, J = 13.9 Hz), 1.9 (m, 2H, CH_2, J = 23.7 Hz). Yield: 1.64 mMol, 40 wt %. The molecular mass of (**2**) was confirmed by liquid-chromatography LC-MS (Shimadzu 2010A LCMS, ESI/ APCI) as it yielded m / z $[M + H]^+$ = 171.80. The FT-IR spectrum of (**2**) was obtained using a Nicolet 8700 FT-IR. The spectra were recorded over a range of 4000–400 cm^{-1} at a resolution of 4 cm^{-1}.

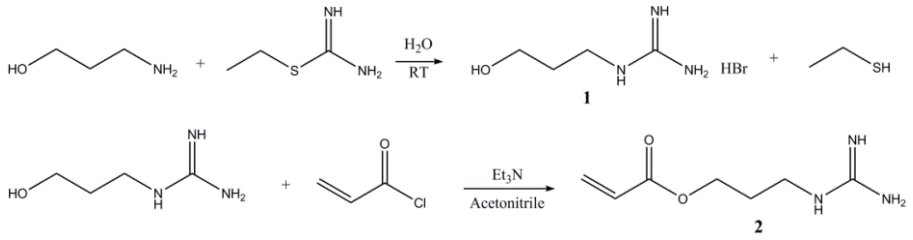

Scheme 4.1 Reaction scheme for the two-step synthesis of: (**1**) guanidinium propanol and (**2**) the guanidinium acrylate monomer.

Membrane fabrication

The guanidinium acrylate based AEM was prepared via a UV-polymerization reaction initiated by free-radicals from the active double bonds of the Darocure1173 photo-initiator. In detail, 0.053 mol of (**2**) and 0.017 mol of cross-linker were added to 2 mL of demi-water and 1.7 mL of *iso*-propanol and mixed until a clear solution was obtained. Next, 1 wt % of TEGO®Glide, 1 wt % of MEHQ, and 0.05 wt % of Darocure1173 were added to the mixture. The mixture was cast into films by coating a non-woven polypropylene substrate with a 12 µm wire-wound coating bar. The membrane was exposed to UV-irradiation (240 W/cm) through a bench-top conveyor system (Heraeus Noblelight Fusion UV inc. USA). A mercury H-bulb (240-280 nm) working at 100% intensity was used, and the conveyor speed was 30 m·min^{-1} with a single pass. The obtained membrane was referred to as Gu-100, indicating that 100% of the exchange sites are Gu groups. The membrane formulation was prepared such that the amount of exchange sites was comparable to the amount of quaternary groups present in the reference AEM, *i.e.* a standard grade Fuji membrane, here referred to as Gu-0 (2.71 mMol·g^{-1} and 2.83 mMol·g^{-1} for Gu-100 and Gu-0, respectively). The membrane thickness was found to be 142 ± 2 µm for Gu-0 and 148 ± 2 µm for Gu-100 as measured with a digital screw micrometer (Mitutoyo Corporation, Japan, model 293-240-30).

Membranes characterizations

The membrane water uptake (w_{uptake}) was determined by application of the following equation:[35]

$$w_{\text{uptake}} = \frac{m_{\text{wet}} - m_{\text{dry}}}{m_{\text{wet}}} \quad [\%] \qquad (4.1)$$

where m_{wet} and m_{dry} are the membrane masses in the wet and dry state, respectively. The wet mass was obtained after immersing the membrane in Milli-Q water for 48 h. The excess of water on the membrane surface was quickly removed using laboratory wipes. For the dry mass, samples were dried in vacuum oven at 50°C for 48 h. The w_{uptake} is reported as an average of the measurements for three different membranes.

Elemental composition by X-ray Photoelectron Spectroscopy (XPS, Thermo Fisher Scientific, K-Alpha model) was used to determine the surface atomic composition of Gu-100 and Gu-0 membranes. A monochromatic Al K_α X-ray source with a spot size of 400 µm at a pressure of 10^{-7} mbar, a constant pass energy of 400 eV for the survey spectra and 50 eV for the detailed high-resolution spectra were used. The flood gun was turned on during the measurement to compensate for potential charging of the surface. The peak position was adjusted based on the internal standard C1s peak at 284.8 eV, with an accuracy of ±0.05 eV. Avantage processing software was used to analyze all spectra.

Membrane permselectivity (PS) values indicate to which extent counter-ions (anions) are transported through the membrane and co-ions (cations) are rejected, and was determined from the deviation of the experimental observed membrane potential compared to the calculated membrane potential for 100% permselective membranes (Nernst potential), using the Donnan theory.[36] We measured the PS for a selected number of anions as listed in Table 4.1: chloride, a monovalent anion commonly used as a reference and it is abundantly present in dairy effluent; phosphate, a pH-dependent anion (here measured both at pH = 5 and pH = 10); and sulfate, as a representative divalent anion. Anions where measured separately for a total of four individual experiments and the concentrations were 0.05 M and 0.5 M for each compartment, respectively. Since no current is applied during the PS experiment, ion transport through the membrane is mainly determined by diffusion.[35,37] Membrane PS was determined with a two-compartment cell[38] (custom-made by STT Products, The Netherlands), as illustrated in Figure S3.1 of the supporting information of Chapter 3. The membrane was placed in the sample holder with an effective cross-sectional area of 8.14 cm^2 separating two salt solutions. The potential difference between two Ag/AgCl double-junction reference electrodes (Methrom, the Netherlands) separated with the membrane under investigation (E_x) was measured with the digital multimeter (Digimess). The potential was read out after reaching stabilization (typically after 3-5

min.). The experimental membrane potential (E_m) was then obtained by subtracting the offset potential (E_{offset}) of the electrodes, measured in 3 M KCl solutions[38,39]:

$$E_m = E_x - E_{offset} \quad [mV] \quad (4.2)$$

The final value of permselectivity (%*PS*) was calculated as the ratio between experimental determined E_m and the theoretical calculated Nernst potential (E_{Nernst}) for 100% permselectivity [38,39]:

$$PS = \frac{E_m}{E_{Nernst}} \times 100\% \quad [\%] \quad (4.3)$$

E_{Nernst} was calculated using the following formula:

$$E_{Nernst} = \frac{RT}{nF} ln \frac{C_1 \gamma_1}{C_2 \gamma_2} \quad [mV] \quad (4.4)$$

where *R* is the gas constant, *T* is the temperature in Kelvin, *F* is the Faraday constant, *n* is the valency of the transferring ion and C_1 and C_2 and γ_1 and γ_2 are the concentrations and the activity coefficients of the transferring anion in the diluted and the concentrate compartment, respectively. The electrolyte solutions were continuously recirculated by using two peristaltic pumps (Masterflex Peristaltic pumps, model L/S Economy Pump System with Easy-Load II pump head 230 VAC, the Netherlands) keeping a constant flow rate of 110 mL/min in each compartment. A thermal bath (Thermo Fisher Scientific Inc, USA) was used to maintain a constant temperature of 20 ± 0.5°C.

Membrane electrical resistance (ER) was measured for Gu-100 and Gu-0, and the values reflect the ion mobilities in the membrane. The higher the resistance, the lower the ion mobility[40,41]. Obviously, a low membrane resistance is preferred. The ER was determined by using a conventional six compartment cells (custom-made by STT Products, The Netherlands).[40] Membranes between compartments were placed according to the configuration shown in Figure 4.1. ER was determined with a four-electrode configuration with chronopotentiometry measurements by applying a direct current increased step by step (*i.e.,* 0, 0.05, 0.06…0.3 and every 30 s) via a power supply (Autolab, potentiostat/galvanostat PGSTAT302N).[42] The voltage across the membrane under investigation was measured with a voltage meter through Haber-Lugging capillaries. Compartments containing anode and cathode (compartment 1 and 6 in Figure 4.1) were filled with 0.5 M Na_2SO_4 solution, the other compartments

contained NaH_2PO_4 (at pH = 5), Na_2HPO_4 (at pH = 10), NaCl and Na_2SO_4, which were measured separately at a concentration of 0.5 M for a total of four experiments. Electrolytes solutions were circulated individually at the same flow rate of 250 mL·min^{-1} and temperature was fixed at 25 ± 0.5°C by using a thermal bath (Thermo Fisher Scientific Inc, USA). Prior to the analysis a blank measurement without a membrane was done, and the registered value was subtracted from each measurement. Before usage, the membranes were equilibrated for 48 h in the same salt solution as used in the analysis.

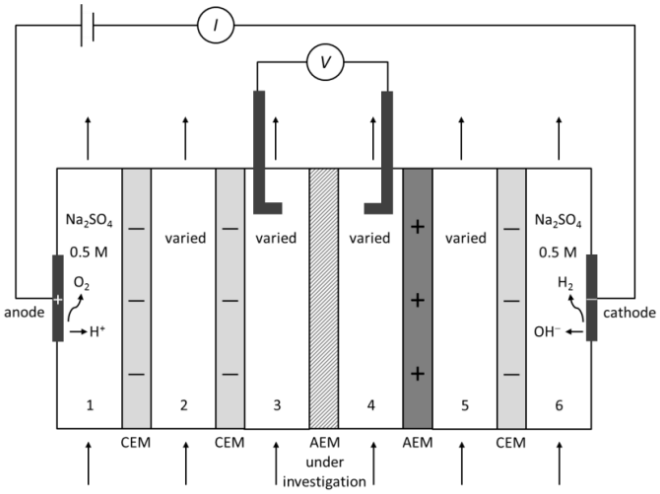

Figure 4.1 Scheme of the set-up used to perform electrochemical impedance spectroscopy and electrodialysis experiments. CEM and AEM stand for cation- and anion-exchange, standard-grade membranes, respectively. The membrane under investigation was positioned between compartment 3 and 4. The current was supplied from two counter electrodes positioned in compartment 1 (anode) and compartment 6 (cathode).

Electrodialysis of model dairy wastewater

Electrodialysis (ED) was performed on both Gu-0 and Gu-100, using the set-up as shown in Figure 4.1. Table 4.1 lists the composition of the model dairy solution. Table 4.2 reports the calculated percentage of phosphate and citrate speciation at the selected pH values. The dairy model solution was used to fill compartments 2, 3, 4 and 5, while a solution of 0.5 M Na_2SO_4 was circulated through the compartments of the cathode and anode electrodes (*i.e.*, compartments 1 and 6). All solutions were continuously pumped at 110 mL·min^{-1} at a fixed temperature of 25°C by using the

peristaltic pump and the thermostatic bath as described in the previous section. The pH was monitored in the feed and the receiving compartments during permeation experiments and was set around pH = 7, chosen as a representative pH value of dairy effluent. In addition, also measurements at a pH = 10 were performed, where divalent phosphate is the dominant specie, in order to better understand the process.[43] The solution pH was adjusted by using 1 M NaOH (Sigma). During ED experiments, a constant direct current of 0.06 A was applied (current density 7.1 mA·cm^{-2}), chosen in the ohmic region, and every 30 min. aliquots of the solution (5 mL) were collected from both feed and receiving compartments until 120 min. Collected samples were analysed by Ion Chromatography (930 Compact IC Flex, 150 mm A Supp 5 column, Metrohm).
In order to evaluate the transport number of each salt (t_{ion})[37], the following equation was used:[44]

$$t_{\text{ion}} = \frac{nF\,V\,\frac{\mathrm{d}C_{\text{ion}}}{\mathrm{d}t}}{iA} = \frac{nF\,J_{\text{ion}}}{i} \qquad [-] \qquad (4.5)$$

where F is the Faraday constant (96485 C·mol^{-1} = 96485 A sec Mol^{-1}), n is the valency of the ion, V is the volume of receiving solution (cm^3), C_{ion} the concentration (mol·cm^{-3}) of anion at time t (sec) and i is the current density (A·cm^{-2}). Considering our experimental conditions (pH = 7 and pH = 10), we calculated the transport numbers with the assumption of n = 3 for citrate and n = 2 for phosphate, since we assume that monovalent phosphate in the membrane turns to divalent [33]. All parameters used to calculate transport numbers, including anionic concentrations as from IC, are reported in the supporting information Table S4.1 and S4.2.

Table 4.1 Composition of model dairy wastewater used in the experiments and their conjugated pK_a, diffusion coefficients (D) and stokes radii (r_s).[45]

Anion*	**mMol**	**pK_a**	***D* (10^{-5} cm^2·s^{-1})****	**r_s (Å)**
Chloride	30	-7	2.032 [-1]	1.21 [-1]
Phosphate	10	2.13;7.21; 12.32	0.959 [-1]; 0.759 [-2]	2.6 [-1]; 2.4 [-2]
Citrate	10	3.13; 4.76; 6.40	0.623 [-3]	3.8 [-3]
Lactate	1	3.78; 15.1	1.033 [-1]	2.3 [-1]
Sulfate	1	-3; 1.99	1.065 [-2]	2.3 [-2]

* all as sodium salts; **numbers between brackets [] indicate the ionic charge.

Table 4.2 Calculated percentages of phosphate and citrate speciation at different pH.

Anion	pH	Monovalent (%)	Divalent (%)	Trivalent (%)
Phosphate	5	100	0	0
	7	62	38	0
	10	0	100	0
Citrate	5	35	61	4
	7	0	19	81
	10	0	0	100

Results and Discussion

Monomer and membrane characterizations

The synthesized and purified guanidinium acrylate monomer (Gu-monomer), compound **2**, was analysed by ^{1}H NMR. The peaks found at δ = 7.4 ppm and δ = 6.8 ppm are attributed to the guanidinium protons, while peaks at δ = 6.4 ppm, δ = 6.1 ppm and δ = 5.9 ppm are the characteristic signals of the protons related to the acrylate double bond. FTIR analysis was used to further characterize the structure of compound **2**. In Figure 4.2, peaks at 3164 cm^{-1} and 811 cm^{-1} are associated with the stretching and bending of the N–H bond, the peak at 1650 cm^{-1} is linked to the stretching of C=N bond, while peaks at 1197 cm^{-1} and 1063 cm^{-1} are assigned to the stretching at and the bending of the N–C bond of the Gu groups.[27,46] The two peaks at 1700 cm^{-1} and 1615 cm^{-1} refer to the stretching of the O=C–O and C=C, respectively, indicating the acrylate moiety and the peak at 1296 cm^{-1} is related to the stretching of the C–O bond of the ester group.[45] Peaks at 3331 cm^{-1}, 1411 cm^{-1} and 982 cm^{-1} are related to the stretching, bending in-plane and bending out-of-plane of the O–H bond, originating from the physically adsorbed water of the hydrophilic monomer.[47]

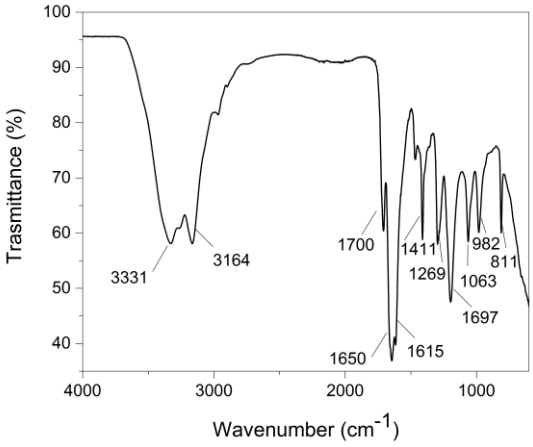

Figure 4.2 FTIR spectrum of compound **2**. Major peaks are indicated with their wavenumber (cm^{-1}) in the figure and explained in the text.

Next, compound **2** was used to fabricate the AEMs, following the procedure described in the materials and method section. Table 4.3 reports the composition, the water uptake measurements and XPS analysis of the Gu-100 and Gu-0 AEMs. The water content is slightly higher for the Gu-100 (1.8 wt %) compared to Gu-0 (1.5%wt). Considering the small difference in membrane ion-exchange capacity, we can calculate that ~37% (1 $mMol_{water}/g$: 2.7 $meq/g_{Gu\text{-}100}$) for Gu-100 and ~28% (0.8 $mMol_{water}/g$: 2.8 $meq/g_{Gu\text{-}0}$) for Gu-0 of water is associated with the anion-exchanging sites, indicating a slightly higher hydrophilicity for guanidinium groups compared to quaternary ammonium. The amount of nitrogen and carbon at the surface of the membranes was determined by XPS (Table 4.3), and found to be 6% and 64% for Gu-0 and 12% and 66% for Gu-100 AEM. Since the ion-exchange site of Gu-0 is a quaternary ammonium group, having one nitrogen atom per site, and in Gu-100 is a guanidinium group, having three nitrogen atoms per site, the estimated ratio of quaternary ammonium to guanidinium is 5.6 : 12.3/3 = 5.6 : 4.1 = 1.4. From the membrane fabrication, the ratio of quaternary ammonium to guanidinium sites in the (bulk and surface of the) membrane was found to be 2.83 : 2.71 = 1.04. It is therefore tentatively suggested that the quaternary ammonium groups are more exposed to the membrane surface compared to the guanidinium groups. The amount of found carbon at the membrane surface is comparable for both membranes; the small difference can be associated with some hydrocarbon contamination.[27,48]

Table 4.3 Membrane properties: type and number of exchange sites, water uptake and surface nitrogen and carbon composition.

AEM	Anion-exchange group* (mMol/g)		Water uptake (in wt % and mMol/g)	Surface composition** (atomic %)	
	$-N(CH_3)_3^+$	$-Gu^+$		N	C
Gu-0	2.83	0	1.52 ± 0.05 0.8	5.6 ± 0.4	64.1 ± 0.1
Gu-100	0	2.71	1.77 ± 0.03 1.0	12.3 ± 0.1	66.4 ± 0.3

*calculated from membrane fabrication; ** from XPS analysis

Permselectivity and membrane electrical resistance

In Table 4.4 the permselectivity (PS) results are presented. Considering the minor differences observed from the water uptake and anion-exchange capacities values (Table 3), we can assume a similar structure density of Gu-0 and Gu-100. Therefore, we attribute the differences observed for the PS values (Table 4.4) mainly to the different interactions of the ions with the fixed charge groups of the membranes. An observed positive value of PS (*i.e.*, a negative measured and negative calculated membrane potential) directly indicates that anions are the dominant exchanging, and thus transporting, species in the membrane. This is the situation for Gu-0 in all investigated situations. For the monovalent anions Cl^- and $H_2PO_4^-$ (pH = 5) the PS values indicate some co-ion (= cation) uptake. For SO_4^{2-} the observed PS is much lower, indicating a much higher co-ion uptake. It seems that the exchanged SO_4^{2-} acts, in part, as an cation exchanging site. Thus, the quaternary ammonium site is interacting with SO_4^{2-}, resulting in a new, overall negative site that is able to exchange cations (co-ions). To find more evidence for this interpretation, phosphate was also investigated at pH = 10, converting the phosphate from the monoanion to the dianion. Indeed, the observed PS is reduced from 88 to 55%. Thus, a phosphate dianion coordinated by the quaternary ammonium group behaves like the sulfate dianion. It is noted that, within this concept, dehydration of the ions is important to enter the membrane and also that the hydration energies of the phosphate dianion and sulfate are similar (-1170 and -1080 kJ/mol, respectively),[49,50] so this does not contribute to the observed differences.

For Gu-100 the situation is different. The monovalent ions Cl^- and $H_2PO_4^-$ (pH = 5) show similar PS values as found for Gu-0. The slightly lower PS found for $H_2PO_4^-$ and Gu-100 compared to Gu-0, might be the result of the expected stronger interaction between $H_2PO_4^-$ and Gu groups (as in Gu-100)[28,33] compared to the interaction to the quaternary ammonium (as in Gu-0). For the sulfate and phosphate dianions (at pH = 10) a remarkable change of sign of the PS is observed. The negative values directly indicate that the dominant exchanging species is no longer the expected anion. In other words, the observed membrane potential has a positive value, indicating that cations are the dominant exchanging species, while in the calculated Nernst potential we assumed that the anions are dominant, resulting in a calculated negative membrane potential.

The situation is more or less similar for sulfate and phosphate dianion. In the Gu-100 membranes, these dianions turn the membranes into cation exchangers: one of the two charges of the counter-ions binds to the Gu groups, while the second negative charge facilitates the interaction with co-ions, which dominate the overall ion transport. That this happens in the Gu-100 membranes and not (to that extent) in the Gu-0 membranes is attributed to the stronger interaction between both sulfate dianion and phosphate dianion to the guanidinium groups compared to their interaction with quaternary ammonium groups.[33] In Table 4.5 the electrical resistance (ER) of the Gu-0 and Gu-100 membranes are shown as determined by separate experiments using sodium chloride, sodium phosphate (at pH = 5 and 10), or sodium sulfate.

Table 4.4 Permselectivities (% PS) and observed membrane potentials (E_m in [mV]) for Gu-0 and Gu-100 membranes in the presence of 0.5/0.05 M of NaCl, NaH_2PO_4, Na_2HPO_4 and Na_2SO_4 measured separately.

	NaCl	**NaH_2PO_4 (pH = 5)**	**Na_2HPO_4 (pH = 10)**	**Na_2SO_4**
Gu-0	90.1 [-43]	87.8 [-38]	54.8 [-4.8]	59.5 [-5.7]
Gu-100	87.1 [-40]	72.1 [-22]	-56.4 [3.1]	-55.6 [3.4]

Table 4.5 Observed electrical resistances (ER) for Gu-0 and Gu-100 membranes in 0.5 M of NaCl, NaH_2PO_4 (pH = 5), Na_2HPO_4 (pH = 10) or Na_2SO_4.

	ER [ohm·cm^2]*			
	NaCl	**NaH_2PO_4 (pH = 5)**	**Na_2HPO_4 (pH = 10)**	**Na_2SO_4**
Gu-0	1.1	6.3	2.3	1.6
Gu-100	0.9	2.7	1.2	3.0

*Error is < 5%, based on triplicate measurements.

The lowest ER values are observed for chloride in both Gu-0 and Gu-100, indicating a high mobility of chloride in both membranes having similar properties regarding the number of ion-exchange sites and observed PS. For the phosphate monoanion (pH = 5) the situation is different. For Gu-0 the ER value is now higher compared to the one of chloride. This is in line with the trend of the diffusion coefficients (Table 4.1): a lower diffusion coefficient results in a lower ion flux through the membrane, and hence in a higher ER.[51] For Gu-100 and phosphate (pH = 5) the ER is reduced to 2.7 ohm·cm^{-2}. Clearly, this is an effect of the mobile cations (co-ions H^+ and Na^+) in the membrane, as observed/interpreted from the PS data. The phosphate monoanion is expected to be bound more strongly to the guanidinium groups compared to the quaternary ammonium groups, and thus resulting in an expected lower mobility, hence raising the ER value. The lower ER values can be attributed to these mobile co-ions.

For the sulfate and phosphate dianions (pH = 10) the understanding of the observed ER data can be supported by the interpretation of our PS data. In more detail, for Gu-0 we observed a significant amount of co-ion exchange and for Gu-100 the co-ion exchange process was even dominant, as evinced from the recorded positive membrane potential. Thus, for Gu-0 the ER values are determined by a combination of *i*) sulfate and phosphate dianions transport, while exchanging with the fixed anionic groups of the membrane, and *ii*) co-ion (cation) transport. The observed lower ER for HPO_4^{2-} and Gu-100 compared to Gu-0 might be related to a somewhat larger co-ion uptake for the Gu-100 membranes compared to the Gu-0 membranes, as can be deduced from the PS measurements; PS is more negative for Gu-100 compared to Gu-0, indicating more co-ion (cation) uptake.

Electrodialysis with model dairy wastewater

Finally, we come to the results of our experiments using the Gu-0 and Gu-100 membranes to separate by electrodialysis a mixed solution containing sodium chloride, sodium phosphate, sodium citrate, sodium lactate and sodium sulfate, as a model dairy wastewater composition at a common pH = 7 and also at pH = 10. We are interested in the effect of changing the quaternary ammonium sites (Gu-0) by the guanidinium sites (Gu-100). Before describing these experiments a short summary is given of the main properties found for the Gu-0 and Gu-100 membranes. This is done to facilitate the interpretation of the electrodialysis results. Briefly, the amount of sites is similar in both membranes, as is the water uptake. From the PS measurements it was found that exchange of the chloride and phosphate monoanions (pH = 5) is hardly influenced by changing the type of anion-exchange sites in the membrane from quaternary ammonium to guanidinium. The phosphate monoanion (pH = 5) is slightly stronger bound to guanidinium compared to quaternary ammonium as deduced from the observed lower PS (indicating more co-ion uptake). The sulfate and phosphate dianions (pH = 10) behave similarly if the membrane is changed from Gu-0 to Gu-100. Both dianions are strongly bound to the guanidinium groups and show a high co-ion uptake. The ER measurements indicate that the mobility of chloride is hardly effected by changing from Gu-0 to Gu-100. Phosphate monoanion (pH = 5) is clearly less mobile compared to chloride in Gu-0. The ER values for the other situations are all influenced by the co-ion uptake and the ER value is not directly a measure of the anion mobility in the membranes.

The composition of the model dairy wastewater is given in Table 4.1 and is shown to i) be rich in sodium chloride (30 mM), ii) have equal concentrations of sodium phosphate and sodium citrate (10 mM), and iii) have low concentrations of sodium lactate and sodium sulfate (both 1 mM).

Both Gu-0 and Gu-100 membranes were operated at an applied constant current of 7.1 $mA \cdot cm^{-2}$, as described in the Materials and Methods section. Samples from feed and receiving phase were collected and analyzed by Ion Chromatography, and the results are represented by their calculated transport numbers (see also Equation 4.5 in Materials and Methods section). The results of the ED performed at pH = 7 are shown in Figure 4.3a. The anion transport is dominated by the chloride transport for both Gu-0 and Gu-100. This is as expected because of its high concentration, compared to the

other present salts, and its low ER value. The transport of lactate and sulfate does play a minor role, due to their very low concentrations compared to the other salts present in the model dairy wastewater we applied. The phosphate transport is observed in Gu-0 and the amount transported increases for Gu-100. At pH = 7 phosphate is present as monoanion (62%) and as dianion (38%), see Table 4.2. The present guanidinium groups in Gu-100 are clearly responsible for the increased phosphate transport, as was also deduced from our PS measurements. No citrate transport is found for Gu-0, but it is observed for Gu-100. At pH = 7 citrate is present as a dianion (19%) and as a trianion (81%), see Table 4.2. Thus, the difference observed between phosphate and citrate transport for Gu-0 can be attributed to the differences in diffusion coefficient (Table 4.1) and valency; the phosphate monoanion can be exchanged by the quaternary ammonium groups present in Gu-0, while the di- and trianion of citrate does not. In the presence of guanidinium exchanging sites (Gu-100) there is an additional affinity towards the oxyanions (*e.g.,* phosphate), compared to quaternary ammonium. This affinity is responsible for the increased uptake and transport of phosphate and citrate at pH = 7.

To find further support for this interpretation we have also performed electrodialysis experiments at pH = 10. The results are presented in Figure 4.3b. At this pH, phosphate is present as dianion (100%) and citrate as trianion (100%), see Table 4.2. It is expected now that the phosphate dianion is also not taken up by the Gu-0 as was citrate before. This is indeed what we have observed: there is a complete absence of any phosphate transport for Gu-0 at pH = 10. In the presence of Gu groups (Gu-100) phosphate transport is taking place again. At this pH value also citrate (as trianion) transport is observed for the Gu-100 membranes. It was a surprise to observe some citrate transport under these conditions for the Gu-0 membrane (though only 0.025). We can only speculate why the citrate trianion does transport under these conditions, while the phosphate dianion does not. It is suggested that both citrate and phosphate equilibrate to some extent with the membrane, and that the citrate trianion experiences a larger electrophoretic force compared to the phosphate dianion.

Finally, for both pH = 7 and 10, we can conclude that the uptake of citrate and phosphate is stronger for the Gu-100 membrane compared to Gu-0. To obtain more insight into the interaction between the Gu-100 membrane and citrate/phosphate anions, we compared the relative differences in the transport number to the ratio of the diffusivity values (Table 4.1). We calculate that the diffusivity ratio for

phosphate/citrate is 1.2, while the ratio of the transport numbers is 2.6 at pH = 7 and 0.69 at pH = 10. The difference in the ratio of diffusion coefficients and those of the transport numbers point to a complexation between these anions and the exchange sites of the membrane occurs.

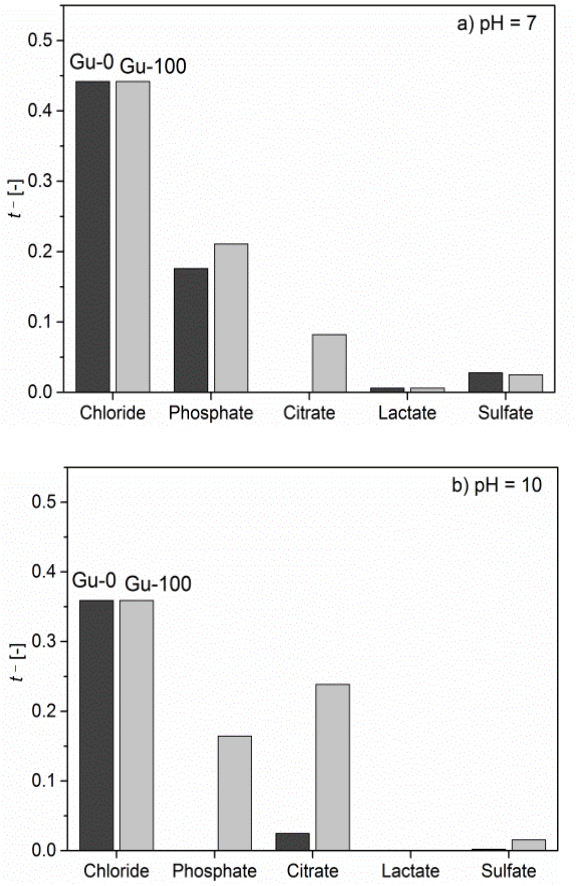

Figure 4.3 Transport number (t^-) of anions for Gu-0 (black) and Gu-100 (grey) membrane in a model dairy wastewater solution a) at pH 7 and b) at pH 10.

Implications

A new, functionalized anion-exchange membrane containing guanidinium groups as the anion-exchange sites (Gu-100) was made, characterised in detail and applied in ED experiments. By making use of a functionalized acrylate, our focus is on the bulk modification rather than the surface modication[52] or nanomaterial-assisted[53]

strategies. This way, high densities of the functional groups in anion- and cation-exhange membranes can be obtained. In the current study, guanidinium groups were chosen as the functional moiety because of their specific interactions with oxyanions, *e.g.,* phosphate. Apart from its relevance in dairy wastewater streams, uncontrolled discharge of P-containing products as present in aqueous streams from agricultural and cosmetic sectors has increased the eutrophication processes, *i.e.,* the rapid growth of aquatic algae in lakes and rivers. Next to the observed increased phosphate transport, the current study also shows an effect of the functionalization of the ion-exchange membrane to the transport of citrate. Citrate is not only an intermediate in the Krebs cycle, it is also used as a chelating agent in water treatment processes and as a descaling agent to remove limescale.

The synthesis of the functionalized acrylate monomer is based on a two-step modification of a 1-amino- ω-alcohol. This synthesis strategy is not only facile, but also modular as it allows the integration of other functional moieties. As such, the presented approach has the potential to prepare ion-exchange membranes that address other ions that are environmentally relevant. As a final remark it is noted that functionalized anion- and cation-exchange membranes are not only relevant for ED processes, they are also of importance in other fields, including those of fuel cells and capacitive deionization. This further illustrates the (environmental) scope of the ability to control the selective transport of ions.

Supporting Information

Table S4.1 List of parameters used to calculate the anionic transport numbers.

	Value	Unit
Faraday constant (*F*)	96485	C mol^{-1}
Membrane Area (*A*)	8.41	cm^2
Current density (*i*)	7.1	mA cm^{-2}
Volume (*V*)	0.5	L
Time	7200	s
Chloride valency (*n*)	-1	
Phosphate *n*	-2	
Sulphate *n*	-2	
Lactate *n*	-1	
Citrate *n*	-3	

Table S4.2 Anionic concentrations (mol L^{-1}) as measured by IC.

	Gu-0		Gu-100	
	Initial	**Final**	**Initial**	**Final**
Lactate	0.8592 ± 0.005	0.8425 ± 0.001	0.906 ± 0.002	0.333 ± 0.001
Chloride	31.03 ± 0.01	34.41 ± 0.06	28.77 ± 0.05	32.16 ± 0.08
Phosphate	10.75 ± 0.05	10.56 ± 0.01	9.687 ± 0.018	10.46 ± 0.05
Sulfate	1.093 ± 0.035	1.103 ± 0.072	0.978 ± 0.023	1.051 ± 0.012
Citrate	8.292 ± 0.082	8.370 ± 0.030	8.291 ± 0.058	9.041 ± 0.025

References

(1) Hudson, J. J.; Taylor, W. D.; Schindler, D. W. Phosphate Concentrations in Lakes. *Nature* 2000, *400*, 55–56.

(2) Service, R. F. Desalination Freshens Up. *Science* 2006, *313* (5790), 1088–1090.

(3) Strathmann, H. Electrodialysis, a Mature Technology with a Multitude of New Applications. *Desalination* 2010, *264*, 268–288.

(4) Dlugolecki, P.; van der Wal, A. Energy Recovery in Membrane Capacitive Deionization. *Environ. Sci. Technol.* 2013, *47* (9), 4904–4910.

(5) AlMarzooqi, F. A.; Al Ghaferi, A. A.; Saadat, I.; Hilal, N. Application of Capacitive Deionisation in Water Desalination: A Review. *Desalination* 2014, *342*, 3–15.

(6) Dlugolecki, P.; Nijmeijer, K.; Metz, S.; Wessling, M. Current Status of Ion Exchange Membranes for Power Generation from Salinity Gradients. *J. Memb. Sci.* 2008, *319*, 214–222.

(7) Galama, A. H.; Vermaas, D. A.; Veerman, J.; Saakes, M.; Rijnaarts, H. H. M.; Post, J. W.; Nijmeijer, K. Membrane Resistance: The Effect of Salinity Gradients over a Cation Exchange Membrane. *J. Memb. Sci.* 2014, *467*, 279–291.

(8) Chen, G. Electrochemical Technologies in Wastewater Treatment. *Sep. Purif. Technol.* 2004, *38*, 11–41.

(9) Liu, R.; Wang, Y.; Wu, G.; Luo, J.; Wang, S. Development of a Selective Electrodialysis for Nutrient Recovery and Desalination during Secondary Effluent Treatment. *Chem. Eng. J.* 2017, *322*, 224–233.

(10) Zhang, Y.; Van der Bruggen, B.; Pinoy, L.; Meesschaert, B. Separation of Nutrient Ions and Organic Compounds from Salts in RO Concentrates by Standard and Monovalent Selective Ion-Exchange Membranes Used in Electrodialysis. *J. Memb. Sci.* 2009, *332*, 104–112.

(11) Strathmann, H. Ion-Exchange Membrane Processes in Water Treatment. *Sustain. Sci. Eng. Elsevier* 2010, *2*, 141–199.

(12) Chapotot, A.; Lopez, V.; Lindheimer, A.; Aouad, N.; Gavach, C. Electrodialysis of Acid Solutions with Metallic Divalent Salts: Cation-Exchange Membranes with Improved Permeability to Protons. *Desalination* 1995, *101*, 141–153.

(13) Bazinet, L. Electrodialytic Phenomena and Their Applications in the Dairy Industry: A Review. *Crit. Rev. Food Sci. Nutr.* 2005, *45* (4), 307–326.

(14) Boniardi, N.; Rota, R.; Nano, G.; Mazza, B. Analysis of the Sodium Lactate Concentration Process by Electrodialysis. *Sep. Technol.* 1996, *6* (1), 43–54.

(15) Fidaleo, M.; Moresi, M. Concentration of Trisodium Citrate by Electrodialysis. *J. Memb. Sci.* 2013, *447*, 376–386.

(16) Andrés, L. J.; Riera, F. A.; Alvarez, R. Skimmed Milk Demineralization by Electrodialysis: Conventional versus Selective Membranes. *J. Food Eng.* 1995, *26* (1), 57–66.

(17) van der Horst, H. C. Timmer, J. M. K. Robbertsen, T. Leenders, J. Use of Nanofiltration for Concentration and Demineralization in the Dairy Industry. *J. Memb. Sci.,* 1995, *104* (3), 205–218.

(18) Zhang, Y.; Desmidt, E.; Van Looveren, A.; Pinoy, L.; Meesschaert, B.; Van Der Bruggen, B. Phosphate Separation and Recovery from Wastewater by Novel Electrodialysis. *Environ. Sci. Technol.* 2013, *47* (11), 5888–5895.

(19) Luo, T.; Abdu, S.; Wessling, M. Selectivity of Ion Exchange Membranes: A Review. *J. Memb. Sci.* 2018, *555*, 429–454.

(20) White, N.; Misovich, M.; Yaroshchuk, A.; Bruening, M. L. Coating of Nafion Membranes with Polyelectrolyte Multilayers to Achieve High Monovalent/divalent Cation Electrodialysis Selectivities. *ACS Appl. Mater. Interfaces* 2015, *7* (12), 6620–6628.

(21) Mulyati, S.; Takagi, R.; Fujii, A.; Ohmukai, Y.; Matsuyama, H. Simultaneous Improvement of the Monovalent Anion Selectivity and Antifouling Properties of an Anion Exchange Membrane in an Electrodialysis Process, Using Polyelectrolyte Multilayer Deposition. *J. Memb. Sci.* 2013, *431*, 113–120.

(22) Rijnaarts, T.; Shenkute, N. T.; Wood, J. A.; de Vos, W. M.; Nijmeijer, K. Divalent Cation Removal by Donnan Dialysis for Improved Reverse Electrodialysis. *ACS Sustain. Chem. Eng.* 2018, *6* (5), 7035–7041.

(23) Kim, D. H.; Park, H. S.; Seo, S. J.; Park, J. S.; Moon, S. H.; Choi, Y. W.; Jiong, Y. S.; Kim, D. H.; Kang, M. S. Facile Surface Modification of Anion-Exchange Membranes for Improvement of Diffusion Dialysis Performance. *J. Colloid Interface Sci.* 2014, *416*, 19–24.

(24) Lee, W.; Saito, K.; Furusaki, S.; Sugo, T.; Makuuchi, K. Design of Urea-Permeable Anion-Exchange Membrane by Radiation-Induced Graft Polymerization. *J. Memb. Sci.* 1993, *81*, 295–306.

(25) Hosseini, S. M.; Nemati, M.; Jeddi, F.; Salehi, E.; Khodabakhshi, R.; Madaeni, S. S. Fabrication of Mixed Matrix Heterogeneous Cation Exchange Membrane Modified by Titanium Dioxide Nanoparticles: Mono/bivalent Ionic Transport Property in Desalination. *Desalination* 2015, *359*, 167–175.

(26) Pantos, A.; Tsogas, I.; Paleos, C. M. Guanidinium Group: A Versatile Moiety Inducing Transport and Multicompartmentalization in Complementary Membranes. *Biochim. Biophys. Acta - Biomembr.* 2008, *1778*, 811–823.

(27) Paltrinieri, L.; Wang, M.; Sachdeva, S.; Besseling, N. A. M.; Sudhölter, E. J. R.; de Smet, L. C. P. M. Fe3O4 Nanoparticles Coated with a Guanidinium-Functionalized Polyelectrolyte Extend the pH Range for Phosphate Binding. *J. Mater. Chem. A* 2017, *5*, 18476–18485.

(28) Cao, Z.; Gordiichuk, P. I.; Loos, K.; Sudhölter, E. J. R.; de Smet, L. C. P. M. The Effect of Guanidinium Functionalization on the Structural Properties and Anion Affinity of Polyelectrolyte Multilayers. *Soft Matter* 2016, *12*, 1496–1505.

(29) Liu, L.; Li, Q.; Dai, J.; Wang, H.; Jin, B.; Bai, R. A Facile Strategy for the Synthesis of Guanidinium-Functionalized Polymer as Alkaline Anion Exchange Membrane with Improved Alkaline Stability. *J. Memb. Sci.* 2014, *453*, 52–60.

(30) Park, J.; Yi, J.; Tachikawa, T.; Majima, T.; Choi, W. Guanidinium-Enhanced Production of Hydrogen on Nafion-Coated Dye/TiO 2 under Visible Light. *J. Phys. Chem. Lett.* 2010, *1* (9), 1351–1355.

(31) Zhang, Q.; Li, S.; Zhang, S. A Novel Guanidinium Grafted Poly(aryl Ether Sulfone) for High-Performance Hydroxide Exchange Membranes. *Chem. Commun. (Camb).* 2010, *46* (40), 7495–7497.

(32) Sajjad, S. D.; Hong, Y.; Liu, F. Synthesis of Guanidinium-Based Anion Exchange Membranes and Their Stability Assessment. *Polym. Adv. Technol.* 2014, *25*, 108–116.

(33) Paltrinieri, L.; Poltorak, L.; Chu, L.; Puts, T.; van Baak, W.; Sudhölter, E. J. R. .; de Smet, L. C. P. M. Hybrid Polyelectrolyte-Anion Exchange Membrane for Phosphate Removal. *React. Funct. Polym.* 2018.

(34) Funhoff, A. M.; van Nostrum, C. F.; Lok, M. C.; Fretz, M. M.; Crommelin, D. J. a; Hennink, W. E. Poly(3-Guanidinopropyl Methacrylate): A Novel Cationic Polymer for Gene Delivery. *Bioconjug. Chem.* 2004, *15* (6), 1212–1220.

(35) Sata, T. *Ion Exchange Membranes Preparation, Characterization, Modification and Application*; RSC, 2004.

(36) Sata, T. Studies on Ion Exchange Membranes with Permselectivity for Specific Ions in Electrodialysis. *Journal of Membrane Science*. 1994, pp 117–135.

(37) Sata, T. Studies on Anion Exchange Membranes Having Permselectivity for Specific Anions in Electrodialysis - Effect of Hydrophilicity of Anion Exchange Membranes on Permselectivity of Anions. *J. Memb. Sci.* 2000, *167*, 1–31.

(38) Geise, G. M.; Cassady, H. J.; Paul, D. R.; Logan, B. E.; Hickner, M. A.; Logan, E.; Hickner, M. A. Specific Ion Effects on Membrane Potential and the Permselectivity of Ion Exchange Membranes. *Phys. Chem. Chem. Phys.* 2014, *16* (39), 21673–21681.

(39) Cassady, H. J.; Cimino, E. C.; Kumar, M.; Hickner, M. A. Specific Ion Effects on the Permselectivity of Sulfonated Poly(ether Sulfone) Cation Exchange Membranes. *J. Memb. Sci.* 2016, *508*, 146–152.

(40) Dlugolecki, P.; Ogonowski, P.; Metz, S. J.; Saakes, M.; Nijmeijer, K.; Wessling, M. On the Resistances of Membrane, Diffusion Boundary Layer and Double Layer in Ion Exchange Membrane Transport. *J. Memb. Sci.* 2010, *349*, 369–379.

(41) Geise, G. M.; Hickner, M. A.; Logan, B. E. Ionic Resistance and Permselectivity Tradeoffs in Anion Exchange Membranes. *ACS Appl. Mater. Interfaces* 2013, *5*, 10294–10301.

(42) Galama, A. H.; Hoog, N. A.; Yntema, D. R. Method for Determining Ion Exchange Membrane Resistance for Electrodialysis Systems. *Desalination* 2016, *380*, 1–11.

(43) Sarapulova, V.; Nevakshenova, E.; Pismenskaya, N.; Dammak, L.; Nikonenko, V. Unusual Concentration Dependence of Ion-Exchange Membrane Conductivity in Ampholyte-Containing Solutions: Effect of Ampholyte Nature. *J. Memb. Sci.* 2015, *479*, 28–38.

(44) Güler, E.; van Baak, W.; Saakes, M.; Nijmeijer, K. Monovalent-Ion-Selective Membranes for Reverse Electrodialysis. *J. Memb. Sci.* 2014, *455*, 254–270.

(45) Lide, D. R. CRC Handbook of Chemistry and Physics, 84th Edition, 2003-2004. *Handb. Chem. Phys.* 2003, *53*, 2616.

(46) Tristán, F.; Palestino, G.; Menchaca, J.-L.; Pérez, E.; Atmani, H.; Cuisinier, F.; Ladam, G. Tunable Protein-Resistance of Polycation-Terminated Polyelectrolyte Multilayers. *Biomacromolecules* 2009, *10* (8), 2275–2283.

(47) Wong, J. E.; Gaharwar, A. K.; Müller-Schulte, D.; Bahadur, D.; Richtering, W. Magnetic Nanoparticle-Polyelectrolyte Interaction: A Layered Approach for Biomedical Applications. *J. Nanosci. Nanotechnol.* 2008, *8* (8), 4033–4040.

(48) Stevens, J. S.; De Luca, A. C.; Pelendritis, M.; Terenghi, G.; Downes, S.; Schroeder, S. L. M. Quantitative Analysis of Complex Amino Acids and RGD Peptides by X-Ray Photoelectron Spectroscopy (XPS). *Surf. Interface Anal.* 2013, *45*, 1238–1246.

(49) Eiberweiser, A.; Nazet, A.; Hefter, G.; Buchner, R. Ion Hydration and Association

in Aqueous Potassium Phosphate Solutions. *J. Phys. Chem. B* 2015, *119* (16), 5270–5281.

(50) Smith, D. W. Ionic Hydration Enthalpies. *J. Chem. Educ.* 1977, *54* (9), 540–542.

(51) Kamcev, J.; Paul, D. R.; Manning, G. S.; Freeman, B. D. Ion Diffusion Coefficients in Ion Exchange Membranes: Significance of Counterion Condensation. *Macromolecules* 2018, *51* (15), 5519–5529.

(52) Khoiruddin; Ariono, D.; Subagjo; Wenten, I. G. Surface Modification of Ion-Exchange Membranes: Methods, Characteristics, and Performance. *J. Appl. Polym. Sci.* 2017, *134*, 1–13.

(53) Alabi, A.; AlHajaj, A.; Cseri, L.; Szekely, G.; Budd, P.; Zou, L. Review of Nanomaterials-Assisted Ion Exchange Membranes for Electromembrane Desalination. *npj Clean Water* 2018, *1* (1), 10.

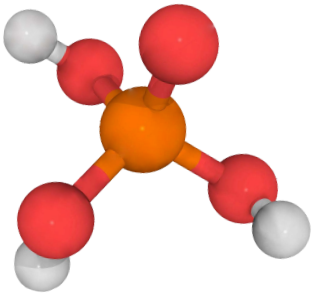

CHAPTER 5

Improved phosphoric acid recovery from sewage sludge ash using Layer-by-Layer modified membranes

We report an advanced treatment for phosphoric acid recovery from leached sewage sludge ash. Layer-by-layer (LbL) polyelectrolyte deposition has been used as a tool to modify and convert a hollow ultrafiltration membrane into a nanofiltration (NF) LbL membrane for H_3PO_4 recovery. To build the LbL membrane, poly(styrenesulfonate) PSS was chosen as polyanion, while three types of polycations were used: a permanently charged polyelectrolyte, poly(diallyldimethylammonium chloride), PDADMAC; a pH-dependent charged polyelectrolyte poly(allylamine hydrochloride), PAH; and a PAH modified with guanidinium groups (PAH-Gu). Based on detailed surface characterizations (AFM, XPS and Zeta-potential), it was concluded that both the charge density and the pH-responsiveness of the polycations are key parameters to control the final membrane surface structure and transport properties. The surface properties of LbL membranes were with the membrane filtration performance, when exposed to the real leached sewage sludge ash solution. The highest permeability was recorded for $(PDADMAC/PSS)_6$, which had a loose and less interpenetrated structure, followed by $(PAH\text{-}Gu/PSS)_6$ characterized by a more dense, compact layer. H_3PO_4 recovery was the highest in the case of $(PDADMAC/PSS)_6$, but the retention of multivalent metals (Fe^{3+} and Mg^{2+}) was low, leading to a more contaminated permeate. The opposite trend was observed for $(PAH\text{-}Gu/PSS)_6$, resulting in a less metal-contaminated, but also a less H_3PO_4-concentrated permeate. Our LbL-modified membranes were found to improve the permeability and H_3PO_4 recovery compared to a commercially available acid-resistant NF membrane.

Introduction

Phosphorus (P) an essential element and a limited resource. Used mainly as fertilizer, it is of global importance to the food supply of the ever-growing human population.[1] P-containing ore is extracted from mines located in a limited number of countries (*e.g.*, Morocco, Western Sahara, Australia and China)[2], making most nations heavily dependent on P imports. In 2014, the European Commission added P to its revised list of Critical Raw Materials.[3] Since then, the recovery of P from wastewater has been recognized as a strategic, sustainable solution to the depletion of mineral deposits.[4,5] Given that most of the P is transferred from wastewater to sludge (around 90%),[6] P has been found to be abundant in sewage sludge ash after incineration. Sewage sludge ash, therefore, is the ideal raw source for P-recovery in the form of phosphoric acid (H_3PO_4).

The selective P-recovery is of interest to many countries. For instance, in January 2016 Switzerland revised its Technical Ordinance on Waste to require the recovery of P from P-rich waste streams, such as sewage sludge and sewage sludge ash.[7] Over the past years, a wide range of P-recovery processes from sewage sludge have been developed.[8] The most studied are the thermal processes (*e.g.*, *Ash-Dec®* process) for calcium-phosphate precipitation[9], and the wet chemical treatment to produce struvite (also known as the *Stuttgarter®* and the *Gifhorn®* process)[9] which have been tested at both lab- and pilot scale. In addition to these technologies, a solvent extraction, the *Phos4life®* process, has been developed recently in a pilot-plant.[10] Current techniques require extensive use of chemicals and by-product disposal, limiting their use in "green" and "chemical-free" processes. Furthermore, their main recycling products are P-containing minerals used directly as fertilizer, while their regulatory and market acceptance is still unclear[9] and their economic feasibility often unknown.[11] A possible alternative is the *TetraPhos®* process, which combines acidic leaching, ion exchange and nanofiltration. The final product is H_3PO_4, which itself has a high market potential.[12] Its advantages include not only that H_3PO_4 is the final product, but also the use of the membrane technology for the treatment process,[9] enabling continuous operation and limiting chemical usage.

Within the family of membrane processes, nanofiltration (NF) is a suitable purification method for H_3PO_4 recovery.[13] The transport mechanism in NF is based on both size exclusion (molecular weight cutoff, MWCO = 80 – 2,000 Da) and electrostatic interactions governed by the Donnan exclusion principle.[14] The separation efficiency of the NF process depends on the charge and size of the compounds of interest in relation to the charge of the membrane and its apparent pore size. Monovalent and neutral compounds (e.g., ions pairs, inorganic acids) can pass through the NF membranes, while multivalent ions and molecules are retained.[15] H_3PO_4 is an ampholytic compound with three distinct pK_a values: 2.2, 7.2 and 12.3[16]. Using leached sewage sludge ash in a strong acidic environment (pH < pK_{a1} = 2.2), P is an uncharged H_3PO_4 and can permeate through NF membranes, while charged multivalent ions are rejected. The proof of concept to use NF for P-recovery from leached sewage sludge was shown by Schütte *et al.*[17] and Niewersch *et al.*[18]. In these studies, it has been concluded that commercially available, acid-resistant NF membranes (NF270 from DOW, DL and Duracid from GE, and AMS A-3012-1812 from AMS) can be employed to recover H_3PO_4 from metal-contaminated sources. Among the four tested membranes, the acid-resistant AMS membrane achieved the highest H_3PO_4 yields and the highest permeate purity, setting the benchmark in H_3PO_4 recovery from sewage sludge.[17,19] However, the permeability of AMS membranes showing high H_3PO_4 recovery was relatively low, so improvements in this area are needed.

Polyelectrolytes (PEs) are charged polymers and attractive materials for use in membrane modification. Due to their good applicability and large chemical and structural variations, PEs are recognized as key compounds tailoring membrane performances.[20][21][2223] PEs are primarily applied by Layer-by-Layer (LbL) deposition.[24] A positively charged PE and a negatively charged PE are deposited in alternation to form a multilayer on top of a charged substrate; the multilayer stability mostly relies on electrostatic interactions.[25] The sulfonated ultrafiltration (UF) membrane has been shown to be the best support for LbL formation.[26] The LbL deposition on UF membranes forms a stable, thin coating, decreasing the membrane pore size, changing the surface charge and converting the UF membrane into a NF membrane, as measured by separation characteristics.[26] The overall surface charge of the LbL NF membrane depends on both the number of deposited layers and the type of PEs applied. It has been

shown that after a certain number of bi-layer deposits the membrane surface charge is overall positive.[26,27] When using a LbL NF membrane with a sufficient amount of PEs, multivalent charged ions are usually rejected by the membrane and uncharged compounds (*e.g.,* H_3PO_4) are transported through the membrane by the convective water flux.[26,29,30]

Recently, LbL membranes have been applied as NF membranes for H_3PO_4 recovery in the presence of divalent ions. Remmen *et al.*[31] report an optimized LbL NF membrane for recovery of H_3PO_4 contaminated with Al^{3+}, as a representative multivalent ion. The LbL NF membranes showed high permeability, high H_3PO_4 yields and sufficient Al^{3+} retention values. However, only one type of polycation was used for multilayer formation and only model solution was tested. Consequently, there is a lack of understanding on the LbL membranes performance when exposed to real solutions (*i.e.,* leached sewage sludge ash), and on the effect of the PE type on the H_3PO_4 recovery.

Using three types of amino-based polycations we studied the modification of the interior of sulfonated polyethersulfone (sPES) UF hollow fiber membranes via LbL deposition, as shown in Figure 5.1. In more detail, polystyrene sulfonate (PSS) was always used as the polyanion. As polycations we used poly(diallyldimethylammonium chloride) PDADMAC, a permanently charged PE; poly(allylamine hydrochloride) PAH, a pH-dependent PE with pK_a = 8-9,[32] and a functionalized PAH containing 30 wt % of guanidinium groups (PAH-Gu). Compared to non-oxoanions, the guanidinium group (pK_a = 13) shows enhanced interactions towards phosphate ions.[33–36] The sPES support material was chosen according to an MWCO of 10 kDa, leading to a retention of all selected PE molecular weights (M_ws).

The aim of this work is to show the advantages of acid-resistant LbL NF membranes, with respect to permeability and H_3PO_4 recovery, compared to the benchmark acid-resistant NF membrane (AMS) and to correlate membrane structure-properties with its performances. A secondary aim is to improve the technology by demonstrating a real-life application using leached sewage sludge ash.

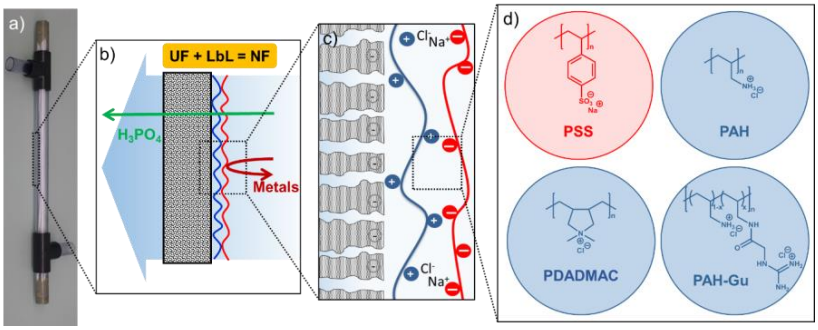

Figure 5.1 a) Picture of a sulfonated sPES UF membrane from Pentair, and schematic presentations of b) alternately deposited PEs (only 2 PEs are given for maters of simplicity), including a summary of the separation properties, c) a zoom-in of the interfaces inside the lumen, d) molecular structures of the Pes used in this study.

Materials and Methods

Materials for membrane modification

A sulfonated polyethersulfone (sPES) hollow-fiber membrane with an MWCO of 10 kDa was provided by Pentair X-Flow (the Netherlands) as a substrate for LbL deposition.37 The inner diameter of each fiber was 0.8 mm, and in our study a length of 300 mm was chosen, resulting in a surface area of 0.00075 m^2 per fiber. Positively charged poly(diallyldimethylammonium chloride) (PDADMAC, Mw = 300 - 400 kDa, 20 wt% in water) and poly(allylamine hydrochloride) (PAH Mw = 50 kDa) and negatively charged poly(sodiumstyrenesulfonate) (PSS, Mw = 1,000 kDa, 25 wt% in water) were purchased from Sigma-Aldrich (Switzerland). Guanidine acetic acid (GAA, 99%), 1-Ethyl-3-(3-Dimethylaminopropyl) Carbodiimide (EDC, commercial grade) and N-Hydroxy-Succinimide (NHS, 98%) were all purchased from Sigma-Aldrich and used to synthesize polyallyamine hydrochloride functionalized with guanidine groups (PAH-Gu). According to the procedure developed in our research group 30% of primary amine groups where modified with Gu moieties.33 The chemical structures of the three polycations and the relative pKa values are shown in Fig. 5.1. For LbL formation, a solution containing sodium chloride (≥ 99.8% purity) from Sigma was used. All the chemicals were used without any further purification. A commercially available acid resistant NF membrane spiral wound

module (AMS A-3012-1812, purchased from AMS Technologies, Israel) was employed during the sewage sludge ash filtration for comparison with the optimized LbL-modified membranes modules containing 10 hollow fibers (*i.e.*, a surface area of 0.0075 m^2). The membrane area of the AMS module was 0.4 m^2.

Membrane coating procedure

The sPEs UF hollow fiber membrane modification with PEs was realized through the dynamic coating method, following the set-up described in previous studies.26 A dead-end filtration set-up was used at a constant pressure of 3 bar, and the PE was deposited inside the lumen of the membrane, followed by a rinsing step with demiwater at pH around 5-6. Modules containing one and ten hollow fiber membranes were potted, with an overall membrane area of 7.5 cm^2 and 75 cm^2, respectively. Next, the modules were soaked in ultrapure water for at least 24 hours, followed by rinsing with ultrapure water for at least 1 hour (pH around 5-6). The sPES UF membrane has sulfonated groups, making it negatively charged. For that reason the multilayer deposition was always achieved by starting with the positively charged PE, followed by consecutively alternating adsorption of polyanions and polycations, until six bi-layers were reached (a bi-layer consists of two oppositely charged PE layers). The number of layers was chosen based on the previous study, as the optimal configuration for phosphoric acid retention from a model solution.[27] Each filtration cycle was carried out until 2 $g \cdot m^{-2}$, and 0.2 $g \cdot m^{-2}$ PE were retained in the membrane, keeping in consideration the pore size of the support membrane used was smaller than the hydrodynamic radius of the PE applied. After each cycle (*i.e.*, the deposition of one PE), the membrane was flushed with deionized water until a conductivity less than 3 µS/cm was reached to ensure the excess of PE solution was completely washed out. The conductivity was measured using a GMH 3451 conductivity meter (Greisinger, Germany).

Multilayer optimization

To find the optimum LbL configuration, the effect of polyelectrolyte concentration (0.1 g L^{-1} vs. 1 $g \cdot L^{-1}$) used for the build-up of $(PDADMAC/PSS)_6$ and $(PAH\text{-}Gu/PSS)_6$ on H_3PO_4 recovery was determined by employing a model

solution containing H_3PO_4 at 10 wt % and 2 g·L^{-1} Al, dosed as $Al(OH)_3$ and used as the representative metal (pH = 0.7). A single hollow fiber membrane was assembled in a module and filtered at a constant pressure of 5 bar using a custom-made testing device (Fig. 5.2). A gear pump (Ismatec, Switzerland) was used to establish a cross flow velocity of 2.65 m·s^{-1} reaching a Reynolds number (R_e) of more than 2,300, thus operating in turbulent mode. Each membrane configuration was tested in triplicate. The concentrations of selected ions in the feed and permeate were analyzed in triplicate with ion-coupled plasma optical emission spectroscopy (ICP-OES) at a power of 1,400 W (coolant flow: 13 L min^{-1}, auxiliary flow: 1 L·min^{-1}, nebulizer flow: 0.75 L·min^{-1}, Spectroblue SOP, Spectro Analytical Instruments). Finally, the following optimized concentrations were used for further characterizations: PDADMAC/PSS 1 g·L-1 each in 0.5 M NaCl; and PAH and PAH-Gu 0.1 g· L^{-1} with PSS 0.1 g L^{-1} in 0.05 M NaCl. The obtained modified membranes were labelled as $(PDADMAC/PSS)_6$, $(PAH\text{-}Gu/PSS)_6$ and $(PAH/PSS)_6$ based on their composition.

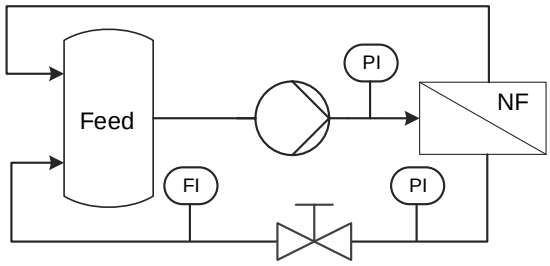

Figure 5.2 Flow chart of the self-designed and constructed filtration unit used for the optimization experiments using one hollow fiber module with a surface area of 0.00075 m^2 at TMP = 5 bar and v = 2.65 m·s^{-1}, where NF, FI (flow measurement) and PI(pressure measurement) stand for membrane unit, flow measurement, and pressure measurement, respectively.

Membrane surface characterization

Atomic force microscopy (AFM) measurements were carried out on the bare and LbL membranes to investigate membrane surface morphology. Before the analysis, the hollow-fiber membranes were cut and opened to analyze the inner (modified) section. The membranes were then fixed with a double-faced tape to an aluminium substrate to maintain a flat surface for the analysis. A SOLVER

NEXT AFM instrument from NT-MDT was used in all the AFM experiments. An NSG03 silicon tip from NT-MDT, with a nominal value for the tip radius of 7 nm (guaranteed < 10 nm) and a nominal spring constant of 0.4-2.7 $N \cdot m^{-1}$ was used in the height imaging and adhesive force measurements. The actual value of the spring constant was measured as 0.87 $N \cdot m^{-1}$ using the thermal noise method.38 While scanning the surface morphology, 512 x 512 points were recorded in 2 μm x 2 μm area. The height images were all scanned at a rate of 0.3 Hz. During all experiments, the relative humidity of the room was maintained constant at 48%.
X-ray Photoelectron Spectroscopy (XPS, Thermo Fisher Scientific, K-Alpha model) was employed to determine the surface elemental composition of all the membranes studied. In detail, a monochromatic Al K_α X-ray source with a spot size of 400 μm at a pressure of 10^{-7} mbar, a constant pass energy of 400 eV for the survey spectra, and 50 eV for the detailed high-resolution spectra were used. During the measurement, the flood gun was turned on to compensate for potential charging of the surface. The peak position was adjusted based on the internal standard C_{1s} peak at 284.8 eV, with an accuracy of ±0.05 eV. Avantage processing software was used to analyze all the spectra. Sample preparation was performed as it is described in the previous AFM section.

The zeta potential of the inner surface of the LbL membranes was determined by using a SurPassTM 3 (Anton Paar, Switzerland) instrument. A 10-cm-long membrane was covered by a heat shrink to prevent leakage. The membrane studied was inserted into the measuring cell by using flexible tubing. During measurement, a silver electrode was used. An aqueous 0.001 $Mol \cdot L^{-1}$ KCl solution was the background electrolyte. The pH was adjusted with a 0.05 M HCl and 0.05 M NaOH solution. The zeta potential was measured using one membrane at pH 2, 4, and 6. Each point was measured in triplicate, and after each measurement, the membranes were rinsed with demi water.

Sewage sludge ash leaching

Sewage sludge ash leachate from a mono incineration plant in Luzern, Switzerland was prepared with a sulfuric acid solution (≥95-98%, Sigma). Table 5.1 shows the chemical composition of the leached sewage sludge ash. To obtain 2 L of leachate, 700 g of sewage sludge ash was mixed with 2.92 L of demi water.

During stirring (500 rpm) of sulfuric acid was slowly added until pH = 1 was reached. Afterwards, the solution was stirred for an additional 10 min. In the next step, the leachate was filtered with 0.45 µm filter paper to remove solid residuals. For each experiment, 2 L of sludge ash leachate were prepared. The final pH of the solution was 1.15, measured by WTW inoLab® Multi 9310 IDS (Germany).

Filtration performances with sewage sludge ash leachate

The filtration experiments were performed using a bench-scale setup (MaxiMem unit from PS Prozesstechnik, Basel, Switzerland). During the filtration experiments, the cross-flow velocity for the LbL-modified membranes was v = 3.32 $m \cdot s^{-1}$, corresponding to R_e > 2,300 resulting in a turbulent flow. The commercially available acid-resistant AMS membrane was used as a benchmark and it was operated at 0.32 $m \cdot s^{-1}$, according to the manufacturer's data. For all the membranes, the temperature was set at 20°C (Thermofisher, Switzerland). The concentrations of elements in the feed and permeate were analyzed in triplicate with ICP-OES at a power of 1,400 W (coolant flow: 13 $L \cdot min^{-1}$, auxiliary flow: 1·L min^{-1}, nebulizer flow: 0.75 $L \cdot min^{-1}$, Spectroblue SOP, Spectro Analytical Instruments). The samples were diluted with 0.5 M HNO_3 (Sigma), were collected from the feed and the permeate at 7, 8, and 9 bar after at least 30 minutes of stabilization. During permeate recovery, the samples were taken at intervals of approximately 10 % of the permeate recovery until 50% of the initial feed was recovered.

Table 5.1 Sewage sludge ash leachate composition at pH = 1.15 and conductivity 50 $mS \cdot cm^{-1}$, P indicates the total phosphorus mostly present as H_3PO_4; S indicates the total sulfate mostly present as H_2SO_4.

Element	Concentration ($mg \cdot L^{-1}$)	Concentration ($mmol \cdot L^{-1}$)
Na^+	126 ± 9.6	2.9
K^+	209 ± 13	8.2
Mg^{2+}	903 ± 47	22
Al^{3+}	2,232 ± 110	60
P	9,729 ± 397	301
S	5,616 ± 212	180
Ca^{2+}	575 ± 39	23
Fe^{3+}	1,617 ± 63	90
Cu^{2+}	48.7 ± 7.3	3.1
Zn^{2+}	80 ± 13	5.2
Cr^{3+}	0.98 ± 0.08	0.05
Cd^{2+}	0.18 ± 0.01	0.02
Ni^{2+}	1.1 ± 0.2	0.06

Results and Discussion

Optimization of the membrane modification by LbL deposition.

A key advantage of LbL membranes is the option to tailor the membrane by parameter adjustments during the production process. One design parameter is the applied PE and its concentration. Table 5.2 reports the effects of PDADMAC/PSS, PAH-Gu/PSS and PAH/PSS concentrations used for coating (0.1 $g \cdot L^{-1}$ *vs.* 1 $g \cdot L^{-1}$) on H_3PO_4 recovery from a model solution containing H_3PO_4 and Al^{3+}.

Table 5.2 Percentage values of H_3PO_4 retention from a model solution containing H_3PO_4 at 10 wt% and 2 g·L^{-1} of Al^{3+}, dosed as $Al(OH)_3$, for $(PDADMAC/PSS)_6$, $(PAH\text{-}Gu/PSS)_6$ and $(PAH/PSS)_6$ LbL membranes at 1 g·L^{-1} and 0.1 g·L^{-1} of polyelectrolyte concentration.

Type of PE	PE Concentration [g·L^{-1}]	Al^{3+} retention [%]	H_3PO_4 retention [%]
$(PDADMAC/PSS)_6$	1	98 ± 1	10 ± 2
	0.1	85 ± 1	26 ± 1
$(PAH\text{-}Gu/PSS)_6$	1	94 ± 4	19 ± 2
	0.1	96 ± 2	14 ± 7
$(PAH/PSS)_6$	1	99 ± 1	17 ± 1
	0.1	97 ± 1	16 ± 2

For $(PDADMAC/PSS)_6$ the highest metal retention was obtained with a PE concentration of 1 g·L^{-1}. Clearly, a dense, concentrated multilayer leads to a higher retention of multivalent ions than a less concentrated, PE multilayer.[13] The H_3PO_4 retention was low at high $(PDADMAC/PSS)_6$ concentrations (26% at 0.1 g·L^{-1} *vs.* 10% at 1 g·L^{-1}). Similar observations were obtained previously when a lower number of PDADMAC/PSS bi-layers (indicating a low PE concentration on at the surface) led to higher H_3PO_4 retention values.[27] Despite differences in H_3PO_4 retentions, high metal retentions were often achieved, indicating a better separation. Consequently, 1 g·L^{-1} was set as the concentration for further analysis of the $(PDADMAC/PSS)_6$ NF membrane. For $(PAH\text{-}Gu/PSS)_6$ and $(PAH/PSS)_6$ similar values of Al^{3+} and H_3PO_4 retention were obtained. From the economic perspective of scaling-up the modification process, a low concentration of PEs is obviously preferred.[20] Thus 0.1 g·L^{-1} was chosen as the optimum membrane configuration for PAH-Gu/PSS and PAH/PSS multilayers.

Surfaces characterizations

We used XPS to map the elemental composition at the membrane surface before and after modification and to confirm the deposition of PE-multilayers at the optimized concentrations. Table 5.3 reports the values (%) of the detected elements for the membranes under investigation. A clear indication of the PE coating was the detection of nitrogen (N), which was absent in the bare sPES membrane and present in all LbL-coated membranes. The percentage of N

increased upon PE modification according to the following trend: PDADMAC ≤ PAH < PAH-Gu. The same order was found for C atoms with minor differences, which could be explained by the hydrocarbon contamination always present at the membrane surface or by interference of the C content from the sPES substrate.[35] The observed trend for N can be related to both the chemical structure of the polycations and the amount of PEs deposited on the analyzed area. The number of N atoms per monomeric unit is 1.9 N per repeating unit for PAH-Gu (4 N × 30% Gu + 1 N × 70% NH_2) and 1 N per monomeric unit for PAH and PDADMAC. The percentage of N found for $(PAH\text{-}Gu/PSS)_6$ was 5.3%, which is around 3 times higher than in the case of $(PDADMAC/PSS)_6$, yielding a value of 1.8%. This is probably due to the different chemical structure. To our surprise, we found for $(PAH/PSS)_6$ N = 4.6%, which was 2.5 times higher than the N detected for the PDADMAC/PSS multilayer. This might indicate a higher degree of coverage for PAH/PSS multilayer. The percentage of Si, known to be present in the inner part of the UF membrane as reported by the manufacturer, decreases upon the LbL deposition. The Si drops to a value of 15% for $(PDADMAC/PSS)_6$ and around 4% for both $(PAH\text{-}Gu/PSS)_6$, and $(PAH/PSS)_6$. This indicates a lower layer thickness for the PDADMAC-based multilayer, compared to the other two types of multilayers. We can further explain this with the respective pK_a value of the polycations. When the pH-independent polycation is applied (PDADMAC), less polymer is required to compensate for the negative charge of PSS, so more Si (16%) and less N (1.8%) is detected. For pH-dependent PEs (*e.g.,* PAH and PAH-Gu), the opposite can be assumed.[36] Indeed, for PAH layers less Si (4%) and more N (4.5%) is detected.

The XPS data also shows that Cl and Na (the respective counter-ions of the used PEs) were found high for PAH layers, and less for PAH-Gu. Almost no Na or Cl was found for PDADMAC. This can point to different levels of polyelectrolyte complexation. In case of PDADMAC/PSS multilayers polyelectrolyte complexation occurs, so no counter-ions are present within the polymeric network. It is known that the concentration of counter-ions in PDADMAC/PSS is strongly dependent on the number of bi-layers deposited.[24] The presence of counter-ions has been detected in the multilayer only if more than 7 bi-layers were applied[25], here a lower number of bi-layers were used. The low M_w of the PAH monomeric unit contributes to a higher charge density than PSS, around 50% more as reported

by Riegler *et al.*[37] when PAH/PSS layers were assembled, therefore counter-ions might have been involved in adsorption to maintain electroneutrality. According to Jaber *et al.*[38] around 30% of the PAH charges can be neutralized by Cl^-. This is less pronounced for PAH-Gu, which had a slighty higher M_w (having 30% of Gu groups in the sidechains of the PAH structure), and thus a lower charge density, than PAH.

Table 5.3 Selected XPS data from inner part of the sPES membranes and LbL-modified membranes. (n.d.: not detectable).

	C (%)	Si (%)	N (%)	Cl (%)	Na(%)
sPES	52.2 ± 2.8	21.6 ± 2.0	n.d.	n.d.	n.d.
$(PDADMAC/PSS)_6$	58.4 ± 1.2	15.6 ± 1.6	1.8 ± 0.5	0.3 ± 0.0	n.d.
$(PAH\text{-}Gu/PSS)_6$	66.1 ± 3.0	4.3 ± 2.2	5.3 ± 0.4	0.9 ±0.2	0.8 ± 0.0
$(PAH/PSS)_6$	60.0 ± 1.3	5.5 ± 1.4	4.6 ± 0.1	2.7 ± 0.6	2.6 ± 0.9

Previous XPS data suggested differences on the multilayer formation based on the nature of the polycation employed. An additional understanding of the differences between LbL structures can be found with AFM analysis (Figure 5.3). The study of the membrane morphology with AFM provides a more complete qualitative view of the multilayer conformation compared to XPS. As expected, the morphology of the bare sPES membrane (Figure 5.3a) reflects a generally smooth surface.[19] The LbL structure is confirmed by change of surface roughness. The surface becomes slightly denser in the case of PDADMAC/PSS multilayers (Figure 5.3b), and has a definitely rougher and more spiky-like structure when the PAH-Gu/PSS (Figure 5.3c) and PAH/PSS (Figure 5.3d) layers are deposited. As pointed out in the XPS interpretation, the PAH/PSS multilayers have more counter-ions, and therefore a more interpenetrated structure suggesting a higher degree of coverage.[39] AFM data support this observation, showing PAH/PSS with rough and dense conformation.[21,40,41] Also, PAH-Gu/PSS shows a high level of interpenetration, thus a dense structure, yet less than PAH/PSS. The PDADMAC/PSS morphology appears definitely lose and less dense compared to the others. The can be explained by the swollen nature of the PDADMAC, as reported in literature[38,40], and the absence of counter-ions, as found from XPS.

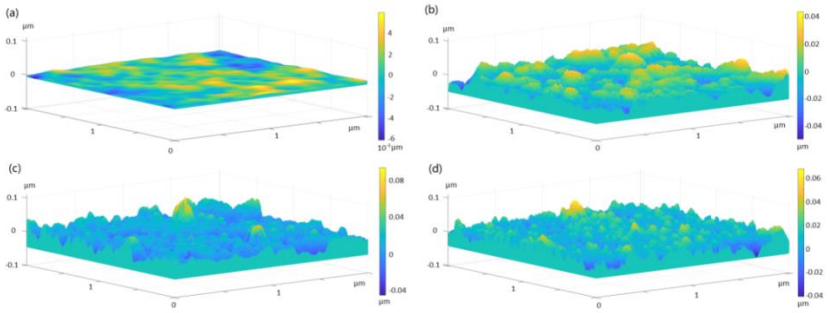

Figure 5.3 AFM topography images of a a) bare sPES membrane; and of membranes coated with the following PEMs: b) $(PDADMAC/PSS)_6$; c) $(PAH\text{-}Gu/PSS)_6$; d) $(PAH\ /PSS)_6$.

Given the importance of surface charge in the PEM build-up and ionic interactions, we measured the ζ-potential values of the sPES and as-prepared LbL-coated membranes (Figure 5.4). Given the highly acidic conditions of the intended filtration conditions (pH = 1.15), the ζ-potential was monitored in acidic solutions (pH = 2-6). As expected, the bare sPES membrane is negatively charged in the full pH range, which is attributed to the negative sulfonic groups present at the membrane surface. For the LbL membranes, the ζ-potential gradually decreases with increasing pH. While $(PDADMAC/PSS)_6$ remains positive throughout the whole pH-range, $(PAH/PSS)_6$ and $(PAH\text{-}Gu/PSS)_6$ turns negative at pH > 5.

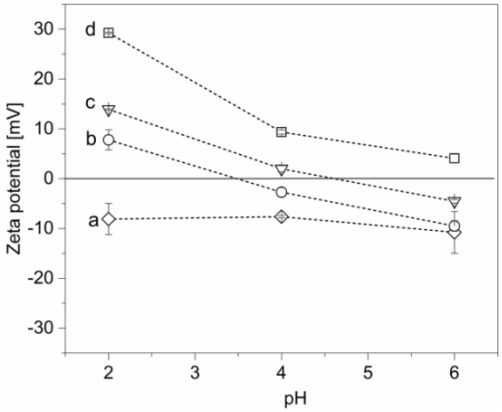

Figure 5.4 ζ-potential in acidic conditions (from pH 6 to 2) for the a) sPES bare membrane; b) PAH-Gu c) PAH and d) PDADMAC type of multilayers. The lines serve as a guide for the eyes.

Taking into account the experimental error during the measurement, again the differences in the acidic dissociation constant (pK_a) play a significant role. PDADMAC is a permanently charged polycation, while PAH and PAH-Gu are pH-dependent, with a pK_a of 8-9 for the primary amine and pK_a ~ 13 for the Gu moiety, allowing counter-ions within the polymer network (as we concluded from XPS).[28] Therefore, the amount of total positive charges of the multilayers is expected to be lower for PAH and PAH-Gu than PDADMAC[24,25] since local pH changes can affect the charge density, leading to decreased ζ-potential values.[25]

To conclude, the surface characterizations revealed that differences in the physicochemical properties of polycations lead to specific surface morphologies, related to different degrees of coverage and charge density in the PEs multilayer. Membrane surface properties play relevant roles in membrane filtration. Knowing the characteristics of membrane surface, such as charge, elemental composition and morphology, it, therefore, is important to deeply understand the mechanism of separation and later to correlate H_3PO_4 recovery results with the membrane type used.

Filtration experiments of sewage sludge ash leachate

In the second part of this study, we conducted bench-scale filtration experiments with the LBL NF membranes using sewage sludge ash leachate (for the composition, see Table 5.1). The optimized membranes with, 1 $g \cdot L^{-1}$ $(PDADMAC/PSS)_6$, 0.1 $g \cdot L^{-1}$ $(PAH\text{-}Gu/PSS)_6$ and 0.1 $g \cdot L^{-1}$ $(PAH/PSS)_6$ were compared in terms of their H_3PO_4 retention, cation retention and permeability. The conventional NF membrane AMS was used as a benchmark. As addressed in the introduction, this specific membrane achieved the lowest H_3PO_4 retention values and ~ 100% of metal retention among other commercially available acid-resistant NF membranes.[15] In Table 5.4, we report pure water and feed solution permeabilities at 0% permeate recovery, for LbL-modified NF membranes, the bare sPES UF membrane and the AMS acidic-resistant NF membrane.

Table 5.4 Pure water and the feed solution permeability at 0% permeate recovery, for bare sPES UF membranes, $(PDADMAC/PSS)_6$, $(PAH\text{-}Gu/PSS)_6$, $(PAH/PSS)_6$ LbL-modified membranes and AMS NF membrane at 20°C. Permeability for sPES and LbL-modified membranes were considered at TMP = 9 bar, and for AMS at TMP = 12 bar. (N.a.: not available.)

Membrane	Pure water permeability $L/m^2/h/bar$	Leachate sewage sludge ash permeability $L/m^2/h/bar$
sPES	80 [42]	N.a.
$(PDADMAC/PSS)_6$	6.1 ± 0.12	2.1 ± 0.065
$(PAH\text{-}Gu/PSS)_6$	5.4 ± 0.31	1.5 ± 0.051
$(PAH/PSS)_6$	2.5 ± 0.09	1.2 ± 0.037
AMS	2.1[a]	0.3 ± 0.04

[a] According to the specifications of the manufacturer.

Pure water permeability decreases more than 90% for all three LbL NF membranes compared to the bare sPES membrane, which reaches the highest value of 80 $L/m^2/h/bar$, clearly due to the high MWCO. Comparing the LbL-modified membranes, the lowest water permeability is observed for $(PAH/PSS)_6$, followed by $(PAH\text{-}Gu/PSS)_6$ and $(PDADMAC/PSS)_6$ with values of 2.5, 5.4 and 6.1 $L/m^2/h/bar$, respectively. The polycation-dependent trend of the flux is in line with the finding related to XPS and AFM. A loose and less interpenetrated multilayer structure, as it is for PDADMAC/PSS, generates a high flux; while the dense and rough surface morphologies, as observed for PAH and PAH-Gu layers, is correlated to a low flux. Water permeability values were compared with the permeability at 0% permeate recovery of leached sewage sludge ash (Table 5.4). Given the high MWCO of the unmodified sPES UF membrane, it was not tested for H_3PO_4 recovery. For the LbL-modified membranes, the permeabilities recorded for leached sewage sludge ash followed the same trend as for water permeability (*i.e.*, PAH < PAH-Gu < PDADMAC), but with remarkably lower values, attributable to the difference in osmotic pressure in the feed solutions ($\Pi_{\text{leached sewage sludge ash}}$ = 16 bar).

It must be noticed that the permeabilities of all the LbL-modified membranes are still much higher than the acid-resistant AMS NF benchmark membrane, with a flux of 2.1 $L/m^2/h/bar$ for pure water and only 0.3 $L/m^2/h/bar$

for sewage sludge ash leachate. The reason for such low values, is related to the dense selective surface layer, inhibiting the flux. We can already conclude that LbL deposition achieves a higher permeability than conventional NF membranes, and this is true for all the type of PEs applied.

Figure 5.5 shows the retention values for the $(PDADMAC/PSS)_6$ and $(PAH\text{-}Gu/PSS)_6$ LbL membranes and the AMS membrane of H_3PO_4 with Mg^{2+}, representing divalent charged ions and Fe^{3+}, as a representative metal, as a function of TMP. Other metals and ions present in the feed solution (Table 5.3) show comparable trends. Due to an extremely low permeability in the applied pressure range, the results obtained from $(PAH/PSS)_6$ LbL membrane were not considered.

Mass transport in NF membranes can be convective and/or diffusive. Diffusion originates from a concentration gradient, whereas convection arises from forced water flux, as described by the conventional extended Nernst-Planck model.[43] Changes in ion retention as a function of TMP can point to one of these two mechanisms. In Figure 5.5a, the H_3PO_4 retention for the $(PDADMAC/PSS)_6$ and $(PAH\text{-}Gu/PSS)_6$ LbL membranes was TMP independent, hence the transport of H_3PO_4 through the LbL membrane is pure convective. For the AMS membrane, H_3PO_4 retention increased with the applied TMP, reaching 65% at 10 bar and over 75% at 15 bar. Here, the H_3PO_4 transport also depends on diffusion. Increasing pressure led to lower H_3PO_4 yields when using the benchmark AMS membrane.

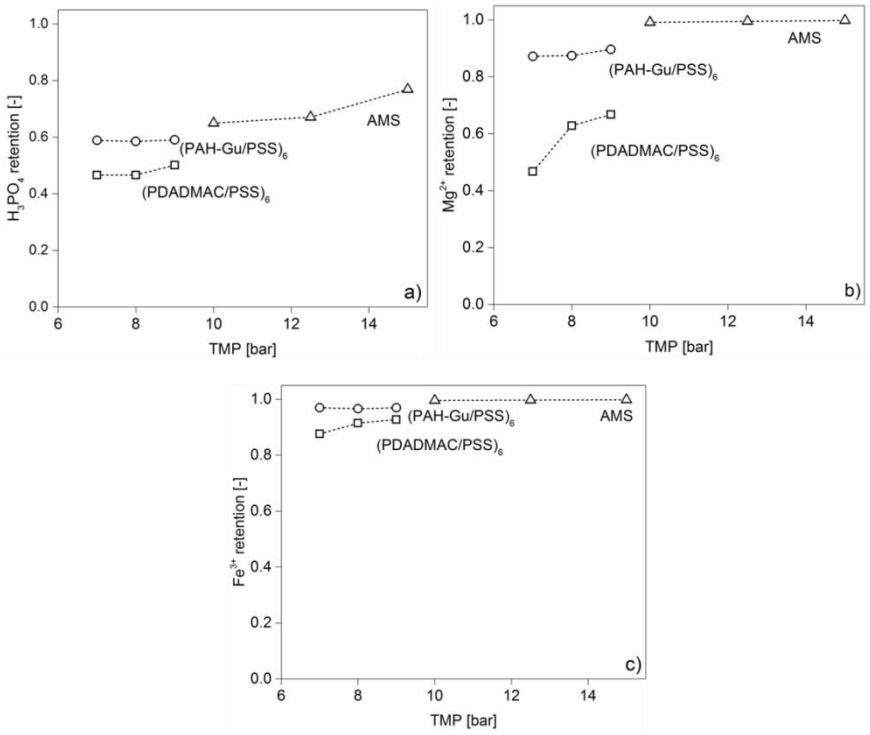

Figure 5.5 Retention values as a function of TMP for H_3PO_4, Mg^{2+}, and Fe^{3+} for two LbL-modified membranes $(PDADMAC/PSS)_6$ and $(PAH\text{-}Gu/PSS)_6$ and a conventional acid-resistant AMS NF membrane using sewage sludge ash leachate as a feed solution at T= 20°C and pH = 1.15.

The retention values of Mg^{2+} and Fe^{3+} for PAH-Gu/PSS and for AMS membranes is not dependent on the applied pressure (Figure 5.5b and c). The dense, packed top layer at the membrane surface probably contributed to maintaining a retention value of multivalent cations independently on the applied pressure. In contrast, for $(PDADMAC/PSS)_6$, the retention of Mg^{2+} and Fe^{3+} gradually increases along with TMP. We understand that at low applied pressure, the multivalent cations are partially rejected by the electrostatic forces present at the membrane surface, and mass transport is mainly determined by diffusion.[17,44,45] When a high pressure is applied, the drag forces increase due to water fluxes into the pores of the loose PDADMAC/PSS multilayer.[19] Meanwhile, the surface electrostatic forces remained constant, and the diffusive membrane transport stayed low compared to the overall permeate flow.

Figure 5.6 shows the retention values of H_3PO_4, Mg^{2+} and Fe^{3+} as a function of permeate recovery of up to 50% for the $(PDADMAC/PSS)_6$ and $(PAH\text{-}Gu/PSS)_6$ LbL membranes and the AMS membrane (benchmark membrane). Again the $(PAH/PSS)_6$ membrane was not further considered due to the insufficient flux. The lowest H_3PO_4 retention (highest recovery) was obtained for $(PDADMAC/PSS)_6$ followed by the $(PAH\text{-}Gu/PSS)_6$ and the AMS membrane (Figure 5.6a). Again, the differences between the two LbL-modified membranes can be explained by multilayer conformation as observed from AFM and XPS. As mentioned, $(PDADMAC/PSS)_6$ has a more open, loose structure favouring the transport of phosphorus by convective flux as H_3PO_4, compared to the denser $(PAH\text{-}Gu/PSS)_6$ membranes (Table 5.4). Moreover, the Gu moieties in the PAH-Gu enable specific interactions with oxyanions such as monovalent phosphate (present as a small fraction at this low pH conditions)[31] as already mentioned in Chapters 2 and 3, and this could partially contribute to higher retention of the total measured H_3PO_4 compared to PDADMAC.[43] For all three membranes, the H_3PO_4 retention values tend to increase over permeate recovery. This might be a consequence of changed concentration polarization (increasing of ionic strength at membrane surface), and/or changes in steric effects during permeate recovery. However H_3PO_4 retention values for LbL membranes tend to be higher at a given permeate recovery as compared to commercially available acidic-resistant AMS NF membrane.

As shown in Figure 5.6b, the Fe^{3+} retentions for $(PAH\text{-}Gu/PSS)_6$ and $(PDADMAC/PSS)_6$ are >90% during the recovery process. However, these values are lower than the values measured for the conventional AMS membrane which showed a constant value >99%. Similar results were observed for Mg^{2+} in Figure 5.6c. The AMS membrane maintains a retention >99% for Mg^{2+}, while for the LbL membranes Mg^{2+} retention is on average 85% for the PAH-Gu/PSS and 60% for the PDADMAC/PSS membrane. Another time, we can associate this with the morphological differences between the two multilayers. Obviously, a loose layer as for PDADMAC would retain fewer multivalent cations than a more compact, dense layer. Clearly, the effect was enhanced for the divalent- compared to trivalent cations, having a higher charge density. Both LbL membranes showed decreased cation retention over permeate recovery. We can explain this tendency by shielding effect of the membrane.[46] As the ionic strength of the

sewage sludge ash leachate increases during filtration, the concentration at the membrane surface rise, which might result in a screening of membrane charges[47,48], and decreasing the retention of multivalent cations. This phenomenon has been observed for other types of conventional membranes (*e.g.*, DL (GE), NF270 (DOW) and Duracid (GE)[15], so it can be attributed not only to the LbL deposition but also to the general NF principle.

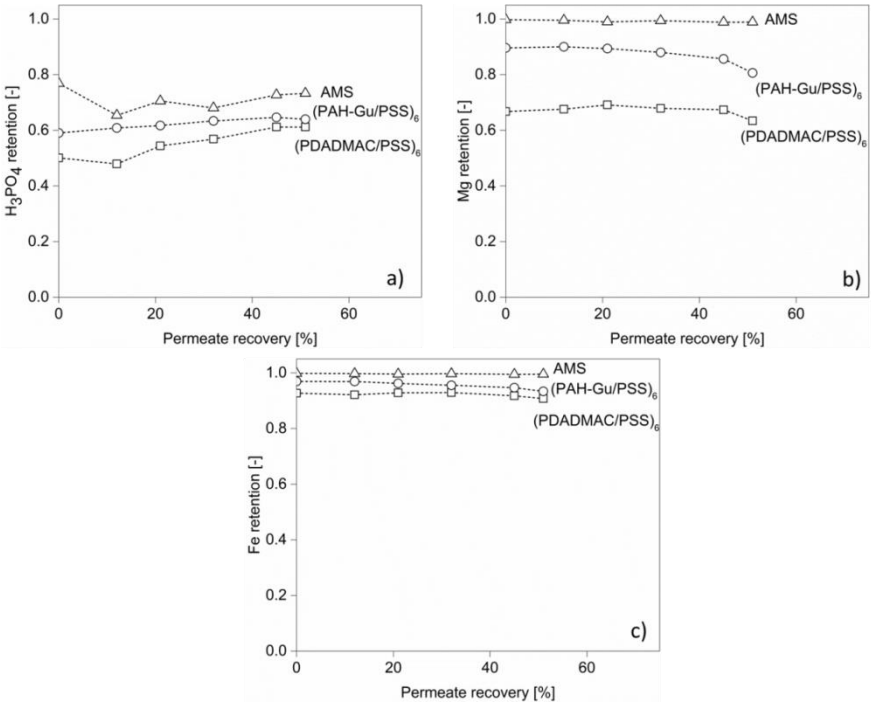

Figure 5.6 Retention values over permeate recovery of (a) H_3PO_4, (b) Fe^{3+}, and(c) Mg^{2+} for $(PDADMAC/PSS)_6$ and $(PAH\text{-}Gu/PSS)_6$ using sewage sludge ash leachate as a feed solution at TMP = 9 bar, T= 20°C and pH = 1 and for AMS A-3012-1812 (AMS) membrane using sewage sludge ash leachate as a feed solution at TMP = 12.5 bar, T= 20°C and pH = 1.

Figure 5.7 displays the permeability for LbL membranes, and the AMS membrane during sewage sludge ash leachate filtration for permeate recovery. The permeability of LbL membranes decreases linearly with increasing permeate recovery, due to higher osmotic pressure. Scaling is not very likely to occur in this harsh acidic conditions. The AMS membrane has a low, almost constant permeability value during filtration (0.3 L/m^2/h/bar, see also Table 5.4). The LbL-

modified membranes exhibit higher permeability throughout the experiment. Even after 50% of permeate recovery, the permeability for $(PDADMAC/PSS)_6$ is 10 times higher compared to the AMS membrane. The $(PAH\text{-}Gu/PSS)_6$ reaches values 5 times higher than the benchmark membrane. Higher permeability leads to a favourable process design based on the operational and investment costs of the NF unit, requesting less membrane area. This implies smaller membrane units, and thus lower investments costs (CAPEX) for the unit.

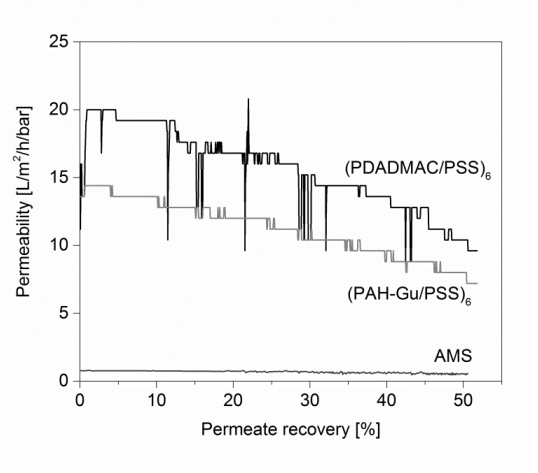

Figure 5.7 Permeability as function of permeate recovery for three tested membranes: $(PDADMAC/PSS)_6$ and $(PAH\text{-}Gu/PSS)_6$ using sewage sludge ash leachate as a feed solution at TMP = 9 bar, T= 20°C and pH = 1 and AMS membrane using sewage sludge ash leachate as a feed solution at TMP = 12.5 bar, T= 20°C and pH = 1.

To generate the same permeate flow at the same pressure, the $(PDADMAC/PSS)_6$-modified membrane needs four times less membrane area than the AMS membrane. Estimating the specific investment cost for a membrane unit, following Samhaber *et al.*[49] more than 50% of CAPEX can be saved when applying an LbL membrane. Compared to the LbL-modified membranes, the AMS membrane can be operated at higher pressure, so the membrane area can be decreased. However, this generates high energy consumption, increasing the operational cost (OPEX) of the process. Energy costs would rise by more than 80% to reach comparable fluxes. An increase in CAPEX occurs due to higher material requirements for the pressure resistance of the membrane unit. Another important factor is the high packing density of hollow-

fiber membranes.[50] A small number of modules is needed, and the membrane unit size is reduced. From an economic perspective, the application of LbL-modified, hollow-fiber membranes offers lower CAPEX and OPEX than conventional spiral wound membrane modules.

Conclusions

In this work, LbL-modified, hollow-fiber UF membranes were employed as NF membranes to recover P from leached sewage sludge ash. This research was conducted to fill the knowledge gap on the correlation between the LbL NF membrane structure properties (here investigated with XPS and AFM) and the H_3PO_4 recovery under industrially relevant conditions. The LbL-coated membranes proved to increase the permeability and H_3PO_4 recovery compared to commercially available acidic-resistance NF membranes (AMS). The LbL-modified membranes were tested with a leached sewage sludge ash solution, and we discovered that $(PDADMAC/PSS)_6$ had a higher P recovery (low retention) compared to the $(PAH\text{-}Gu/PSS)_6$ membrane. However, the latter had better retention of multivalent cations, which must be completely retained for a clean H_3PO_4 permeate. We can conclude that LbL-modified membranes produce better results in term of H_3PO_4 recovery from sewage sludge ash than the commercially available acid-resistant nanofiltration membrane (AMS). Finally, this work aims to demonstrate that LbL-coated NF membrane can be employed for real-life application with advantages in term of CAPEX and OPEX.

References

(1) Van Vuuren, D. P.; Bouwman, A. F.; Beusen, A. H. W. Phosphorus Demand for the 1970-2100 Period: A Scenario Analysis of Resource Depletion. *Glob. Environ. Chang.* 2010, *20*, 428–439.

(2) Jasinski, S. M. Phosphate Rock. *U.S. Bur. Mines, Miner. Resour. Progr.* 2017, No. 703.

(3) European Commission. *On the Review of the List of Critical Raw Materials for the EU and the Implementation of the Raw Materials Initiative*; 2014.

(4) Desmidt, E.; Ghyselbrecht, K.; Zhang, Y.; Pinoy, L.; Van der Bruggen, B.; Verstraete, W.; Rabaey, K.; Meesschaert, B. Global Phosphorus Scarcity and Full- Scale P-Recovery Techniques: A Review. *Crit. Rev. Environ. Sci. Technol.* 2015, *45*, 336–384.

(5) Conley, D. J. H. Paerl, W. Howarth, R. W. Boesch, D. F. Seitzinger, S. P. Havens, K. E.Lancelot, C. Likens, G. E. Controlling Eutrophication: Nitrogen and Phosphorus. *Science* 2009, *323*, 1014–1015.

(6) Blöcher, C.; Niewersch, C.; Melin, T. Phosphorus Recovery from Sewage Sludge with a Hybrid Process of Low Pressure Wet Oxidation and Nanofiltration. *Water Res.* 2012, *46* (6), 2009–2019.

(7) Schweizerischer Bundesrat. Vermeidung Und Die Entsorgung von Abfällen. *Abfallverordnung, VVEA* 2015, 1–46.

(8) Beurteilung, G.; Nachhaltigkeit, D. Beurteilung von Technologien Zur Phosphor-Rückgewinnung Inhalt. *BAFU* 2017.

(9) Nogueira, G. . Phos4life Process: Joint Industrial Development towards Efficient Phosphorus Urban Mining. *Phosphor-Mining Der Stoffkreislauf schliesst sich, Informationsveranstaltung* 2017, *9* (September).

(10) Nattorp, A.; Remmen, K.; Remy, C. Cost Assessment of Different Routes for Phosphorus Recovery from Wastewater Using Data from Pilot and Production Plants. *Water Sci. Technol.* 2017, *76* (413–424).

(11) Egle, L.; Rechberger, H.; Krampe, J.; Zessner, M. Phosphorus Recovery from Municipal Wastewater: An Integrated Comparative Technological, Environmental and Economic Assessment of P Recovery Technologies. *Sci. Total Environ.* 2016, *571*, 522–542.

(12) Mohammad, A. W.; Teow, Y. H.; Ang, W. L.; Chung, Y. T.; Oatley-Radcliffe, D. L.; Hilal, N. Nanofiltration Membranes Review: Recent Advances and

Future Prospects. *Desalination* 2015, *356*, 226–254.

(13) Cheng, W.; Liu, C.; Tong, T.; Epsztein, R.; Sun, M.; Verduzco, R.; Ma, J.; Elimelech, M. Selective Removal of Divalent Cations by Polyelectrolyte Multilayer Nanofiltration Membrane: Role of Polyelectrolyte Charge, Ion Size, and Ionic Strength. *J. Memb. Sci.* 2018, *559*, 98–106.

(14) Lide, D. R. CRC Handbook of Chemistry and Physics, 84th Edition, 2003-2004. *Handb. Chem. Phys.* 2003, *53*, 2616.

(15) Schütte, T.; Niewersch, C.; Wintgens, T.; Yüce, S. Phosphorus Recovery from Sewage Sludge by Nanofiltration in Diafiltration Mode. *J. Memb. Sci.* 2015, *480*, 74–82.

(16) Niewersch, C.; Battaglia Bloch, A. L.; Yüce, S.; Melin, T.; Wessling, M. Nanofiltration for the Recovery of Phosphorus - Development of a Mass Transport Model. *Desalination* 2014, *346*, 70–78.

(17) Niewersch, C. Nanofiltration for Phosphorus Recycling from Sewage Sludge. *Ph.D. Diss. RWTH Aachen Univ.* 2013, 158.

(18) Liu, G.; Dotzauer, D. M.; Bruening, M. L. Ion-Exchange Membranes Prepared Using Layer-by-Layer Polyelectrolyte Deposition. *J. Memb. Sci.* 2010, *354* (1–2), 198–205.

(19) Menne, D. Layer-by-Layer Design of Nanofiltration Membranes. *Layer-by-Layer Des. Nanofiltration Membr.* 2017.

(20) Richardson, J. J.; Bjornmalm, M.; Caruso, F. Technology-Driven Layer-by-Layer Assembly of Nanofilms. *Science* 2015, *348*, 1–11.

(21) Tang, K.; Besseling, N. A. M. Formation of Polyelectrolyte Multilayers: Ionic Strengths and Growth Regimes. *Soft Matter* 2016, *12* (4), 1032–1040.

(22) Menne, D.; Kamp, J.; Erik Wong, J.; Wessling, M. Precise Tuning of Salt Retention of Backwashable Polyelectrolyte Multilayer Hollow Fiber Nanofiltration Membranes. *J. Memb. Sci.* 2016, *499*, 396–405.

(23) Joseph, N.; Ahmadiannamini, P.; Hoogenboom, R.; Vankelecom, I. F. J. Layer-by-Layer Preparation of Polyelectrolyte Multilayer Membranes for Separation. *Polym. Chem.* 2014, *5* (6), 1817–1831.

(24) Schlenoff, J. B.; Dubas, S. T. Mechanism of Polyelectrolyte Multilayer Growth: Charge Overcompensation and Distribution. *Macromolecules* 2001, *34*, 592–598.

(25) Adusumilli, M.; Bruening, M. L. Variation of Ion-Exchange Capacity , ζ

Potential , and Ion-Transport Selectivities with the Number of Layers in a Multilayer Polyelectrolyte Film. *Langmuir* 2009, No. 35, 7478–7485.

(26) Femmer, R.; Mani, A.; Wessling, M. Ion Transport through Electrolyte/polyelectrolyte Multi-Layers. *Sci. Rep.* 2015, *5*, 1–12.

(27) Remmen, K.; Muller, B.; Joachim, K.; Wessling, M.; Wintgens, T. Phosphorus Recovery in an Acidic Environment Using Layer-by-Layer Modified Membranes. *under Submiss.*

(28) Choi, J.; Rubner, M. F. Influence of the Degree of Ionization on Weak Polyelectrolyte Multilayer Assembly. *Macromolecules* 2005, *38* (1), 116–124.

(29) Cao, Z.; Gordiichuk, P. I.; Loos, K.; Sudhölter, E. J. R.; de Smet, L. C. P. M. The Effect of Guanidinium Functionalization on the Structural Properties and Anion Affinity of Polyelectrolyte Multilayers. *Soft Matter* 2016, *12*, 1496–1505.

(30) Pantos, A.; Tsogas, I.; Paleos, C. M. Guanidinium Group: A Versatile Moiety Inducing Transport and Multicompartmentalization in Complementary Membranes. *Biochim. Biophys. Acta - Biomembr.* 2008, *1778*, 811–823.

(31) Schug, K.; Lindner, W. Noncovalent Binding between Guanidinium and Anionic Groups: Focus on Biological- and Synthetic-Based Arginine/guanidinium Interactions with Phosph[on]ate and Sulf[on]ate Residues. *Chem. Rev.* 2005, *105*, 67–114.

(32) Paltrinieri, L.; Wang, M.; Sachdeva, S.; Besseling, N. A. M.; Sudhölter, E. J. R.; de Smet, L. C. P. M. Fe3O4 Nanoparticles Coated with a Guanidinium-Functionalized Polyelectrolyte Extend the pH Range for Phosphate Binding. *J. Mater. Chem. A* 2017, *5*, 18476–18485.

(33) de Grooth, J.; Oborný, R.; Potreck, J.; Nijmeijer, K.; de Vos, W. M. The Role of Ionic Strength and Odd-Even Effects on the Properties of Polyelectrolyte Multilayer Nanofiltration Membranes. *J. Memb. Sci.* 2015, *475*, 311–319.

(34) Hutter, J. L.; Bechhoefer, J. Calibration of Atomic-Force Microscope Tips. *Rev. Sci. Instrum.* 1993, *64*, 1868–1873.

(35) Stevens, J. S.; De Luca, A. C.; Pelendritis, M.; Terenghi, G.; Downes, S.; Schroeder, S. L. M. Quantitative Analysis of Complex Amino Acids and RGD Peptides by X-Ray Photoelectron Spectroscopy (XPS). *Surf. Interface*

Anal. 2013, *45*, 1238–1246.

(36) Maroni, P.; Montes Ruiz-Cabello, F. J.; Cardoso, C.; Tiraferri, A. Adsorbed Mass of Polymers on Self-Assembled Monolayers: Effect of Surface Chemistry and Polymer Charge. *Langmuir* 2015, *31* (22), 6045–6054.

(37) Riegler, H.; Essler, F. Polyelectrolytes: Intrinsic or Extrinsic Charge Compensation? Quantitative Charge Analysis of PAH/PSS Multilayers. *Langmuir* 2002, *18* (17), 6694–6698.

(38) Jaber, J. A.; Schlenoff, J. B. Counterions and Water in Polyelectrolyte Multilayers: A Tale of Two Polycations. *Langmuir* 2007, *23* (2), 896–901.

(39) Lourenço, J. M. C.; Ribeiro, P. A.; Do Rego, A. M. B.; Fernandes, F. M. B.; Moutinho, A. M. C.; Raposo, M. Counterions in Poly(allylamine Hydrochloride) and Poly(styrene Sulfonate) Layer-by-Layer Films. *Langmuir* 2004, *20* (19), 8103–8109.

(40) V Klitzing, R. Internal Structure of Polyelectrolyte Multilayer Assemblies. *Phys. Chem. Chem. Phys.* 2006, *8* (43), 5012–5033.

(41) Szilagyi, I.; Trefalt, G.; Tiraferri, A.; Maroni, P.; Borkovec, M. Polyelectrolyte Adsorption, Interparticle Forces, and Colloidal Aggregation. *Soft Matter* 2014, *10*, 2479–2502.

(42) de Grooth, J.; Haakmeester, B.; Wever, C.; Potreck, J.; de Vos, W. M.; Nijmeijer, K. Long Term Physical and Chemical Stability of Polyelectrolyte Multilayer Membranes. *J. Memb. Sci.* 2015, *489*, 153–159.

(43) Mudler, M. *Basic Principles of Membrane Technology*, 2nd ed.; Kluwer Academic Publishers, The Netherlands, 1996.

(44) Pontalier, P. Y.; Ismail, A.; Ghoul, M. Mechanisms for the Selective Rejection of Solutes in Nanofiltration Membranes. *Sep. Purif. Technol.* 1997, *12* (2), 175–181.

(45) Paugam, L.; Taha, S.; Dorange, G.; Jaouen, P.; Quéméneur, F. Mechanism of Nitrate Ions Transfer in Nanofiltration Depending on Pressure, pH, Concentration and Medium Composition. *J. Memb. Sci.* 2004, *231* (1–2), 37–46.

(46) Rautenbach, T. M. R. *Membranverfahren. Grundlagen Der Modul- Und Anlagenauslegung,*; 2007.

(47) Bargeman, G.; Westerink, J. B.; Guerra Miguez, O.; Wessling, M. The Effect of NaCl and Glucose Concentration on Retentions for Nanofiltration Membranes Processing Concentrated Solutions. *Sep. Purif.*

Technol. 2014, *134*, 46–57.

(48) Liu, C.; Shi, L.; Wang, R. Enhanced Hollow Fiber Membrane Performance via Semi-Dynamic Layer-by-Layer Polyelectrolyte Inner Surface Deposition for Nanofiltration and Forward Osmosis Applications. *React. Funct. Polym.* 2015, *86*, 154–160.

(49) Samhaber, W. M. Erfahrungen Und Anwendungspotential Der Nanofiltration. *VDI-Wissensforum "Membrantechnik der Prozessindustrie* 2006, *20*.

(50) Frank, M.; Bargeman, G.; Zwijnenburg, A.; Wessling, M. Capillary Hollow Fiber Nanofiltration Membranes. *Sep. Purif. Technol.* 2001, *22–23*, 499–506.

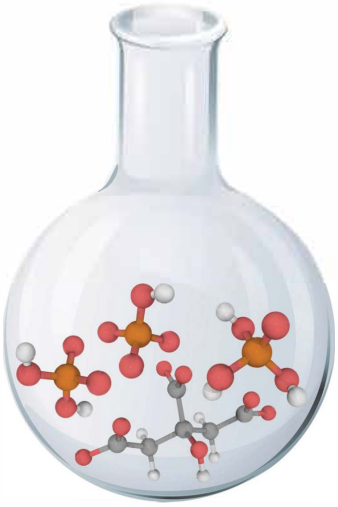

CHAPTER 6

General discussion and outlook

General discussion

I summarize the results described in this thesis with the take-home message that materials functionalized with guanidinium (Gu) receptor groups are able to interact with phosphate from water, and thus are able to be used in its recovery. Yet, this comes with several challenges, mostly related to the presence of competing ions and the pH conditions. Changing the pH of the solution influences the phosphate species involved in the separation process, and adding to the complexity of the selective capture of phosphate from a mixed solution.[1] To address these challenges different Gu-functionalized materials were synthesized, investigated and tested in advanced water treatment technologies at different pH values.

In **Chapter 2**, a functionalized polyelectrolyte with Gu groups (PAH-Gu, having 30% of the monomeric units carrying a Gu group) is used as a surface coating of Fe_3O_4 nanoparticles. These Fe_3O_4@PAH-Gu NPs were able to adsorb a constant amount phosphate (~4 mg P/g of adsorbent) independently of the pH condition (pH range 5 – 10). In addition, Fe_3O_4@PAH-Gu NPs showed a higher colloidal stability compared to the unmodified Fe_3O_4 NPs, resulting in an improvement of their long-term effectiveness. Phosphate removal by adsorption to Fe_3O_4@PAH-Gu NPs is a fast and straightforward method, however, the system needs an extensive use of chemicals during the regeneration process, causing additional costs and chemical disposal issues.

Another approach is based on anion-exchange membranes (AEMs), as described in **Chapters 3** and **4**. Offering a permselective transport for anions over cations, AEMs can provide a continuous and controlled separation process avoiding the use of chemicals for regeneration. In **Chapter 3** a new AEM composition was proposed, containing the same polyelectrolyte as used in the previous chapter (PAH-Gu). This polymer was blended with a cross-linker and a charged quaternary ammonium acrylate monomer to obtain a blended/hybrid membrane upon photo-polymerization. The amount of blended PAH-Gu blended was optimized in terms of the density of functional groups and the miscibility of

the membrane components, and the optimum was found to be 5 wt%. The PAH-Gu@AEM yielded an enhanced interaction with phosphate at pH = 5 compared to the reference (PAH-Gu free) AEM. By this example of an AEM, prepared by the addition of a polyelectrolyte that is only partially composed of Gu-groups, we have shown the potential of such a facile membrane fabrication procedure to tune the ion-selective properties of AEMs.

Remarkable improvements of the ion selectivity of Gu-based membranes are presented in **Chapter 4**. Here, the anion-exchange sites of the AEM were completely determined by Gu groups (Gu-100). The Gu-100 was obtained by the UV-initiated polymerization of a newly synthesized Gu-acrylate monomer. Observed differences between the Gu-100 and the Gu-free (Gu-0; only quaternary ammonium sites) were substantial during the electrodialysis of model dairy wastewater streams. Phosphate and citrate transport was enhanced in Gu-100 membranes compared to Gu-0 at pH = 7, and at pH = 10 Gu-100 was able to selectively transport phosphate and citrate, while transport of these ions was almost absent for the Gu-0 AEM. In this study, the phosphate removal properties of the Gu-100 were determined in a complex aqueous stream in the presence of abundant competing anions.

In the previous chapters, the removal of phosphate by Gu-based materials (*i.e.*, nanoparticles and AEMs) was always explored at alkaline or neutral/slightly acidic pH conditions (pH = 7-10). In **Chapter 5** the recovery of phosphate under harsh strongly acidic conditions was investigated. At a pH value of 1, phosphoric acid itself is the main species (pK_{a1} = 2.2). The earlier-mentioned Gu-functionalized polyelectrolyte (PAH-Gu) was deposited by the layer-by-layer (LbL) method on the lumen part of a hollow fibre ultrafiltration membrane. By this modification, the membrane porosity decreased to the nanofiltration (NF) range (having typical molecular weight cutoff = 80 – 2,000 Da). The LbL-modified NF membranes were able to recover phosphoric acid from a real leachate sewage sludge ash stream. The observed permeability of the LbL NF membranes were higher than a commercial, acidic-resistance (reference) NF membrane, and the recovery of the phosphoric acid was also significantly improved. In this work, we proved the effectiveness of PAH-Gu modified membranes in phosphoric acid recovery from real waste streams.

In general, this research shows a wide range of applications of the guanidinium receptor:

i) in the form of a polyelectrolyte modifying nanoparticles (Ch 2) and hollow fiber membranes (Ch 5), as well as blended in an anion-exchange membrane (Ch 3);

ii) in the form of an acrylate monomer polymerised to a novel anion-exchange membrane (Ch 4).

The Gu receptor was of use under harsh acidic conditions as well as in basic and at neutral pHs (and this is all attributed to the high pK_a value of 13). Moreover, the level of complexity of the water stream at which Gu-based materials were exposed gradually increases with the research chapters, going from a single salt solution (Ch 2) to a binary mixture (Ch 3), to a complex model solution (Ch 4), and finally, to a real wastewater stream (Ch 5). The Gu polyelectrolyte was employed as adsorption layer on the surface of nanoparticles to extend the pH range for phosphate binding. Furthermore it has been used to facilitate transport in all the other research topics. The strength of the Gu-phosphate interaction is such that it potentially allows both capturing and transport of phosphate throughout the membrane. In other words, the binding is reversible.

Yet, besides phosphate, guanidinium has shown also favourable interactions with others oxyanions, like sulphate (Ch 3) and citrate (Ch 4), hence the selectivity between different oxyanions might be difficult to achieve. However, guanidinium groups hold interesting properties regarding their binding properties with oxyanions as well as their use in a wide pH range, showing great potential for different applications, for example, to improve membrane stability in alkaline fuel cells or to improve the capture of anions in capacitive deionization systems.

Outlook

Increased awareness of the limited amounts of global phosphorus resources and on the uncontrolled discharge of phosphate-containing waste streams, is the motivation to recover and re-use phosphate. As materials scientists in the field of

water technology, our contribution primarily lies in the development of new precision materials with selective properties and their integration into well-known separation technologies. Membranes are often used for advanced water treatments, and in the past years, a number of methodologies have been proposed to improve their selectivity, not only for phosphate removal but in general for the recovery of valuable compounds present in wastewater streams.[2]

In this thesis, polyelectrolytes have been used to improve the membrane selectivity, as additional fixed charges in blended membranes (Ch 3) and as applied by a layer-by-layer (LbL) modification on nanofiltration membranes (Ch 5). Certainly, polyelectrolytes offer several advantages in term of costs and versatility, and recent studies[3–5] have shown their potential as LbL on top of ion-exchange membranes. The modification of ion-exchange membranes via LbL is an attractive procedure due to their easy fabrication process. However, the method still holds a few limitations and this is why the methodology was not explored in this research. For instance, their interaction with the membrane substrate is only driven by non-covalent interactions, thus determined by the available charges on the surface of the substrate. In addition, the number of layers that can be potentially deposited is limited, since it should not lead to a too strong increase of the overall membrane thickness, which would reduce the ion transport too much. Moreover, when polyelectrolytes are used as a selective layer on top of an ion-exchange membrane, the fixed-charges of the substrate itself (usually present at a higher concentration compared to the charged groups of the polyelectrolyte multilayer) might interfere with the overall membrane selectivity.

New frontiers in the field of selective ion-exchange membranes point towards the need of developing new bulk rather than surface modification strategies.[6] In this way, improvements on ion-exchange membrane selectivity can be achieved by creating interconnected ion-conducting functional channels inside the membrane.

The first chapter of this thesis presents the results obtained with modified magnetic nanoparticles, showing their potential for phosphate binding and it would be very interesting to incorporate such modified nanomaterials inside ion-

exchange membranes. Given their nano-sized dimensions, nanoparticles can be homogeneously distributed inside the membrane[7] creating such desired interconnected pathways for ion-selective transport. Moreover, the distribution of iron oxide nanoparticles might be tuned or aligned with the use of external magnetic fields.[8] As shown in Chapter 1, iron oxide nanoparticles can be easily modified at the surface, and numerous functional groups can be explored to improve their selectivity towards specific target compounds. In general, the incorporation of functionalized nanomaterials inside ion-exchange membrane shows great potential to the design of novel ion-selective membranes and the topic definitely worth to be further explored. In Figure 6.1a, an illustration is given of the concept of a novel anion-exchange membrane loaded with functionalized magnetic nanoparticles. By the use of a magnetic field well-aligned nanodomains are created (Figure 6.1b), facilitating ion conductivity along predefined pathways.

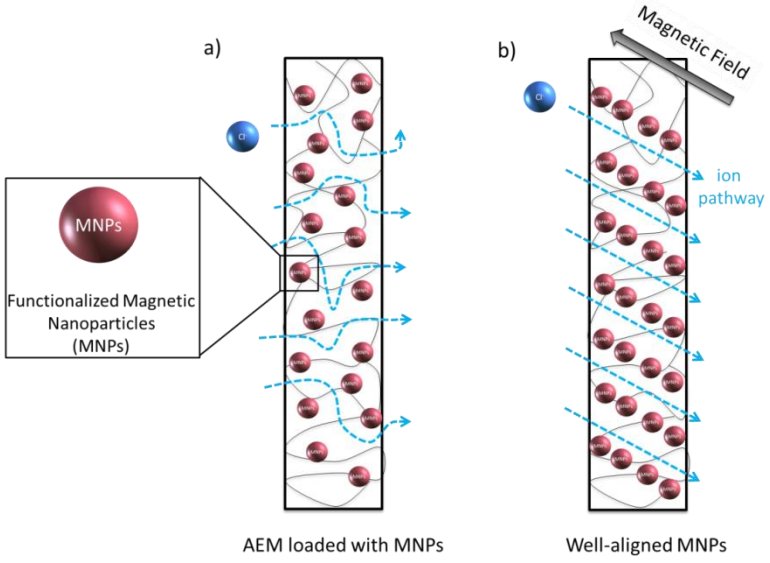

Figure 6.1 Schematic illustration of ion pathways (chloride as an example) in an a) AEM loaded with randomly distributed functionalized magnetic nanoparticles (MNPs) and b) AEM loaded with well-aligned MNPs as obtained by the use of an external magnetic field.

Besides exploring all the possible configurations for membrane modification, one should always keep in mind that the key of a good selective transportation is

to find the right balance between affinity and mobility. To selectively recover a target compound from water the binding between the functional group (*i.e,* the receptor) and the ion (*i.e,* the target) should be reversible, allowing for transport. Creating strong interactions with a specific ion would favour partitioning to the functional groups of the membrane, however, the ion mobility would inevitably be decreased or can be even lost. If the affinity is strong, additional energy is required to allow the ion to jump between successive binding sites. Finding the right balance between mobility and selectivity is still a great challenge for most of the research to be done in this field, and the introduction of external driving-forces, such electrical fields or pressure, can be of help to improve the mobility, if affinity is too strong.

Indeed, the proper choice of the receptor to improve the membrane selectivity is only one aspect to realize to a successful separation. Also important are the operational parameters, which have a certain control over ion-transport (*i.e.,* for nanofiltration, these include transmembrane pressure, the cross-flow velocity, the module geometry; for ion-exchange membranes, these include the current density, flow rate, stacks design). As an illustration, in Chapter 4 we performed electrodialysis experiments using model dairy water containing a high concentration of chloride ions. Chloride is a relatively small anion with a high diffusion coefficient (Table 1.1), thus under an externally applied current density, its electrophoretic mobility would always prevail over the other anions present with a larger size and lower diffusion coefficient. In this case, it is clear that the selectivity of a 'perfect' membrane would not overcome the intrinsic response of certain anions to external parameters, *i.e.,* applied current/voltage. Thus, if the final goal is to discriminate chloride from other anions, selective membranes as proposed in this thesis cannot do the job in one step. Of great importance are pre-treatments, which contribute to reduce the complexity of the composition of the aqueous solution during the separation process. For example, combining an ion-exchange resin process (to remove chloride by adsorption) with electrodialysis, using selective anion-exchange membranes, is a possible strategy to improve the recovery process of valuable compounds. Another solution may be found in multistep processes during electrodialysis. Monovalent selective membranes (which are commercially available) can be assembled in a stack to first transport monovalent undesired compounds before addressing the

separation of the multivalent ions. Here, in the case of phosphate recovery (or others ampholytic compounds), the starting pH of the feed solution should be adjusted to maintain desired multivalent species during the first electrodialysis step.

References

(1) Sarapulova, V.; Nevakshenova, E.; Pismenskaya, N.; Dammak, L.; Nikonenko, V. Unusual Concentration Dependence of Ion-Exchange Membrane Conductivity in Ampholyte-Containing Solutions: Effect of Ampholyte Nature. *J. Memb. Sci.* 2015, *479*, 28–38.

(2) Luo, T.; Abdu, S.; Wessling, M. Selectivity of Ion Exchange Membranes: A Review. *J. Memb. Sci.* 2018, *555* (December 2017), 429–454.

(3) Femmer, R.; Mani, A.; Wessling, M. Ion Transport through Electrolyte/polyelectrolyte Multi-Layers. *Sci. Rep.* 2015, *5*, 1–12.

(4) Abdu, S.; Marti-Calatayud, M.-C.; Wong, J. E.; Garcia-Gabaldon, M.; Wessling, M. Layer-by-Layer Modification of Cation Exchange Membranes Controls Ion Selectivity and Water Splitting. *Appl. Mater. Interfaces* 2014, *6*, 1843–1854.

(5) White, N.; Misovich, M.; Alemayehu, E.; Yaroshchuk, A.; Bruening, M. L. Highly Selective Separations of Multivalent and Monovalent Cations in Electrodialysis through Nafion Membranes Coated with Polyelectrolyte Multilayers. *Polym. (United Kingdom)* 2016, *103*, 478–485.

(6) Alabi, A.; AlHajaj, A.; Cseri, L.; Szekely, G.; Budd, P.; Zou, L. Review of Nanomaterials-Assisted Ion Exchange Membranes for Electromembrane Desalination. *npj Clean Water* 2018, *1* (1), 10.

(7) He, Y.; Tong, C.; Geng, L.; Liu, L.; Lü, C. Enhanced Performance of the Sulfonated Polyimide Proton Exchange Membranes by Graphene Oxide: Size Effect of Graphene Oxide. *J. Memb. Sci.* 2014, *458*, 36–46.

(8) Hasani-Sadrabadi, M. M.; Majedi, F. S.; Coullerez, G.; Dashtimoghadam, E.; VanDersarl, J. J.; Bertsch, A.; Moaddel, H.; Jacob, K. I.; Renaud, P. Magnetically Aligned Nanodomains : Application in High- Performance Ion Conductive Membranes. *Appl. Mater. Interfaces* 2014, *6*, 7099–7107.

Samenvatting

Ik vat in het algemeen de resultaten beschreven in dit proefschrift samen met mee naar huis te nemen boodschap dat gefunctionaliseerde materialen met guanidinium (Gu) receptorgroepen in staat zijn om te interageren met fosfaat uit water en dus kunnen worden gebruikt bij het herstel ervan. Toch komt dit met verschillende uitdagingen, vooral gerelateerd aan de aanwezigheid van concurrerende ionen en pH-omstandigheden. Verandering van de pH in de oplossing beïnvloedt de fosfaat soort die bij het scheidingsproces is betrokken en draagt bij aan de complexiteit van de selectieve vastlegging van fosfaat uit een gemengde oplossing. Om op te lossen werden verschillende Gu-gefunctionaliseerde materialen gesynthetiseerd, onderzocht en getest in geavanceerde waterzuiveringstechnologieën bij verschillende pH-waarden.

In **Hoofdstuk 2** wordt een gefunctionaliseerde polyelektrolyt met Gu-groepen (PAH-Gu, met 30% van de monomeer eenheden die een Gu-groep dragen) gebruikt als een oppervlaktelaag van Fe_3O_4-nanodeeltjes. Deze Fe_3O_4@PAH-Gu ND's waren in staat om een constante hoeveelheid fosfaat (~ 4 mg P/g adsorbent) te adsorberen onafhankelijk van de pH (pH-bereik 5 - 10). Bovendien vertoonden Fe_3O_4 @ PAH-Gu ND's een hogere colloïdale stabiliteit in vergelijking met de ongemodificeerde Fe_3O_4 ND's, wat resulteerde in een verbetering van hun langetermijneffectiviteit. Fosfaat verwijdering door adsorptie aan Fe_3O_4@PAH-Gu ND's is een snelle en eenvoudige methode, maar het systeem heeft een uitgebreid gebruik van chemicaliën nodig tijdens het regeneratieproces, wat extra kosten en chemische verwijderingsproblemen veroorzaakt.

Een andere benadering is gebaseerd op anionenwisselingsmembranen (AWM), zoals beschreven in **Hoofdstukken 3 en 4**. Met een perm-selectief transport voor anionen over kationen, kunnen AWM's zorgen voor een continu en gecontroleerd scheidingsproces dat het gebruik van chemicaliën voor regeneratie vermijdt. In **Hoofdstuk 3** werd een nieuwe AWM-samenstelling voorgesteld, die dezelfde polyelektrolyt bevat als in het vorige hoofdstuk (PAH-Gu). Dit polymeer werd gemengd met een cross-linker en een geladen quaternair ammoniumacrylaat-monomeer om een gemengd/ hybride membraan

na fotopolymerisatie te verkrijgen. De hoeveelheid gemengd PAH-Gu-mengsel was geoptimaliseerd in termen van de dichtheid van functionele groepen en de mengbaarheid van de membraancomponenten, en het optimum bleek 5 gew.% te zijn. De PAH-Gu@AWM leverde een verbeterde interactie met fosfaat op bij pH = 5 in vergelijking met de referentie (PAH-Gu vrij) AWM. Door dit voorbeeld van een AWM, bereid door de toevoeging van een polyelektrolyt dat slechts gedeeltelijk is samengesteld uit Gu-groepen, hebben we het potentieel van een dergelijke eenvoudige membraanvervaardigingsprocedure getoond om de ion selectieve eigenschappen van AWMs af te stemmen.

Opmerkelijke verbeteringen van de ionenselectiviteit van op Gu-gebaseerde membranen worden gepresenteerd in **Hoofdstuk 4**. Hier werden de anion-uitwisselingsplaatsen van de AWM volledig bepaald door Gu-groepen (Gu-100). De Gu-100 werd verkregen door de UV-geïnitieerde polymerisatie van een nieuw gesynthetiseerd Gu-acrylaatmonomeer. De waargenomen verschillen tussen de Gu-100 en de Gu-vrije (Gu-0; alleen quaternaire ammoniumlocaties) waren aanzienlijk tijdens de elektrodialyse van afvalstromen van model afvalzuivel. Fosfaat- en citraat transport was verhoogd in Gu-100 membranen vergeleken met Gu-0 bij pH = 7, en bij pH = 10 was Gu-100 in staat selectief fosfaat en citraat te transporteren, terwijl transport van deze ionen bijna afwezig was voor de Gu-0 AWM. In deze studie werden de fosfaat-verwijderende eigenschappen van de Gu-100 bepaald in een complexe waterige stroom, in aanwezigheid van overvloedige concurrerende anionen. In de vorige hoofdstukken werd de verwijdering van fosfaat door op Gu gebaseerde materialen (*i.e.,* nanodeeltjes en AWM's) altijd onderzocht bij alkalische of neutrale/licht zure pH-omstandigheden (pH = 7-10).

In **Hoofdstuk 5** werd het herstel van fosfaat onder sterk zure omstandigheden onderzocht. Bij een pH van 1 is fosforzuur zelf de belangrijkste soort (pK_{a1} = 2,2). Het eerdergenoemde Gu-gefunctionaliseerde polyelektrolyt (PAH-Gu) werd afgezet door de laag-voor-laag (LVL) methode op het lumendeel van een holle vezel ultrafiltratie membraan. Door deze modificatie nam de porositeit van het membraan af tot het bereik van nanofiltratie (NF) (met kenmerkende uitsluiting molecuulgewicht = 80 - 2000 Da). De met LVL gemodificeerde NF-membranen waren in staat om fosforzuur terug te winnen

uit een echte percolaat van rioolwater uit slijk. De waargenomen permeabiliteit van de LVL NF-membranen was hoger dan een commercieel, zuurbestendig (referentie) NF-membraan en de winning van het fosforzuur was ook aanzienlijk verbeterd. In dit werk hebben we de effectiviteit van met PAH-Gu gemodificeerde membranen bij het winnen van fosforzuur uit echte afvalstromen aangetoond.

Sommario

Riassumo i risultati ottenuti in questa ricerca con il seguente messaggio: i materiali funzionalizzati con il gruppo recettore Guanidinio (Gu) sono in grado di interagire con il fosforo presente nell'acqua, e quindi possono essere utilizzati per il suo recupero. Questo comporta alcune difficoltà correlate alla presenza di altri ioni e alle condizioni di pH iniziale dell'acqua. Il cambiamento del pH iniziale influisce sul tipo di fosforo conivolto nel processo di separazione, aggiungendo ulteriore complessità durante il recupero selettivo del fosforo. In questa ricerca, al fine di superare le molteplici difficoltà, , sono stati sintetizzati diversi materiali contenenti il gruppo Gu. Questi nuovi materiali sono stati testati utilizzando varie tecnologie di trattamento avanzato dell'acqua reflua a diversi valori di pH.

Nel **Capitolo 2** viene presentato un polielettrolita funzionalizzato con il gruppo Gu (chiamato PAH-Gu, avente 30% delle unità monomeriche contenenti il gruppo Gu), il polielettolita e' stato utilizzato come rivestimento superficiale di nanoparticelle (NPs) di Fe_3O_4. In questo capitolo, si dimostra che le NPs di Fe_3O_4@PAH-Gu sono in grado di assorbire una quantità costante di fosforo (~4 mg P/g di NPs) indipedentemente dalle condizioni di pH delle acque di partenza (considerando un intervallo di pH tra 5 e 10). In aggiunta, le NPs di Fe_3O_4@PAH-Gu presentano una stabilità colloidale più alta rispetto a NPs di Fe_3O_4 commerciali, e questo migliora la loro efficacia a lungo termine. La rimozione di fosforo tramite assorbimento con NPs di Fe_3O_4@PAH-Gu è un metodo efficace e veloce, tuttavia il sistema neccessita di un elevato consumo di sostanze chimiche durante il processo di rigenerazione, generando costi aggiuntivi e problemi relativi allo smaltimento dei rifiuti chimici.

Un altro approccio si basa sull'utilizzo di membrane a scambio ionico (AEM), come descritto nei **Capitoli 3** e **4**. Offrendo un trasporto seletivo per anioni rispetto ai cationi, le AEMs garantiscono un processo di separazione continuo e controllato evitando l'utilizzo di agenti chimici per la rigenerazione. Nel **Capitolo 3**, viene proposta una nuova composizione per AEM contenente lo stesso polielettrolita utilizzato nel capitolo precedente (PAH-Gu). Per la prima volta, il polieletrolita è miscelato con un reticolante e un monomero di acrilato di

ammonio quaternario per ottenere una membrana ibrida composta parzialmente da gruppi Gu, utilizzati come siti funzionali a scambio ionico. La membrana è stata ottenuta tramite un processo di fotopolimerizzazione. La quantità di PAH-Gu è ottimizzata in termini di densità di gruppi funzionali e miscibilità dei componenti strutturali della membrana. Il valore ottimale di PAH-Gu all'interno della membrane è risultato 5 m.m%. La membrana PAH-Gu@AEM ha una migliore interazione con il fosforo a pH = 5 comparata con una membrana commerciale di riferimento (Fufjilm) che non contiene PAH-Gu. Dall'esempio di una AEM ibrida contenente un polielettrolita, che è solo parzialmente composto da gruppi di Gu, abbiamo mostrato attraverso una semplice procedura di fabbricazione come sia possiblile migliorare le proprietà selettive di una membrana nel recupero del fosforo.

Importanti miglioramenti riguardo la selettivià di membrane composte da gruppi Gu, sono presentate nel **Capitolo 4**. In questo caso, tutti i siti a scambio anionico della AEM sono completamente sostituiti da gruppi Gu (la nuova membrana viene chiamata Gu-100). La membrana Gu-100 è ottenuta tramite un processo di fotopolimerizzazione di un monomero Gu-acrilato sintetizzato per la prima volta in questa ricerca. Le differenze osservate tra Gu-100 e una membrana Gu-0 commerciale di Fujifilm (avente solo gruppi a scambio ionico a base di ammonio quaternario) sono sostanziali durante l'elettrodialisi di acqua reflua sintetica industriale, preparata sulla base di reflui da latticini. Durante l'eletrodialisi a pH = 7, il trasporto di fosfato e citrato è maggiore per la membrana Gu-100 rispetto a Gu-0; a pH =10 la membrana Gu-100 è in grado di trasportare selettivamente il fosforo e il citrato (quindi di recuperarli), mentre per la membrana commerciale Gu-0 di Fujifilm il transporto di fosfato e citrato è quasi completamente assente. In questa ricerca, la membrana Gu-100 viene caraterizzata per le sue proprietà di recupero del fosforo da una soluzione modello di acqua reflua industriale complessa, abbondante di anioni in competizione tra loro.

Nei capitoli precedenti, il recupero del forforo da materiali contenenti il gruppo Gu (*e.g.,* nanoparticelle e membrane a scambio ionico) è stato sperimentato sempre in condizioni di pH alcalino o neutro/leggermente acidico (intervallo di pH = 7 – 10). Nel **Capitolo 5**, viene studiato il recupero del fosforo

in condizioni a pH acido molto estreme. Ad un valore di pH = 1, il fosfato è maggiormente presente come acido fosforico (pK_{a1} = 2.2). In questa ricerca, il polielettrolita precedentemente utilizzato (PAH-Gu) viene depositato nella parte interna di una membrane cava di ultrafiltrazione tramite il metodo strato-substrato (qua abbrieviato come LbL). Attraverso questa funzionalizzazione, la dimensione dei pori della membrana diminuisce rientrando nel range di una membrane per nanofiltrazione (NF). Abbiamo dimostrato che le membrane di nanofiltratione ottenute tramite la tecnica LbL sono in grado di recuperare il fosforo (nella forma di acido fosforico) da una soluzione reale di fanghi reflui industriali acidificati. Le membrane NF LbL hanno mostrato una permeabilità e una capacità di recupero di fosforo migliore rispetto a membrane nanofiltrazione commerciali utilizzate in applicazioni acide. Questa ricerca mostra l'effettivo utilizzo di un polielectrolita contenente il gruppo Gu (PAH-Gu) applicato su membrane per il recupero di acido fosforico da fanghi reflui da fonte industriale.

List of Publications

This thesis:

1. L. Paltrinieri, K. Remmen [*shared first author*], L. Chu, J. Köser, T. Wintgens, L. C. P. M. de Smet, M. Wessling, E. J. R. Sudhölter, *Improved Phosphoric Acid Recovery from Sewage Sludge Ash using Layer-by-Layer Modified Membranes*, manuscript submitted to J. Memb. Sci.

2. L. Paltrinieri, E. Huerta, T. Puts, W. van Baak, A. Verver, E. J. R. Sudhölter, L. C. P. M. de Smet, *Guanidinium Acrylate-based Anion-Exchange Membrane for the recovery of Citrate and Phosphate from Dairy Wastewater*, Environmental Science and Technology, **2019,** DOI 10.1021/acs.est.8b05558.

3. L. Paltrinieri, L. Poltorak, L. Chu, T. Puts, W. van Baak, E. J. R. Sudhölter, L. C. P. M. de Smet, *Hybrid Polyelectrolyte-Anion Exchange Membrane for Phosphate Removal*, Reactive and Functional Polymers, 133, **2018,** 126-135.

4. L. Paltrinieri, M. Wang, S. Sachdeva, N. A. M. Besseling, E. J. R. Sudhölter, L. C. P. M de Smet, *Fe_3O_4 nanoparticles coated with a guanidinium-functionalized polyelectrolyte extend the pH range for phosphate binding*, Journal of Materials Chemistry A., 5, **2017,** 18476-18485.

Collaborative/previous works:

5. R. di Gesu, C. Gualandi, A. Zucchelli, L. Paltrinieri, M. L. Focarete, *Nutrients recovery through the use of biodegradable electrospun poly(lactic acid) membranes*, under revision in Environmental Science and Technology.

6. A. Cao, M. Shan, L. Paltrinieri, W. Evers, L. Chu, L. Poltorak, J. H. Klootwijk, B. Swoane, J. Garson, E. J. R. Sudhölter, L. C. P. M. de Smet, *Enhanced vapour sensing using silicon nanowire devices coated with Pt nanoparticle functionalized porous organic frameworks*, Nanoscale, 10, **2017,** 6884-6891.

7. C. Cabrera, L. Paltrinieri, L. C. P. M. de Smet, L. A. M. van der Weilen, A. J. J. Straathof, *Recovery and esterification of aqueous carboxylates by using CO_2-expanded alcohols with anion exchange*, Green Chemistry, 19, **2017**, 729-738.

8. J. Feng, E. Hontanon, M. Blanes, J. Meyer, X. Guo, L. Stantos, L. Paltrinieri, N. Ramlawi, L. C. P. M. de Smet, H. Nirschl, F. E. Kruis, A. Schmidt-Ott, G. Biskos,

Scalable and Environmentally Benign Process for Smart Textile Nanofinishing, Journal of Applied Materials and Interfaces, 8 (23), **2016**, 14756-14765.

9. G. Todaro and L. Paltrinieri [*shared first author*], G. Mazzola, M. Vannini, L. Sisti, A. Ballestrazzi, S. Valeri, A. Pollicino, A. Celli, D. Gioia, M. L. Focarete, *Electrospun fibers containing bio-based ricinoleic acid effect of amount and distribution of ricinoleic acid unit on antibacterial properties*, Macromolecular Materials and Engineering, 300 (11) **2015**, 1085-1095.

10. A. Liquori and L. Paltrinieri [*shared first author*], A. Stancampiano, C. Gualandi, M. Gherardi, V. Colombo, M. L. Focarete, *Solid-State Crosslinking of Polysaccharide Electrospun Fibers by Atmospheric Pressure Non-Equilibrium Plasma A Novel Straightforward Approach*, Plasma Polymer and Processes, 12 (11) **2015**, 1195-1199.

11. L. B. Favero, A. Maris, L. Paltrinieri and W. Caminati, *The Rotational Spectrum of Dichloromethane-Ne- Internal Dynamics and Cl Quadrupolar Hyperfine Effects*, Journal of Physical Chemistry A, 119 (49) **2015**, 11813-11819

Conferences:

1. L. Paltrinieri, L. Poltorak, L. Chu, T. Puts, W. van Baak, E. J. R. Sudhölter, L. C. P. M. de Smet, *Electrochemical Properties of Hybrid Anion-Exchange Membrane for Phosphate Removal*, 69th Annual Meeting of the International Society of Electrochemistry, 2-9 September **2018**

2. L. Paltrinieri, L. Poltorak, L. Chu, T. Puts, W. van Baak, E. J. R. Sudhölter, L. C. P. M. de Smet, *Anion-Exchange Membrane blended with a functionalized polyelectrolyte to enhance phosphate transport over sulfate*, Euromembrane, 9-13 July, **2018**

3. L. Paltrinieri, M. J. Eshlaghi, E. J. R. Sudhölter, L. C. P. M. de Smet, *Phosphate transport through Anion Exchange Membranes: Effect of Salt Concentration and Type of Co-ion*, 9th International Membrane Science and Technology Conference, 5-9 December, **2016** [Best Poster Presentation]

Acknowledgements

Coming to the end of this thesis, I would like to thank all people that contributed in their own unique way to this research during these four years.

Firstly, I express my deep gratitude to Prof. Ernst Sudhölter, thanks for your constant support, your constructive feedbacks, and for your confidence in my work. You gave me the freedom to independently conduct my research and I became stronger and more confident with time. My sincere thanks to Dr. Louis de Smet for introducing me to this project. Thanks for your advices, your comments and for your efforts in improving my writing. I would like to thanks the committee members, Prof. Mark van Loosdrecht, Prof. Stephen Picken, Prof. Erik Roesink and Dr. Wilson Smith for their critical remarks which stimulated me to widen my research from various perspectives.

I acknowledge Wetsus for the financial support and all the desalination team members, in particular Dr. Jan Post and Dr. Henk Miedema, for the stimulating discussions during the team meetings. I am also grateful to the industrial partners, especially FrieslandCampina and Fujifilm, for their assistance with the collection of data. A special thanks to Dr. Albert Verver for the substantial scientific contribution for chapter four and to Willem van Baak, who introduced me to membranes production at industrial scale. Your willingness to give your time so generously was a resource for the project, and I wish you the best for Water Future. I also extend my gratitude to the technicians and the researchers of the R&D department of Fujifilm, especially Theo and Elisa, for offering me the technical support in running the experiments.

A special thanks to Prof. Thomas Wintgens, Dr. Joachim Köser and Kirsten Remmen from the FHNW institute in Switzerland, to open the doors of your laboratories for this successful collaboration.

My research would not have been possible without the contribution given by my master students over the past four years, Min, Morez, Arvind, and Kostadin. Guiding you during your thesis has been a true learning process and I am thankful for that. I wish you a great future career. Thanks for the aid and support

of the OMI people, Summit, Anping, Lukasz, Hamid, Mohammad, Liangyong, Naveen, Rajeev, Stijn, Pierre, Nick, Duco and Lars, thanks for being awesome colleagues and for the gold time spent together. Lukasz, thanks for helping me in the co-supervision of two master projects and for all the inputs you gave to this research, your enthusiasm and passion for science is a source of inspiration. Many thanks to the secretaries, Karin, Caroline and Els, for your valuable help in all the practical issues.

Delft is the city where I found precious friends who have made a wonderful time, Leon, Catarina, Miguel, Mathilde, Kars, Nakul, Patrizia, Daniela, Gabriele, Maria, Pasquale, Francesca and Benjamin, you all contributed in different ways to make this experience unforgettable. To my paranymphs, Patrizia and Maria, thanks for accepting standing next to me and for all what we shared, thanks for just being my friends.

Leaving my home town and starting this amazing adventure has been at the same time exiting and difficult. My roots are to me very important, so I have to thanks my old friends Laura, Giorgia, Serena, Giorgia, Sanja, Veronica, Federico e Dino. Despite I was living abroad, you always made me feel as if I never left, thanks for your constant support during these four years. Thanks to my messy, funny, crazy and beloved family members Carlotta, Beatrice, Carmen, Luca, Daniela, Silvia, Giacomo, Cecilia, Giovanni, Lilla, Gigi, Alessandra, Angela and Giuly, you have been close to me even from far. To my brother, Riccardo, my mum, Chiara, and my father, Marco, and to my granparents, Maria e Dino, ho avuto il coraggio di affrontare determinate scelte perche' sapevo di avere un porto sicuro al quale ritornare, grazie per esserci e grazie per tutto quello che avete sempre fatto per me.

Last but not least a special thanks to my sweet half, Roberto, who has always been at my side. Come mi hai detto tu, siamo un squadra e ci supportiamo a vicenda, in ogni passo, dal piú semplice al piú inaspettato. Senza i tuoi consigli, la tua amorevole pazienza e la tua fiducia nelle mie capacitá non sarei mai riuscita a raggiungere questo traguardo. Life with you is amazing!

Laura

About the author

Laura Paltrinieri was born in Carpi, a town in the Emilia Romagna province of Italy. After finishing high school (liceo scientifico M. Fanti) in 2007, she enrolled in University of Bologna to study Chemistry. Laura finished her bachelor *cum laude* with a thesis on physical chemistry which ended up in her first publication "The Rotational Spectrum of Dichloromethane-Ne- Internal Dynamics and Cl Quadrupolar Hyperfine Effects". In 2010, Laura started her Master degree in Chemistry with a specialization in Materials and Analytical Characterizations. Her Master project was conducted at AQUATEAM COWI company in Oslo, Norway. Laura obtained her Master in Chemistry *cum laude* with a thesis on the fabrication of polymeric nanofibrous membranes for nutrients recovery.

In 2012 she joined the Polymeric Materials and Characterization lab at University of Bologna as a Junior Research fellow. She worked for two years in the European Project NEFELE of FP7th for the development of polymeric membranes for water treatments.

In November 2014, Laura started her PhD in the Organic Materials and Interfaces Group at the Chemical Engineering Department of Delft University of Technology, project financed by Wetsus (Center of Excellence for Sustainable Water Technology) in Leeuwarden. The research focused on developing materials for the recovery of phosphate from water and the project was in collaboration with Fujifilm Membrane Development and FrieslandCampina.